Studies on the Biosynthetic Machinery in Polyunsaturated Fatty-Acid Synthases

(多価不飽和脂肪酸合成酵素における
生合成機構に関する研究)

Shohei Hayashi

Graduate School of Chemical Sciences and Engineering

Hokkaido University

TABLE OF CONTENTS

Chapter 1

General introduction

1.1. The role of fatty acids and polyunsaturated fatty acids

Fatty acids are member of lipids and are one of the primary metabolites as with sugars, amino acids, and nucleosides (Figure 1-1-1). Due to their hydrophobic properties, phospholipids with fatty acids, in which palmitic acids (C_{16}) and stearic acids (C_{18}) are mostly involved, are used in cell membranes to separate inside and outside of cells in plants, animal, and microorganisms. Triglycerides, which are a neutral lipid and tri-esterified with fatty acids, are used as energy-storage, and β-oxidation of fatty acids provides more energy than that of carbohydrates and proteins.

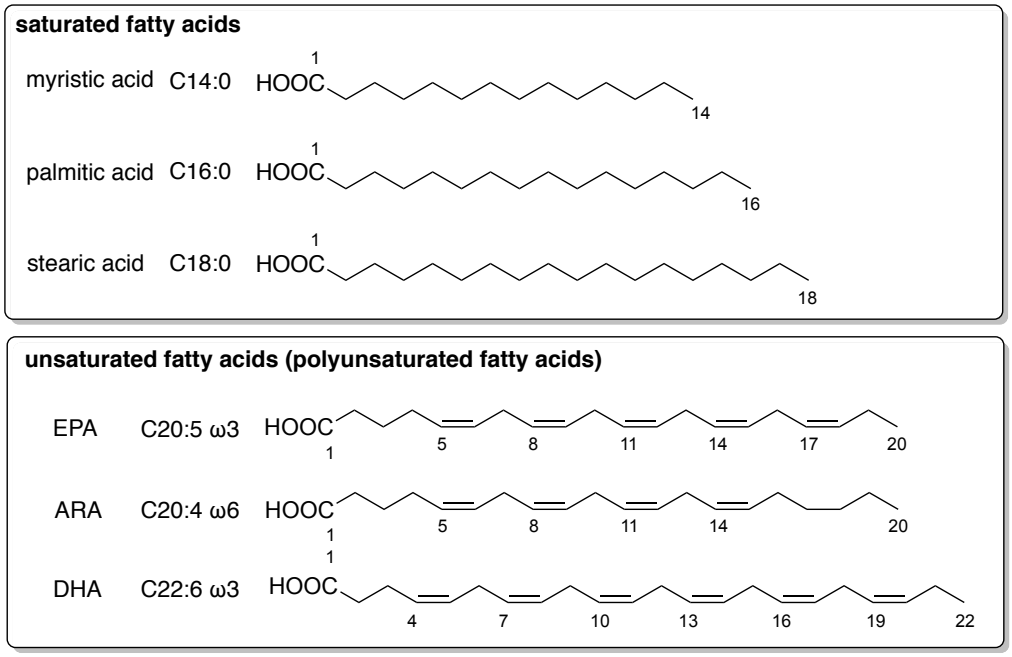

Figure 1-1-1. Chemical structures of saturated and polyunsaturated fatty acids.

Fatty acids are classified into two groups. Former groups are saturated fatty acids that have no double bond in their structure. Latter groups are unsaturated fatty acids that have one or more *cis* double bond. Especially, unsaturated fatty acids containing more than two *cis* double bonds such as docosahexaenoic acids (DHA; C22:6 ω3), eicosapentaenoic acids (EPA; C20:5 ω3), and arachidonic acids (ARA; C20:4 ω6) are collectively called polyunsaturated fatty acids (PUFAs). These PUFAs are

mostly subdivided in omega-3 (ω3) and omega-6 (ω6) depending on position of the first *cis* double bond from methyl end. Because they showed lower melting points than those of saturated fatty acids, membrane phospholipids with PUFAs showed membrane fluidity at low-temperature. Deep-sea bacteria employ them to adapt to low-temperature environments. Indeed, growth of an EPA biosynthetic gene-disrupted *Shewanella* sp. was retarded at low temperature (4℃)[1,2]. Furthermore, PUFAs are precursors of signal molecules such as prostaglandins and leukotrienes in eukaryotes[3,4]. Because human and animals don't have genes for PUFA biosynthesis, they ingest PUFAs from food such as fish and seafoods. ω3 PUFAs showed beneficial biological activities such as prevention of coronary heart diseases and hyperlipidemia. Also, PUFAs showed antibacterial activities against pathogen of stomach cancer *Helicobacter pylori*[5-9]. Therefore, the demands for these PUFAs are increasing in food and pharmaceutical industries. Fish and fish oils have been traditionally the PUFA sources. However, there is concern over the availability of PUFAs because of the unstable supply from marine resources and increasing demand. One of the alternative and sustainable sources of PUFAs are fermentative processes using microorganisms such as filamentous fungi (ARA producer), microalgae (DHA producer), and engineered yeast (EPA producer)[10-12]. In next two section, I described fatty acid and PUFA biosynthetic pathway to understand the biosynthetic system.

1.2. Biosynthetic pathway of fatty acids in microorganisms

All organisms *de novo* biosynthesize fatty acids using Fatty Acid Synthases (FASs), and the process of fatty acid biosynthesis has been well studied in animal, plants, fungi, and bacteria[13-15]. A FAS catalyzes repeated reaction cycles for elongation of fatty acyl chains; β-ketoacyl synthase (KS)-mediated decarboxylative condensation of malonyl-acyl carrier protein (ACP) with acyl-ACP to form β-ketoacyl-ACP, β-ketoacyl reduction catalyzed by β-ketoacyl reductase (KR) using NADPH as a cofactor to form β-hydroxyacyl-ACP, α,β-dehydration catalyzed by dehydratase (DH), and enoyl reduction of 2-*trans* acyl-ACP by enoyl reductase (ER) using NADPH to form saturated acyl-ACP (Figure 1-2-1). These reactions are used for one cycle elongation on fatty acid biosynthesis. Animal FAS and fungal FAS are composed of one large polypeptide and two large polypeptides with several domains catalyzing reaction cycles, respectively. The multifunctional enzyme systems for fatty acid biosynthesis is termed as Type I FAS. In contrast, discreate enzymes catalyzing each reaction step in bacteria and plants. The monofunctional enzyme systems is termed as Type II FAS (Figure 1-2-2).

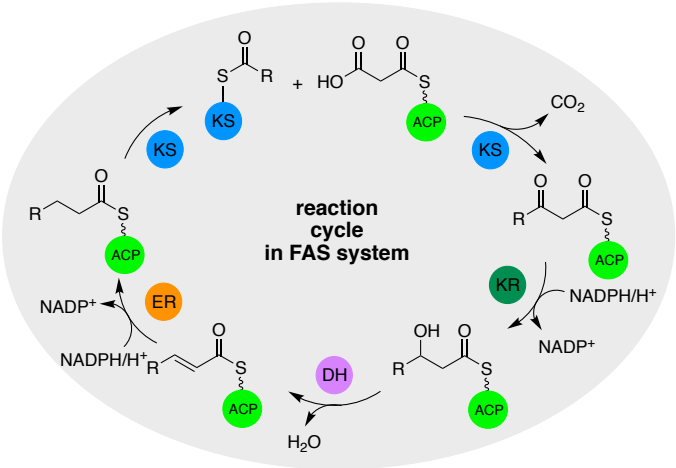

Figure 1-2-1. Schematic illustration of the common fatty acid biosynthetic cycle.

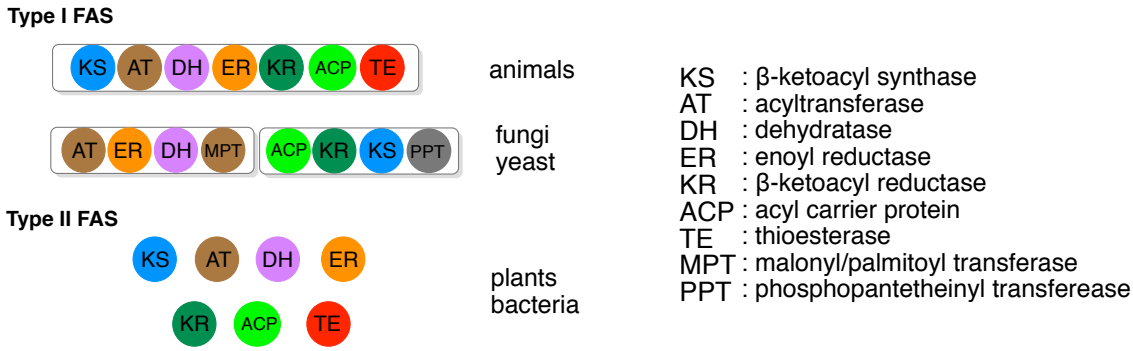

Figure 1-2-2. Domain organization of type I FAS and type II FAS enzymes.

Type I and II fatty acid biosynthetic systems employs common reaction cycle as mentioned above. But there are some differences in initiation and termination steps (Figure 1-2-3). In bacterial Type II FAS, KS III called FabH was responsible for the initial condensation of acetyl-CoA and malonyl-ACP to form 3-oxobutyryl-ACP while condensation of acetyl-ACP generated by the AT or MAT domain was normally catalyzed in Type I FAS[16-18]. As for the termination steps, type I FAS in animals employed thioesterase (TE) domain for off-loading reaction[17]. The TE domain catalyzed a hydrolysis of the thioester-bond of acyl-ACP to form free fatty acids. In fungi FAS, malonyl/palmitoyl-CoA/ACP transferase (MPT) domain was responsible for the direct transfer of palmitoyl unit to CoA[18]. Similarly, acyl units were directly transferred from acyl-ACPs to glycerol-3-phophate derivatives by acyltransferase genes *pls* in *Escherichia coli* Type II FAS[19].

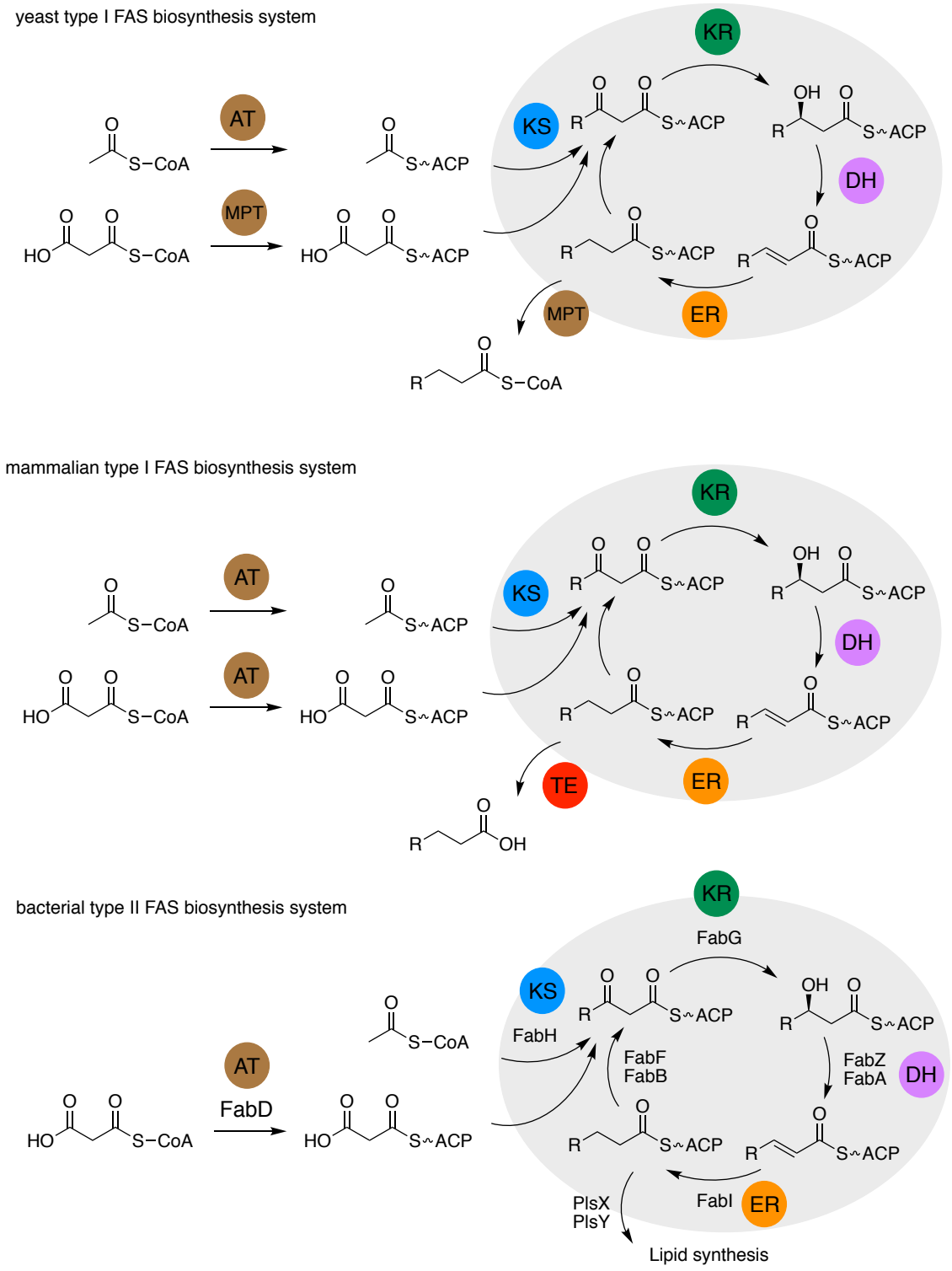

Figure 1-2-3. Schematic illustration of the type I and II fatty acid biosynthesis cycles. Type I FAS in yeast (top), type I FAS in mammalian (middle), and type II FAS in bacteria (bottom). In type II FAS system, three KS enzymes, FabH, FabF, and FabB, and two DH enzymes, FabZ and FabA, are used.

1.3. Biosynthetic pathway of polyunsaturated fatty acids in microorganisms

In PUFAs biosynthesis in fungi, plants, and bacteria, two different pathways are known. One is the well-studied desaturase/elongase pathway found in fungi, plants, and bacteria[20,21]. In the pathway, PUFAs are biosynthesized from saturated fatty acids supplied from the fatty acid biosynthetic pathway through chain elongation and oxygen-dependent desaturation reactions (Figure 1-3-1). Each desaturase introduces site-specific *cis* double bond to saturated fatty acyl chains using molecular oxygen, ferrocytochrome b5, and NADH[18]. The elongase enzymes, β-ketoacyl-CoA/ACP synthases, β-ketoacyl-CoA/ACP reductases, β-hydroxyacyl-CoA/ACP dehydratases, and enoyl-CoA/ACP reductase, catalyzes the same reaction cycles as fatty acid biosynthesis. ω3 and ω6 PUFAs are essential fatty acids for human and animals because they have no genes responsible for Δ12 and Δ15 desaturation reactions. As mentioned previous section, filamentous fungi (ARA producer) and engineered yeast (EPA producer) utilize this pathway for the PUFA biosynthesis[10,11]. Because the reaction in this pathway step-wisely occur, it is easy to perform pathway engineering for desired PUFA production. However, accumulation of intermediates is problem for industrial productions.

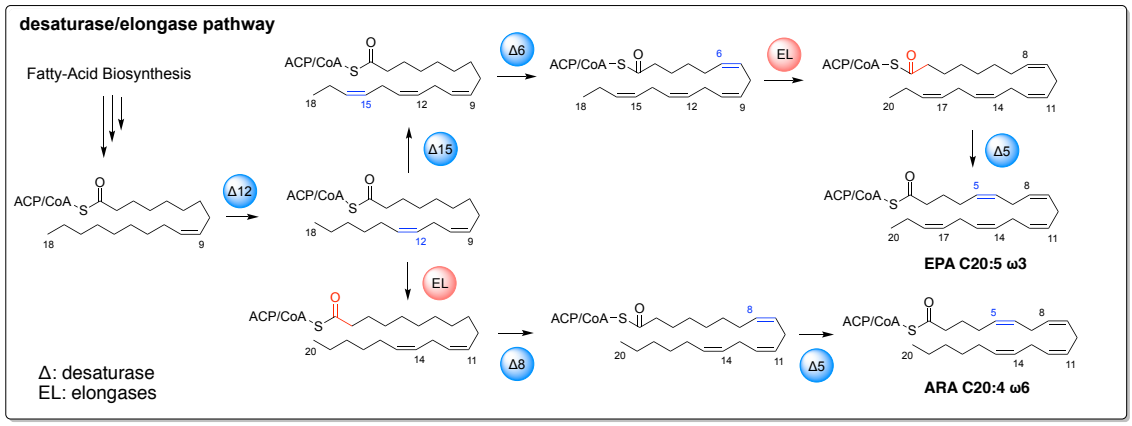

Figure 1-3-1. Schematic illustration of desaturase/elongase pathway

The other pathway is the PUFA synthase pathway, found in microalgae and marine bacteria in 2001[22]. The PUFA synthase is a multi-protein complex composed of three or four polypeptides with catalytic domains like Type I FAS (Figure 1-3-2). PUFAs was believed to be *de novo* biosynthesized from acetyl units using malonyl-ACP as extender units in a similar manner to FAS reaction cycles[22]. However, in this system, β,γ-isomerization and α,β-isomerization of 2-*trans* acyl-ACP are necessary to introduce *cis* double bonds depending on the carbon chain length of acyl-ACPs during reaction cycles (Figure 1-3-3). As mentioned previous section, microalgae *Schizochytrium* sp. (DHA producer) utilize this pathway[12]. From point of view for industrial production of PUFA, this pathway takes more advantage because it requires fewer reducing equivalents such as NADPH and produces smaller amounts of by-products with undesirable chain lengths and unsaturated positions. However, it is difficult to perform molecular engineering on this pathway. Because detailed biosynthetic machinery is still unknown though domain organizations of PUFA synthases suggests putative biosynthetic process.

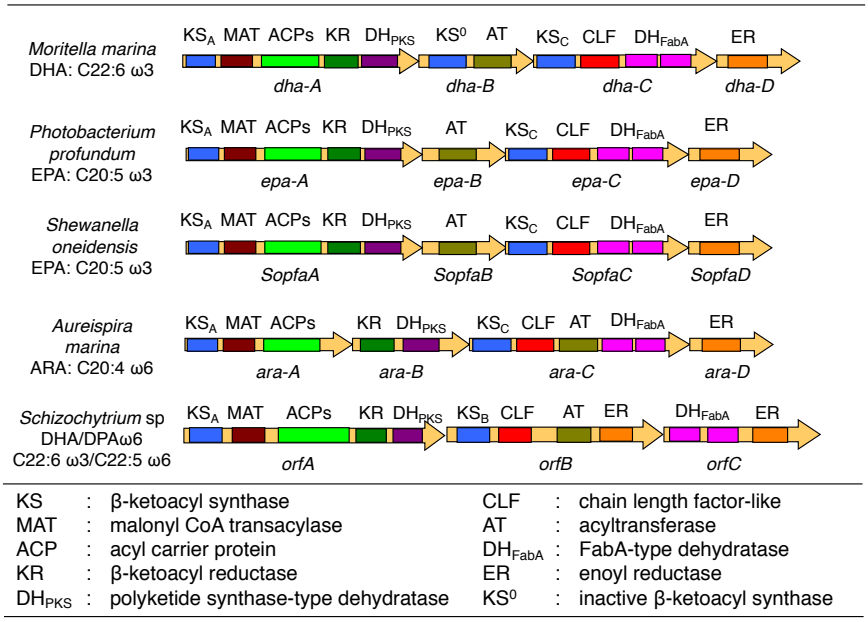

Figure 1-3-2. PUFA synthase genes identified in marine microorganisms.

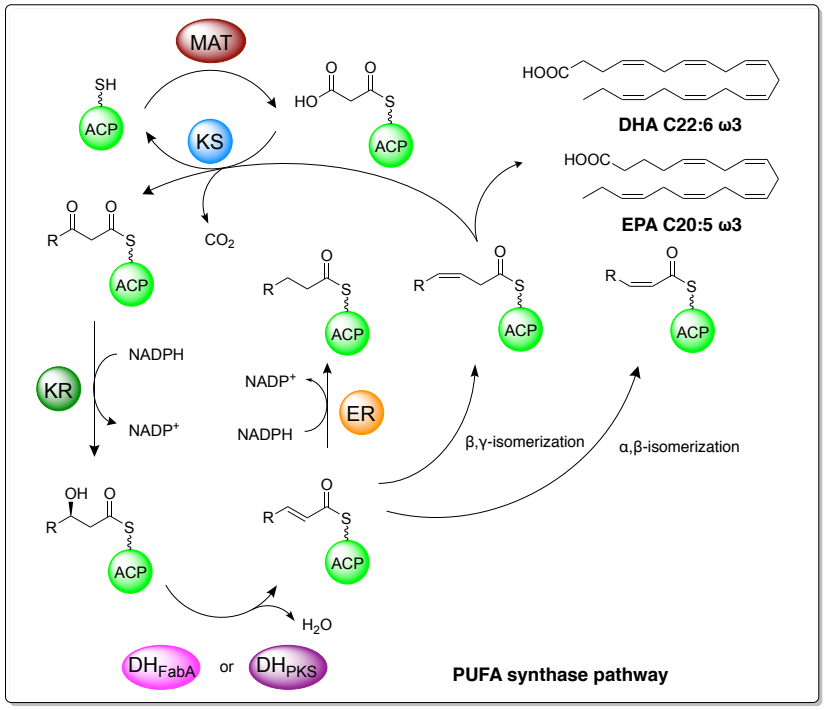

Figure 1-3-3. Schematic illustration of proposed biosynthetic cycles in PUFA synthases.

The PUFA synthase genes responsible for EPA, DHA, and ARA productions were identified not only in marine microorganisms such as *Shewanella oneidensis*, *Photobacterium profundum*, *Moritella marina*, *Aureispira marina*, and *Schizochytrium* sp., but also in terrestrial myxobacteria[22-27] (Figure 1-3-2). Bioinformatic analysis of these genes showed that domain organizations were very similar to each other among all PUFA synthases though the enzymes produced different products (carbon chain length, C_{20} or C_{22}, and *cis* double bond positions, ω3 or ω6). These facts suggested that subtle functional difference of catalytic domains generate a structural diversity of final products. However, the mechanism for control of products is still unknown. Furthermore, PUFA synthases have unique features different from FAS enzymes. They have multiple tandem ACP domains ranging from 4 to 9 while FASs typically have one ACP domain. In addition, while FASs used the TE and MPT domain for chain release from ACP to produce free fatty acids (animal FAS) and fatty acyl-CoA (yeast FAS), respectively, PUFA synthases have no TE domain and hence the off-loading mechanism is unknown. These unveiled biosynthetic machineries are important and essential for molecular

engineering on PUFA synthases for industrial production of PUFAs.

In this study, I dissected the biosynthetic machinery in PUFA synthases. In chapter 2, I examined a mechanism for control of PUFA productivity and showed that unique tandem ACP domains were responsible for control of PUFA productivity. In chapter 3, I examined a mechanism for control of the first *cis* double bond formation on ω3 or ω6 position using EPA and ARA synthase, and showed that PUFA synthases utilized the two-type DH domains depending on the carbon chain length of acyl-ACPs to form *cis* double bonds or saturated form. In chapter 4, I also examined a mechanism for control of carbon chain length, C_{20} or C_{22}, using EPA and DHA synthase, and suggested that substrate recognitions of the KS domains are important for control of products. In chapter 5, I examined the off-loading mechanism in PUFA biosynthetic system and showed that the AT domain was responsible for a hydrolytic reaction of final products.

References

1. J. Kawamoto, T. Kurihara, K. Yamamoto, M. Nagayasu, Y. Tani, H. Mihara, M. Hosokawa, T. Baba, S. B. Sato, N. Esaki. Eicosapentaenoic acid plays a beneficial role in membrane organization and cell division of a cold-adapted bacterium, *Shewanella livingstonensis* Ac10. *J. Bacteriol*., **191**, 632–640. (2009)
2. S. Sato, T. Kurihara, J. Kawamoto, M. Hosokawa, S. B. Sato, N. Esaki.Cold adaptation of eicosapentaenoic acid-less mutant of *Shewanella livingstonensis* Ac10 involving uptake and remodelling of synthetic phospholipids containing various polyunsaturated fatty acids. *Extremophiles.* **12**, 753–761 (2008).
3. E. A. Dennis, P. C. Norris., Eicosanoid storm in infection and inflammation. *Nat. Rev. Immunol.,* **15**, 511–523 (2015).
4. C. D. Funk. Prostaglandins and leukotrienes: advances in eicosanoid biology., *Science*, **294**, 1871–1875 (2001).
5. La Guardia, M., Giammanco, S., Di Majo, D., Tabacchi, G., Tripoli, E. & Giammanco, M. Omega 3 fatty acids: biological activity and effects on human health. *Panminerva Med*. **47**, 245−257 (2005).
6. Swanson, D., Block, R. & Mousa, S. A. Omega-3 fatty acids EPA and DHA: health benefits throughout life. *Adv. Nutr.* **3**, 1−7 (2012).
7. Carlson, S. E., Werkman, S. H., Peeples, J. M., Cooke, R. J. & Tolley, E. A. Arachidonic acid status correlates with first year growth in preterm infants. *Proc. Natl. Acad. Sci. USA* **90**, 1073−1077 (1993).
8. Ander, B. P., Dupasquier, C. M., Prociuk, M. A. & Pierce G. N. Polyunsaturated fatty acids and their effects on cardiovascular disease. *Exp. Clin. Cardiol.* **8**, 164–172 (2003).
9. T. Yamamoto, H. Matsui, K. Yamaji, T. Takahashi, A. Øverby, M. Nakamura, A. Matsumto, K. Nonaka, T. Sunazuka, S. Omura, H. Nakano., Narrow-spectrum inhibitors targeting an alternative menaquinone biosynthetic pathway of *Helicobacter pylori*., *J. Infect. Chemother.*, **22**, 587–592 (2016).
10. Z. Xue, P. L. Sharpe, S. Hong, N. S. Yadav, D. Xie, D. R. Short, H. G. Damude, R. A. Rupert, J. E. Seip, J. Wang, D. W. Pollak, M. W. Bostick, M. D. Bosak, D. J. Macool, D. H. Hollerbach, H. Zhang, D. M. Arcilla, S. A. Bledsoe, K. Croker, E. F. McCord, B. D. Tyreus, E. N. Jackson, Q. Zhu, Production of omega-3 eicosapentaenoic acid by metabolic engineering of *Yarrowia lipolytica*. *Nat. Biotechnol.* **31**, 734–740 (2013).
11. E. Sakuradani, A. Ando, S. Shimizu, J. Ogawa, Metabolic engineering for the production of polyunsaturated fatty acids by oleaginous fungus *Mortierella alpina* 1S-4. *J. Biosci. Bioeng.* **116**, 417–422 (2013).

12. R. J. Winwood, Recent developments in the commercial production of DHA and EPA rich oils from micro-algae. *OCL* **20**, D604 (2013).
13. E. Schweizer, J. Hofmann., Microbial type I fatty acid synthases (FAS): major players in a network of cellular FAS systems., *Microbiol. Mol. Biol. Rev.,* **68**, 501–517 (2004).
14. D. I. Chan, and A. J. Vogel., Current understanding of fatty acid biosynthesis and acyl carrier protein., *Biochem. J.*, **430**, 1–19 (2010).
15. K. Finzel, D. J. Lee, M. D. Burkart., Using modern tools to probe the structure-function relationship of fatty acid synthases., *ChemBioChem*. **16**, 528–547 (2015).
16. R. J. Heath, C. O. Rock., Inhibition of β-ketoacyl-acyl carrier protein synthase III (FabH) by acyl-acyl carrier protein in *Escherichia coli. J. Biol. Chem.,* **271**, 10996–11000 (1996).
17. S. Smith, A. Witkowski, A. K. Joshi., Structural and functional organization of the animal fatty acid synthase. *Progress in Lipid Research.* **42**, 289–317 (2003).
18. F. Lynen., On the structure of fatty acid synthetase of yeast., *Eur. J. Biochem.*, **112**, 431–442 (1980).
19. J. H. Janßen, A. Steinbüchel., Fatty acid synthesis in *Escherichia coli* and its applications towards the production of fatty acid based biofuels. *Biotechnol Biofuels* **7,** 7 doi:10.1186/1754-6834-7-7 (2014).
20. H. Kikukawa, E. Sakuradani, A. Ando, S. Shimizu, J. Ogawa, Arachidonic acid production by the oleaginous fungus Mortierella alpina 1S-4: A review. *Journal of Advanced Research* **11**, 15–22 (2018).
21. J. Shanklin, E. B. Cahoon, Desaturation and related modification of fatty acids. *Annu. Rev. Plant Physiol. Plant Mol. Biol.,* **49**, 611–641 (1998).
22. J. G. Metz, P. Roessler, D. Facciotti, C. Levering, F. Dittrich, M. Lassner, R. Valentine, K. Lardizabal, F. Domergue, A. Yamada, K. Yazawa, V. Knauf, J. Browse, Production of polyunsaturated fatty acids by polyketide synthases in both prokaryotes and eukaryotes. *Science* **293**, 290–293 (2001).
23. J. S. Lee, S. Y. Jeong, U. D. Kim, W. J. Seo, K. B. Hur, Eicosapentaenoic acid (EPA) biosynthetic gene cluster of *Shewanella oneidensis* MR-1: cloning, heterologous expression, and effects of temperature and glucose on the production of EPA in *Escherichia coli*. *Biotechnol. Bioprocess Eng.,* **11**, 510–515 (2006).
24. E. E. Allen, H. D. Bartlett, Structure and regulation of the omega-3 polyunsaturated fatty acid synthase genes from the deep-sea bacterium *Photobacterium profundum* strain SS9. *Microbiology* **148**, 1903–1913 (2002).
25. N. Morita, M. Tanaka, H. Okuyama, Biosynthesis of fatty acids in the docosahexaenoic acid-producing bacterium *Moritella marina* strain MP-1. *Biochem. Soc. Trans*. **28**, 943–945 (2000).

26. T. Ujihara, M. Nagano, H. Wada, S. Mitsuhashi, Identification of a novel type of polyunsaturated fatty acid synthase involved in arachidonic acid biosynthesis. *FEBS Lett.* **588**, 4032–4036 (2014).
27. K. Gemperlein, S. Rachid, O. R. Garcia, C. S. Wenzel, R. Müller, Polyunsaturated fatty acid biosynthesis in myxobacteria: different PUFA synthases and their product diversity. *Chem. Sci.* **5**, 1733–1741 (2014).

Chapter 2
Mechanism for control of PUFA productivity in PUFA synthase

2.1. Introduction

As mentioned in chapter 1, PUFA synthases employ unique multi-tandem ACP domains in its biosynthesis while FASs and most of PKSs typically have single ACP domain for each reaction cycle (Figure 2-1-1). The carrier protein is expressed as *apo*-form. *apo*-ACP is activated by phosphopantetheinyl transferase to form *holo*-ACP, in which 4'-phosphopantetheine arm is attached to the active residue Ser, to shuttle growing acyl chains to appropriate catalytic domains (Figure 2-1-2).

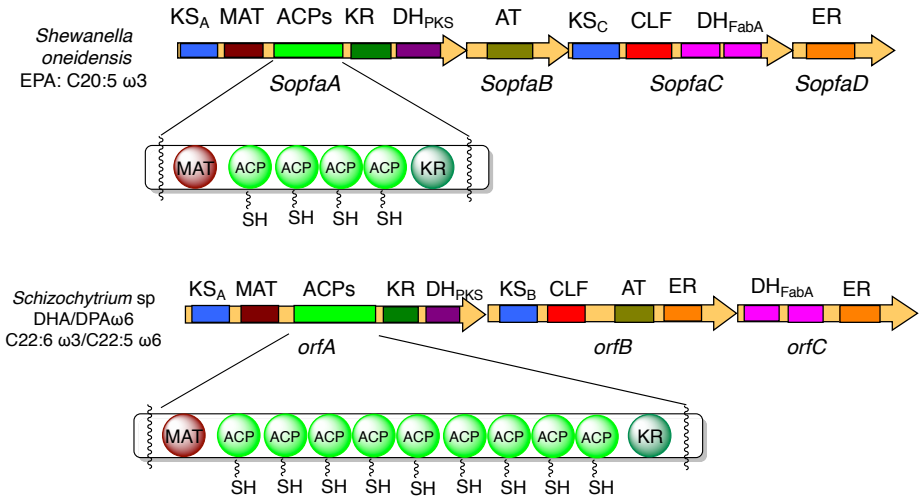

Figure 2-1-1. Multi-tandem ACP domains in PUFA synthases.

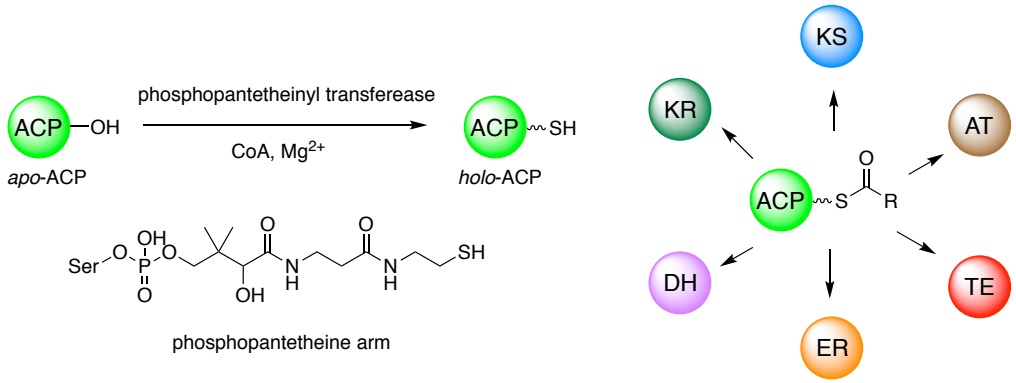

Figure 2-1-2. Activation of *apo*-ACP to form *holo*-ACP by phosphopantetheinyl transferase and shuttling of growing acyl chain to appropriate catalytic domains.

Modular and iterative type I PKSs with a few tandem-repeated ACP domains have also been identified and their biological roles have been studied (Figure 2-1-3). First example was fungal iterative type I PKS with two ACP domains responsible for naphthopyrone biosynthesis. Site-directed mutation of each ACP domain showed that one of the two ACPs was enough to synthesize naphthopyrone but the effect of inactivated ACPs on productivity was not reported[1]. Modular PKS responsible for mupirocin biosynthesis[2] and PKS-nonribosomal peptide synthase, a hybrid enzyme, for curacin biosynthesis[3] also employed two and three ACPs, respectively. Site-directed mutation and in-frame deletion of ACP domains led to a decrease of their productivities. In 2008, Ben Shen's research group showed that inactivation of the ACP domains by site-directed mutagenesis of the active site Ser impacted on the PUFA productivity. They showed that its productivity was decreased depending on the number of inactive ACP domains. Furthermore, they revealed that each of the ACP domains was functionally equivalent for its biosynthesis[4].

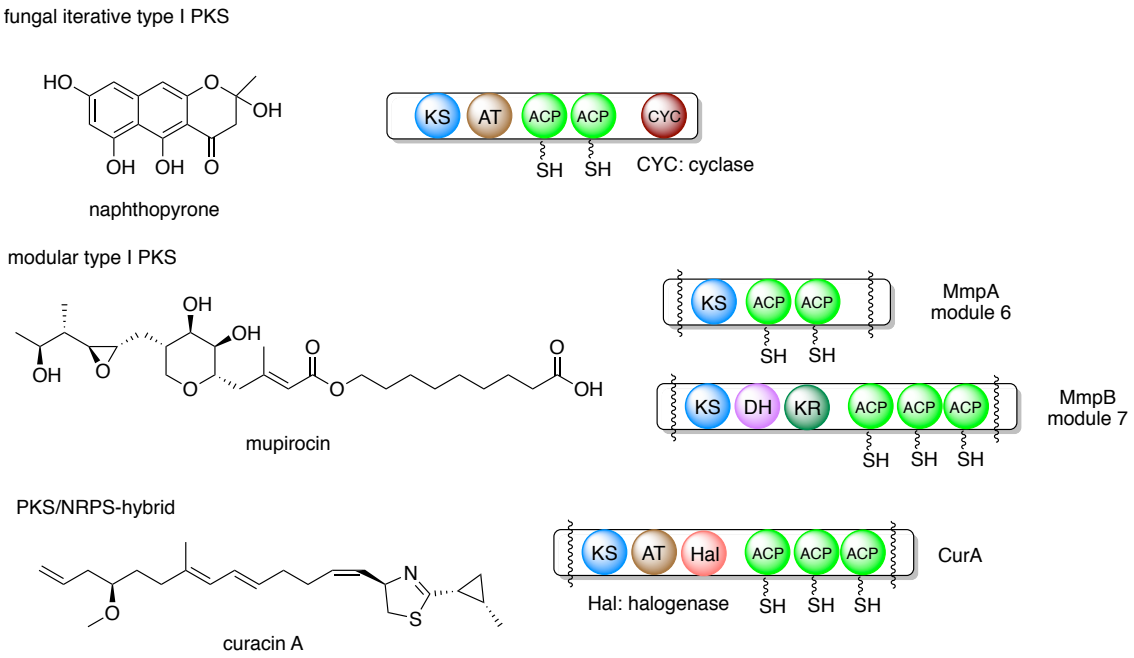

Figure 2-1-3. Examples of PKS enzymes with tandem ACP domains in secondary metabolites.

These results suggest that the number of the ACP domains in PUFA synthases/PKSs and polyketide productivity have a close relationship. Thus, enzyme engineering of ACP domain is an attractive approach for enhancement of its productivity in addition to metabolic engineering approach as described in discussion section. However, only disruption methods have been employed in the reported studies. In this chapter, I constructed bacterial and microalgae PUFA synthase derivatives with more active ACP domains than the native type and examined the effects on their productivities.

2.2. Results

2.2.1. Heterologous expression of PUFA synthase genes in *Escherichia coli*

I first constructed a heterologous expression system in *Escherichia coli* for evaluation of PUFA productivity because it is difficult to prepare recombinant whole PUFA synthase enzymes for *in vitro* assay. Metz *et al.* succeeded in DHA production in *E. coli* harbouring the *orfABC* genes from *Schizochytrium* sp. and phosphopantetheinyl transferase gene, *hetI*, from *Nostoc* sp.[5]. Furthermore, other groups also succeeded in PUFA productions in *E. coli* expressing bacterial PUFA synthase genes[6,7]. Therefore, I selected *E. coli* as heterologous hosts. For easy construction of engineered genes encoding more ACP domains than parental enzyme, PUFA synthase genes were cloned into different and compatible expression vectors, pET-21a, pCDF-1b, pCOLADuet-1, and pSTV or pACYCDuet-1. Microalgae PUFA synthase genes, *orfABC*, and *hetI* were cloned to construct pET-*orfA*, pCDF-*orfB*, pCOLA-*orfC*, and pSTV-*hetI*. Bacterial EPA synthase genes of *Shewanella oneidensis*, *SopfaABCDE*, were also cloned to construct pET-*SopfaA*, pCDF-*SopfaC*, pCOLA-*SopfaD,* pACYC-*SopfaE*-*SopfaB* (Figure 2-2-1-1). To prevent degradation of the synthesized PUFAs, the *fadE* gene encoding an acyl-CoA dehydrogenase, responsible for the β-oxidation pathway in *E. coli* BLR(DE3), was disrupted as described in Experimental section, and the strains was used as host for following experiments.

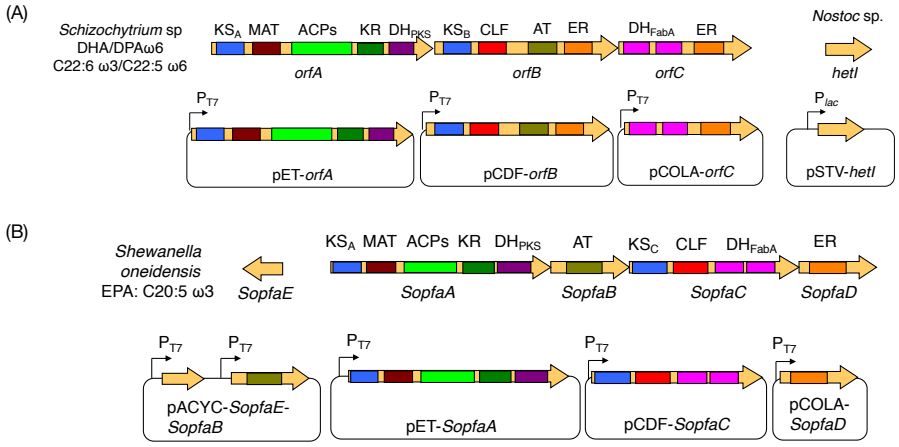

Figure 2-2-1-1. (A) The plasmids set for expression of PUFA synthase genes of *Schizochytrium* sp. (B) The plasmids set for expression of PUFA synthase genes of *S. oneidensis*.

Then, I examined whether the expression system constructed worked well under the experimental conditions. After *E. coli* BLR(DE3)Δ*fadE* harbouring the all plasmids was cultured in terrific broth medium, the products were extracted and analysed by GC/MS. As shown in Figure 2-2-1-2, the transformants expressing *orfABC* and *hetI* produced both DHA and DPAω6 and the yields of DHA and DPAω6 were 4.5 ± 0.08 and 0.71 ± 0.03 μg mL^{-1} OD^{-1}, respectively. I also confirmed that the transformants expressing *SopfaABCDE* produced EPA and DPAω3 in addition to stearidonic acids (SDA, C18:4 ω3) and eicosatetraenoic acids (ETA, C20:4 ω3, Figure 2-2-1-3). Because SDA and ETA are not produced by the original strain, *S. oneidensis*[8], their production were caused by the heterologous expression in *E. coli*. The yields of EPA, DPAω3, SDA, and ETA were 0.10 ± 0.002, 0.013 ± 0.003, 0.22 ± 0.02, and 0.044 ± 0.004 μg mL^{-1} OD^{-1}, respectively.

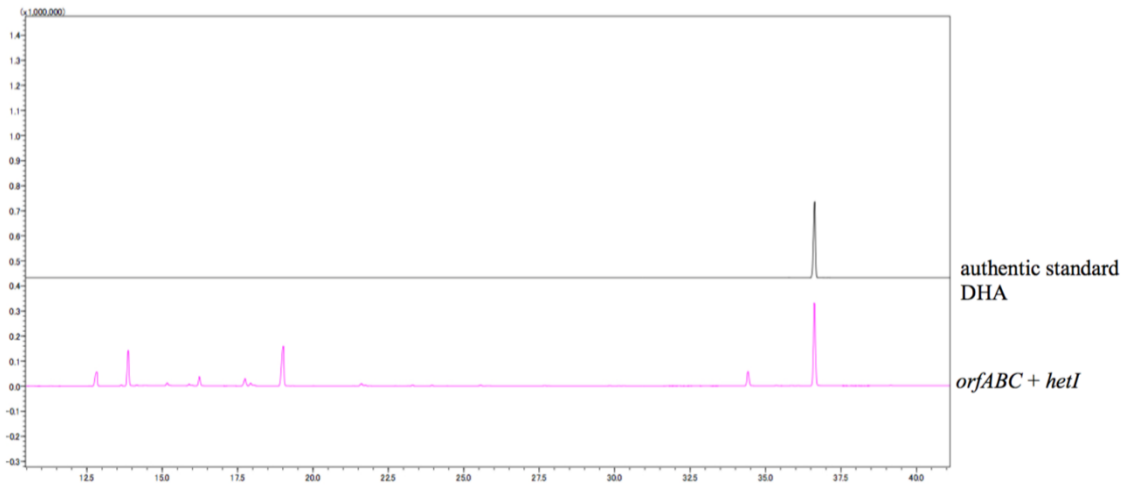

Fig. 2-2-1-2. GC-MS analysis (traced at *m/z* 79) of PUFA methyl esters produced in *E. coli* expressing *orfABC* and *hetI* genes. Upper trace: authentic standard of methyl ester of DHA, lower trace: *E. coli* expressing *orfABC* and *hetI* genes.

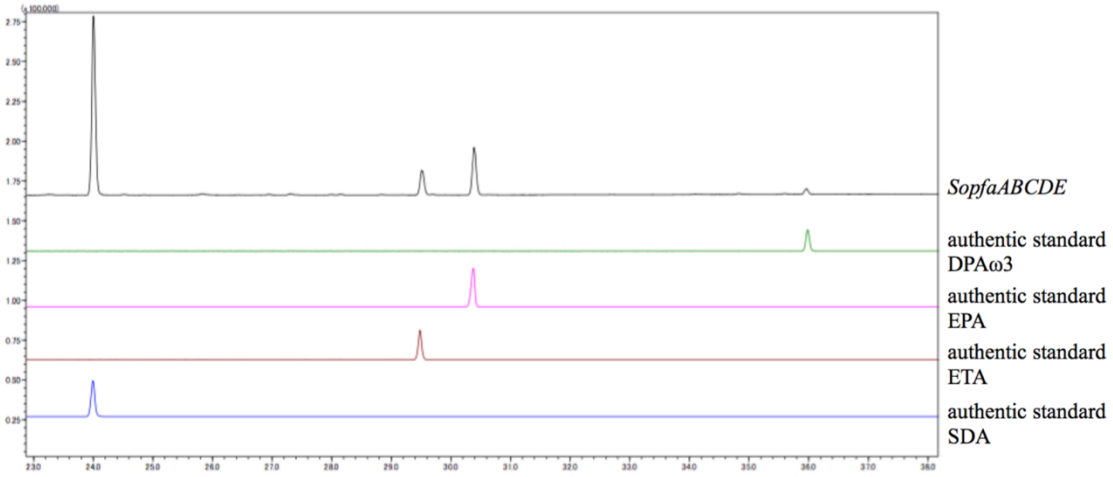

Fig. 2-2-1-3. GC-MS analysis (traced at *m/z* 79) of PUFA methyl esters produced in *E. coli* expressing *SopfaABCDE* genes. Top trace: *E. coli* expressing *SopfaABCDE* genes. Second, third, fourth, and bottom traces were authentic standards of methyl ester of DPAω3, EPA, ETA, and SDA, respectively.

2.2.2. The effect of the number of ACP domains on PUFA productivity

I then constructed pET-*orfA* derivative plasmids with different numbers of ACP domains. Each of the ACP domains is highly conserved and separated by conserved and repeated regions with Ala and Pro rich sequences (Figure 2-2-2-1). This architecture suggested that the regions between the Ala/Pro rich sequences are each one functional ACP unit in the multi-tandem ACP domain of PUFA synthase. Therefore, I increased the number of the unit in a stepwise manner by the method shown in Experimental section. In brief, I first constructed a plasmid with one unit of the ACP domain. Then, this unit was inserted into each plasmid by step-by-step addition to construct all the plasmids. Consequently, I constructed seven engineered *orfA* plasmids with 4×, 5×, 6×, 7×, 8×, 10× and 11×ACP domains (Fig. 2-2-2-2).

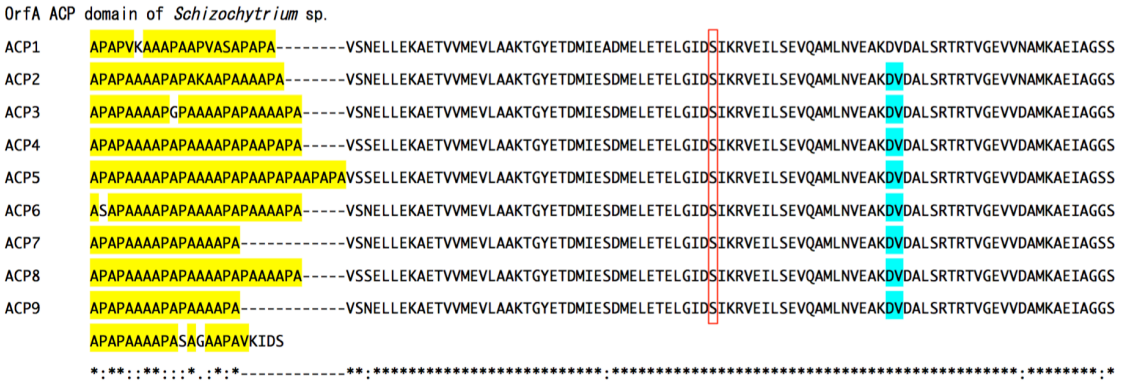

Figure 2-2-2-1. Sequence alignment of the tandem acyl carrier protein domains of *orfA*. The red box, yellow highlighting, and blue highlighting show the active sites of the ACP domains, Ala and Pro rich linkers, and *Zra*I sites, respectively.

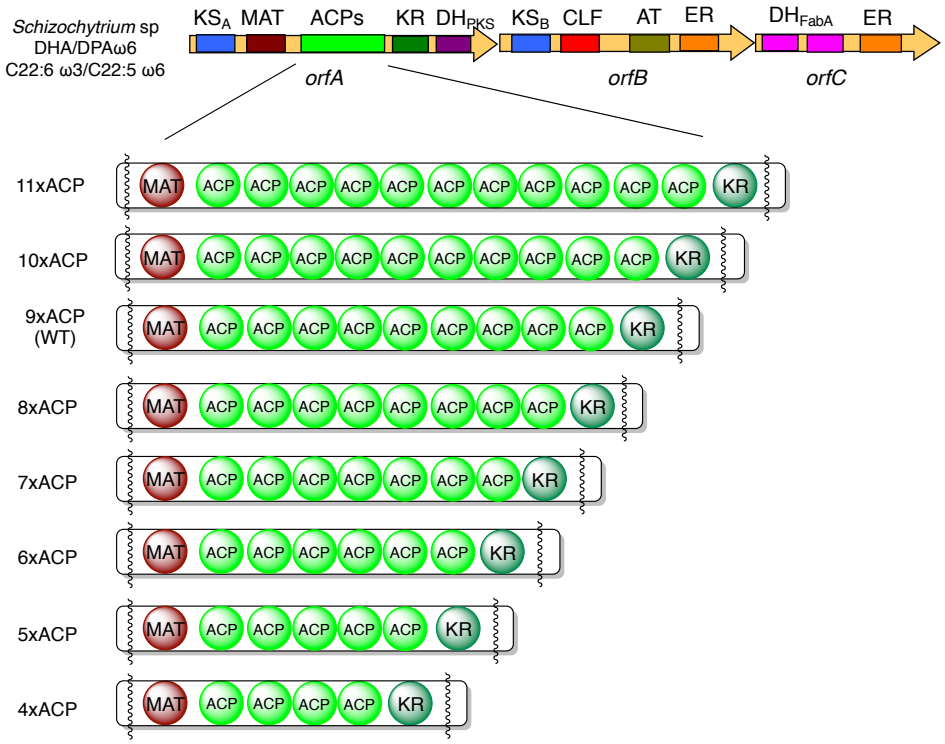

Figure 2-2-2-2. Schematic illustration of engineered *orfA*s with 4× to 11×ACP domains.

Using these plasmids, the PUFA productivity and profile were analysed as described above. As shown in Figure 2-2-2-3, DHA and DPAω6 productivity decreased and increased depending on the number of ACP domains, while the profiles of the PUFA products were the same as those of the native type (9×ACP domains). Notably, the PUFA yields of pET-*orfA* with more ACP domains (10× and 11×)

were higher than those of the native plasmid, pET-*orfA* (1.5-fold DHA and DPAω6 for 10×ACPs, 2.0-fold DPAω6 and 1.8-fold DHA for 11×ACP). These results indicated that the number of ACP domains in OrfA just controls productivity, and that the tandem ACP domain was important for controlling PUFA productivity.

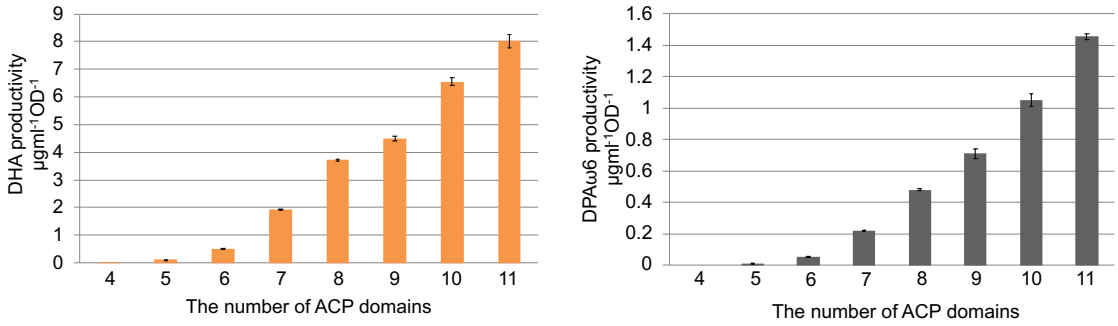

Figure 2-2-2-3. DHA (left) and DPAω6 (right) productivities by the engineered *orfAs, orfBC*, and *hetI* in *E. coli*.

I next carried out the same experiment with the EPA synthase genes, *SopfaABCDE*, of *S. oneidensis*. I constructed five plasmids carrying *SopfaA* genes (Figure 2-2-2-4) with increased numbers of ACP domains (5×, 6×, 7×, 8×, and 9×) by essentially the same method used to construct the pET-*orfA* derivatives as described in Experimental section. The productivities and profiles of the PUFAs produced by *E. coli* BLR(DE3)Δ*fadE* carrying the *SopfaA* derivative genes together with the *SopfaBCDE* were analysed as described above. As shown in Figure 2-2-2-5, EPA productivity linearly increased with increased numbers of ACP domains (5×ACPs, 3.7-fold; 6×ACPs, 5.1-fold; 7×ACPs, 10-fold; 8×ACPs, 16-fold; 9×ACPs, 16-fold). SDA, ETA, and DPAω3 productivities also increased in the same manner. As for the profiles of the PUFA products, no differences between the *SopfaA* derivatives and the native gene were observed. These results again indicated that the number of ACP domains just controls the productivity.

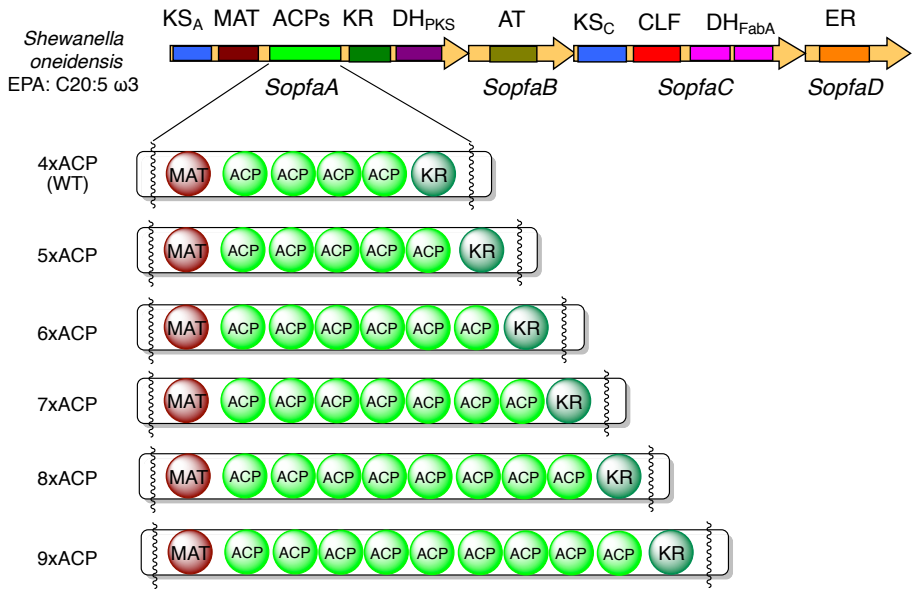

Figure 2-2-2-4. Schematic illustration of the engineered *SopfaA*s with 4× to 9×ACP domains.

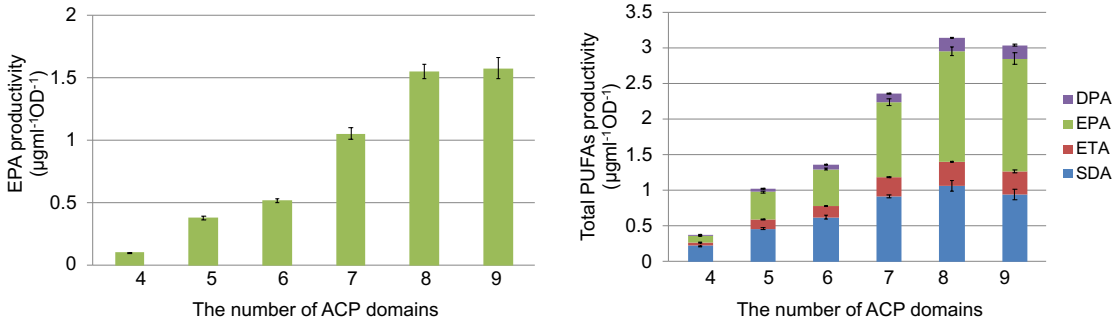

Figure 2-2-2-5. EPA and total PUFAs productivities by the engineered *SopfaAs* and *SopfaBCDE* in *E. coli*.

2.2.3. The Effect of inactivation of ACP domain on PUFA productivity

As demonstrated by the PUFA synthases of both *Schizochytrium* sp. and *S. oneidensis*, which are a eukaryotic and a prokaryotic microorganism, respectively, an increased number of ACP domains up to 9 or 11 linearly enhanced PUFA productivity, suggesting that more ACP domains plausibly supply more substrates to synthesize PUFAs. Therefore, I next investigated the effect of inserting an inactive ACP domain, in which the active Ser residue was mutated to Ala by site-directed mutagenesis,

on PUFA productivity. I constructed five genes, *SopfaA5-1M*, *SopfaA5-2M*, *SopfaA5-3M*, *SopfaA5-4M*, *SopfaA5-5M*, which had the same gene structure as *SopfaA* with 5×ACP domains except that each ACP domain was inactivated. (Figure 2-2-3-1).

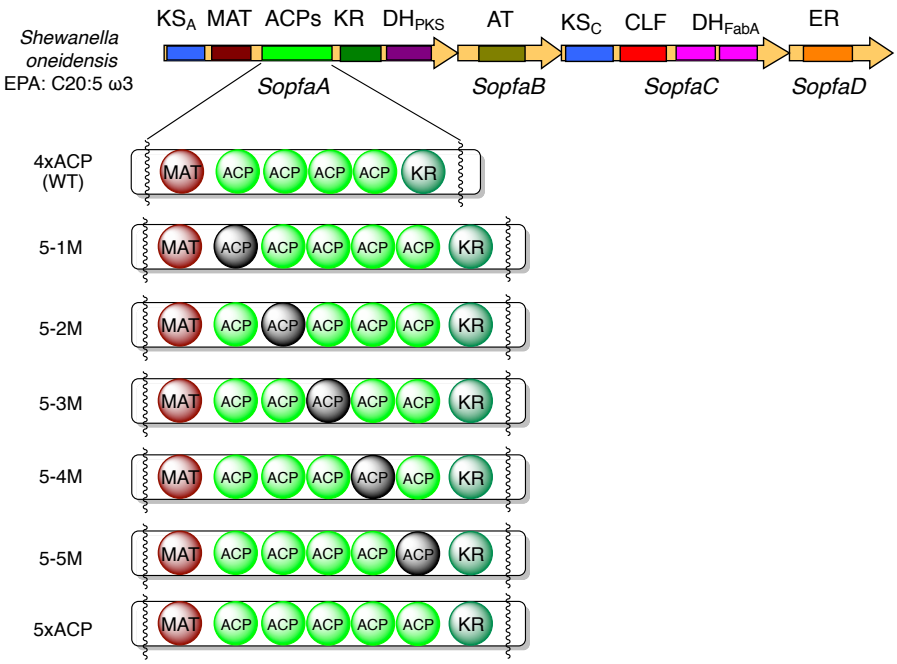

Figure 2-2-3-1. Schematic illustration of the mutated *SopfaA*s. Black ACP showed the inactive ACP domain.

As shown in Figure 2-2-3-2, the transformants harbouring mutated genes produced approximately 18−39 % EPA and 20−38 % total PUFAs compared with those harbouring *SopfaA5*, but unexpectedly produced 230−300 % EPA and 170−220 % total PUFAs compare with those harbouring native *SopfaA* with 4×ACP domains. These results suggested that PUFA productivity was enhanced not only by increasing the number of active ACP domains but also by the insertion of an inactivated ACP domain though the effects were smaller than those of active ACP domains, and that the location of the inactivated ACP in the tandem ACP domain region is not critical.

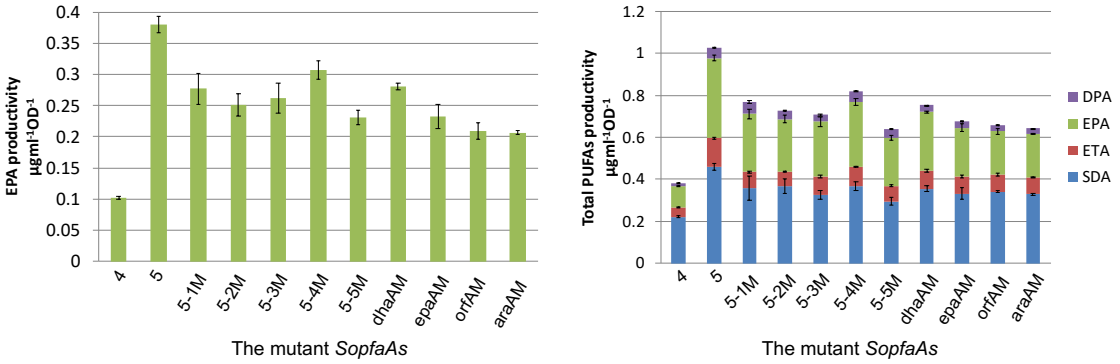

Figure 2-2-3-2. PUFA productivities by the mutated *SopfaAs* and *SopfaBCDE* in *E. coli*.

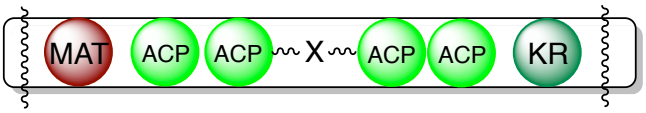

X = Inactive ACP domain from DHA synthase of *M. marina* (identity: 71%)
Inactive ACP domain from DHA synthase of *Schizochytrium sp* (identity: 49%)
Inactive ACP domain from EPA synthase of *P. profumdum* (identity: 70%)
Inactive ACP domain from ARA synthase of *A. marina* (identity: 48%)
No relation amino acid sequence to ACP domain

Figure 2-2-3-3. Schematic illustration of the additional mutated *SopfaAs*.

I next constructed additional *SopfaA5* derivatives. The inactivated ACP domain located at the third position of *SopfaA5-3M* was replaced with another inactive ACP domain of PUFA synthase from *Moritella marina* (a DHA producer), *Photobacterium profundum* (an EPA producer), *Schizochytrium* sp., or *Aureispira marina* (an ARA producer). Their ACP domains show 70%, 71%, 49% and 48% identities to that of SoPfaA, respectively (Figure 2-2-3-3). Each of the constructed plasmids, *dhaAM*, *epaAM*, *orfAM*, and *araAM*, was introduced into *E. coli* BLR(DE3)Δ*fadE* together with the *SopfaBCDE* genes and PUFA productivity was examined. All the enzymes produced similar amounts of PUFAs but the productivities varied slightly depending on the similarity between the native and replaced ACP domains (Figure 2-2-3-2). In contrast, PUFA productivity was lost when third inactive ACP domain was replaced in-frame with sequence S1 or S2 that was a part sequences of ABC transporter HlyB of *S. oneidensis* identified in genome database and had approximately the same length as the native ACP (data not shown). These results suggested that the structure of the tandem

ACP domains is also a key factor controlling PUFA productivity in addition to the number of active ACP domains.

2.3. Discussion

As mentioned in chapter 1, the demand for PUFAs such as DHA and EPA in food and pharmaceutical industries are increasing because of their biological activities. Fermentative processes have been developed as alternative and sustainable sources of PUFAs[9-11]. As for improvement of its productivity, many approaches were reported, such as improvement of reducing equivalent (NADPH) flux, inhibition of the acyl-exchange reaction between phosphatidylcholine and acyl-CoA substrates, and prevention of PUFA degradation by β-oxidation[9,12]. Furthermore, co-expression of catalase[13], addition of cerulenin[14,15], an inhibiter of *de novo* fatty acid synthesis, and metabolic engineering to increase the substrate supply[16] have been employed. However, all these attempts have focussed only on the metabolic flow and no examples of enzyme activation have been reported. In this study, I succeeded in improving PUFA productivity for the first time by the enzymatic engineering. The productivities were linearly increased depending on the number of ACP domains using both the eukaryotic PUFA synthase of *Schizochytrium* sp. and the prokaryotic PUFA synthase of *S. oneidensis* without PUFA product profile change. I believe that this enzymatic approach was useful for enhancement of product productivity to not only PUFA synthase but also FAS and PKSs. Recently, 1.6-fold higher production of total fatty acids in type II FAS were reported by expression of artificial tandem ACP containing three ACPs unit linked with Ala/Pro rich linker sequence[17] (Figure 2-3-1). Furthermore, Wang *et al*. succeeded in 2.5-fold enhancement of polyketide productivity by increasing ACP domains in 6-deoxyerythronolide B synthase[18] (Figure 2-3-1). However, the product profiles of the engineered enzymes were changed from those of native enzyme. The parental enzyme synthesized triketide lactone and triketide ketolactone in a ratio of 1:1.8 whereas the engineered enzyme synthesized only triketide ketolactone. The enzyme unexpectedly skipped β-ketoreduction reaction, suggesting, the quaternary structure of tandem ACP domain was also important for product productivity in addition to the number of ACP domains.

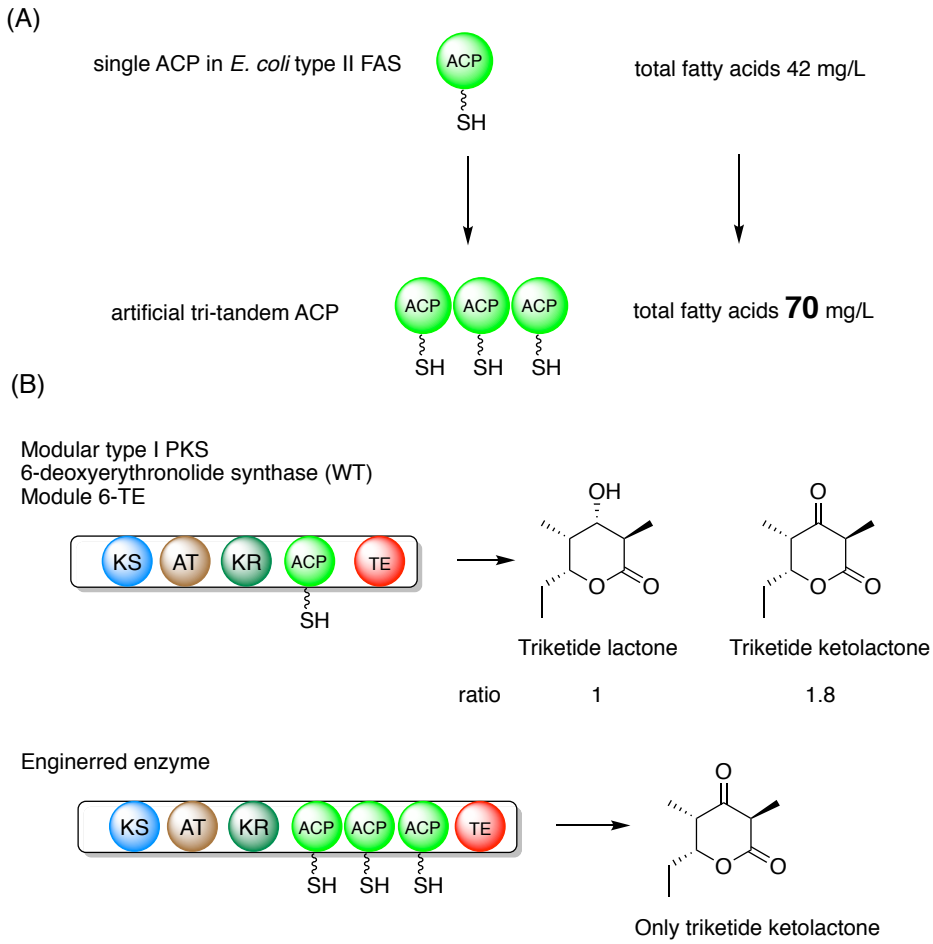

Figure 2-3-1. Enzyme engineering of type II FAS and modular type I PKS 6-deoxyerythronolide synthase with artificial three tandem ACP domains.

The solution structure of the five tandem ACP domains of PUFA synthase was previously investigated using several analytical methods. Small-angle X-ray scattering analysis suggested that the multi-ACP fragment was an elongated monomer with a beads-on-a-string like structure[19] (Figure 2-3-2). This multi-tandem ACP domain structure enabled simultaneous access of other catalytic domains and enhancement of productivity without PUFA profile change. The results, which the mutated enzymes (SoPfaA5-1M to SoPfaA5-5M, dhaAM, epaAM, orfAM, and araAM) still produced more PUFAs, would support the beads-on-a-string structure. The structure of the tandem ACP

domains was a key factor controlling PUFA productivity besides the number of active ACP domains. However, the reasons why the mutated enzymes showed still higher PUFA production than parental enzyme (4×ACP) and why the PUFA synthase complex could allow wide range of tandem ACP domains (4 to 11 ACP domains) to access catalytic domains are still unclear. High-resolution structural information of tandem ACP domains and PUFA synthase complex are needed to answer these questions.

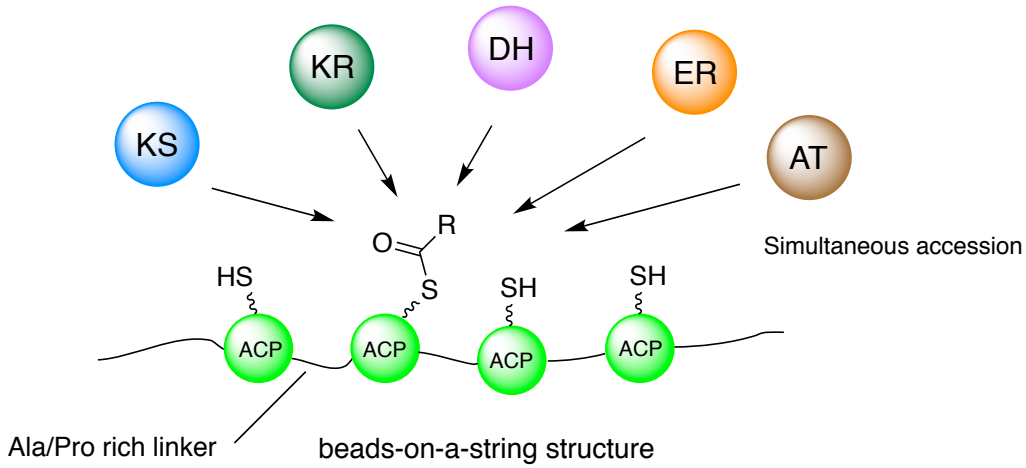

Figure 2-3-2. Beads-on-a-string structure of tandem ACP domains. Each catalytic domain is simultaneously able to access to tandem ACP domains in PUFA synthase complex.

References

1. I, Fujii, A. Watanabe, U. Sankawa, Y. Ebizuka, Identification of Claisen cyclase domain in fungal polyketide synthase WA, a naphthopyrone synthase of *Aspergillus nidulans*. *Chem. Biol.* **8**, 189–197 (2001).
2. S. A. Rahman, J. Hothersall, J. Crosby, J. T. Simpson, M. C. Thomas, Tandemly duplicated acyl carrier proteins, which increase polyketide antibiotics production, can apparently function either in parallel or in series. *J. Biol. Chem*. **280**, 6399–6408 (2005).
3. L. Gu, E. B. Eisman, S. Dutta, T. M. Franzmann, S. Walter, W. H. Gerwick, G. Skiniotis, D. H. Sherman, Tandem acyl carrier proteins in the curacin biosynthesis pathway promote consecutive multienzyme reactions with a synergistic effect. *Angew. Chem. Int. Ed.* **50,** 2795–2798 (2011).
4. H. Jiang, R. Zirkle, J. G. Metz, L. Braun, L. Richter, S. G. Van Lanen, B. Shen, The role of tandem acyl carrier protein domains in polyunsaturated fatty acid biosynthesis. *J. Am. Chem. Soc.* **130,** 6336–6337 (2008).
5. A. Hauvermale, J. Kuner, B. Rosenzweig, D. Guerra, S. Diltz, J. G. Metz, Fatty acid production in *Schizochytrium* sp.: involvement of a polyunsaturated fatty acid synthase and a type I fatty acid synthase. *Lipids* **41**, 739–747 (2006).
6. Y. Orikasa, T. Nishida, A. Yamada, R. Yu, K. Watanabe, A. Hase, N. Morita, H. Okuyama, Recombinant production of docosahexaenoic acid in a polyketide biosynthesis mode in *Escherichia coli*. *Biotechnol. Lett.* **28**, 1841–1847 (2006).
7. J. S. Lee, S. Y. Jeong, U. D. Kim, W. J. Seo, K. B. Hur, Eicosapentaenoic acid (EPA) biosynthetic gene cluster of *Shewanella oneidensis* MR-1: cloning, heterologous expression, and effects of temperature and glucose on the production of EPA in *Escherichia coli*. *Biotechnol. Bioprocess Eng.,* **11**, 510–515 (2006).
8. R. Abboud, R. Popa, V. Souza-Egipsy, C. S. Giometti, S. Tollaksen, J. J. Mosher, R. H. Findlay, K. H. Nealson, Low-temperature growth of *Shewanella oneidensis* MR-1. *Appl. Eonviron. Microbiol*., **71**, 811–816 (2005).
9. Z. Xue, P. L. Sharpe, S. Hong, N. S. Yadav, D. Xie, D. R. Short, H. G. Damude, R. A. Rupert, J. E. Seip, J. Wang, D. W. Pollak, M. W. Bostick, M. D. Bosak, D. J. Macool, D. H. Hollerbach, H. Zhang, D. M. Arcilla, S. A. Bledsoe, K. Croker, E. F. McCord, B. D. Tyreus, E. N. Jackson, Q. Zhu, Production of omega-3 eicosapentaenoic acid by metabolic engineering of *Yarrowia lipolytica*. *Nat. Biotechnol.* **31**, 734–740 (2013).
10. E. Sakuradani, A. Ando, S. Shimizu, J. Ogawa, Metabolic engineering for the production of polyunsaturated fatty acids by oleaginous fungus *Mortierella alpina* 1S-4. *J. Biosci. Bioeng.* **116**, 417–422 (2013).

11. R. J. Winwood, Recent developments in the commercial production of DHA and EPA rich oils from micro-algae. *OCL* **20**, D604 (2013).
12. Y. Gong, X. Wan, M. Jiang, C. Hu, H. Hu, F. Huang, Metabolic engineering of microorganisms to produce omega-3 very long chian polyunsaturated fatty acids. *Prog. Lipid Res.* **56**, 19–35 (2014).
13. Y. Orikasa, Y. Ito, T. Nishida, K. Watanabe, N. Morita, T. Ohwada, I. Yumoto, H. Okuyama, Enhanced heterologous production of eicosapentaenoic acid in *Escherichia coli* cells that co-express eicosapentaenoic acid biosynthesis *pfa* genes and foreign DNA fragments including a high-performance catalase gene, *vktA. Biotechnol. Lett.* **29**, 803–809 (2007).
14. N. Morita, T. Nishida, M. Tanaka, Y. Yano, H. Okuyama, Enhancement of polyunsaturated fatty acid production by cerulenin treatment in polyunsaturated fatty acid-producing bacteria. *Biotechnol. Lett.* **27**, 389–393 (2005).
15. J. Fang, C. Kato, T. Sato, O. Chan, D. McKay, Biosynthesis and dietary uptake of polyunsaturated fatty acids by piezophilic bacteria. *Comp. Biochem. Physiol. B* **137**, 455–461 (2004).
16. K. Gemperlein, G. Zipf, H. S. Bernauer, R. Müller, S. C. Wenzel, Metabolic engineering of *Pseudomonas putida* for production of docosahexaenoic acid based on a myxobacterial PUFA synthase. *Metab. Eng.* **33**, 98–108 (2016)
17. C. Rullan-Lind, M. Ortiz-Rosario, A. Garcia-Gonzalez, V. Stojanoff, N. E. Chorna, R. B. Pietri, A. Baerga-Ortiz. Artificial covalent linkage of bacterial acyl carrier proteins for fatty acid production. *Sci. Rep.*, **9**: 16011 (2019).
18. Z. Wang, S. R. Bagde, G. Zavala, T. Matsui, X. Chen, C. Y. Kim, De novo design and implementation of a tandem acyl carrier protein domain in a type I modular polyketide synthase. *ACS Chem. Biol*., **13**, 3072–3077 (2018).
19. U. Trujillo, E. Vazque-Rosa, D. Oyola-Robles, L. J. Stagg, D. A. Vassallo, I. E. Vega, S. T. Arold, A. Baerga-Ortiz, Solution structure of the tandem acyl carrier protein domains from a polyunsaturated fatty acid synthase reveals bead-on-a-string configuration. *PLoS One* **8**, e57859 (2013).

Chapter 3

Mechanism for control of *cis* double bond positions in PUFA synthases

3.1. Introduction

In chapter 2, I showed that the number of tandem ACP domains and its structure were important factors for controlling PUFA productivity in PUFA synthases through *in vivo* experiments. I next tried to elucidate how the enzymes control *cis* double bond position of PUFA products with EPA and ARA synthases.

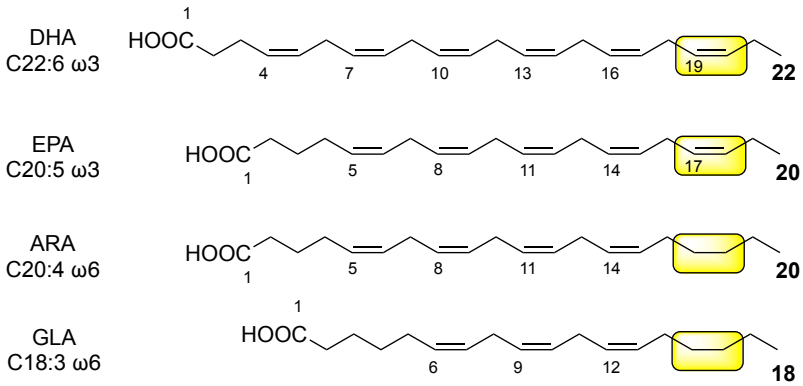

Figure 3-1-1. Chemical structures of DHA, EPA, ARA, and GLA. Yellow highlights show structural difference between ω3 and ω6 PUFAs

As mentioned in chapter 1, PUFAs are classified into ω3 or ω6 PUFAs depending on the first *cis* double bond position from methyl end. EPA and DHA are members of ω3 PUFAs whereas ARA and γ-linoleic acids (GLA) are members of ω6 PUFAs (Figure 3-1-1). From the first discovery of PUFA synthase genes, the genes responsible for ω3 PUFAs production have mainly been identified[1-3]. However, genes responsible for ARA production were identified in *Aureispira marina* in 2014[4]. Interestingly, domain organization of the ARA synthase was similar to that of ω3 PUFAs synthases even though the enzymes synthesized different products (Figure 3-1-2). Based on a putative biosynthetic pathway, the branching reaction steps of ω3 and ω6 PUFAs would be brought during reactions of C_6 to C_8 intermediates. In ω3 PUFAs biosynthesis, a formation of *cis* double bond via β,γ-isomerization of double bond would occur after dehydration of β-hydroxy groups. In contrast, enoyl reduction of *trans* double bond would occur in ω6 PUFAs biosynthesis (Figure 3-1-2). However,

detailed biosynthetic machinery was unclear. In this chapter, I examined the mechanism for controlling the first *cis* double bond positions, ω3 or ω6, of PUFA synthases by *in vivo* and *in vitro* experiments.

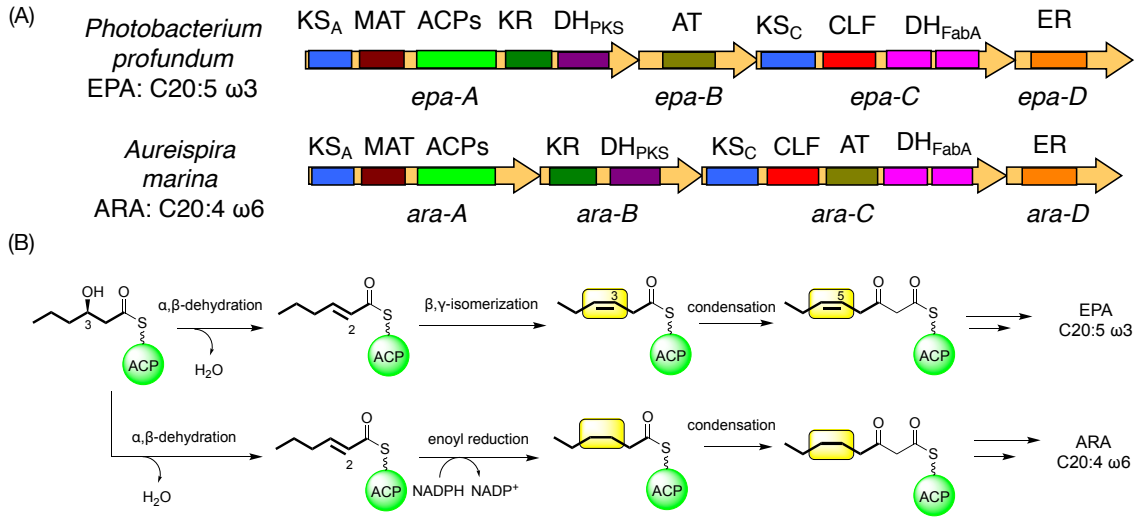

Figure 3-1-2. (A) Domain organizations of EPA and ARA synthases (B) Putative EPA and ARA biosynthetic pathway of C_6 and C_8 intermediates.

3.2. Results

3.2.1. Important domains for control of EPA or ARA production

To get clues how the enzymes control the formation of the first *cis* double bond positions, I carried out *in vivo* gene exchange assays with EPA synthase genes of *Photobacterium. profundum* and ARA synthase genes of *A. marina* using the same heterologous expression system as described in chapter 2. The EPA and ARA synthase genes were cloned into different and compatible expression vectors, pET-21a, pCDF-1b, pACYCDuet-1, and pCOLADuet-1 to construct plasmids (Figure 3-2-1-1). Because a phosphopantetheinyl transferase gene for activation of ACP in Epa-A have not been identified, a phosphopantetheinyl transferase gene, *SopfaE* of *S. oneidensis,* were used as alternative.

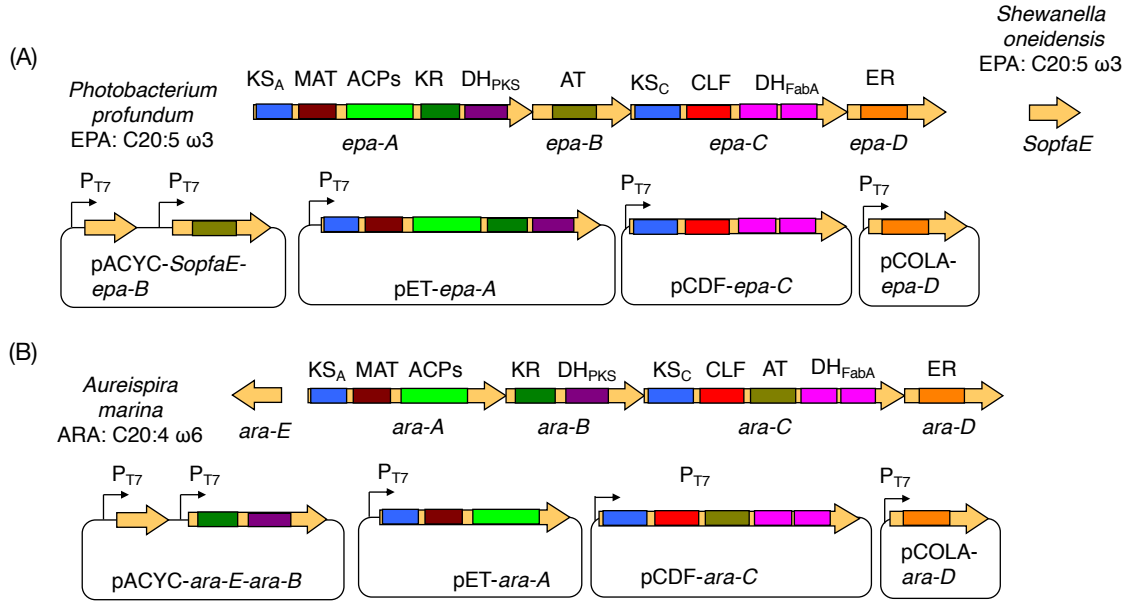

Figure 3-2-1-1. (A) The plasmids set for expression of EPA synthase genes of *P. profundum*. (B) The plasmids set for expression of ARA synthase genes of *A. marina*.

Then, the PUFA profiles were evaluated by replacing each *epa* gene with the corresponding *ara* gene. As shown in Figure 3-2-1-2, the PUFA profiles of transformants expressing *epa-ABC* with *ara-D* were almost the same as those of transformants expressing *epa-ABCD*. In contrast, the

transformants expressing *epa-ABD* with *ara-C* produced both EPA and ARA, suggesting *ara-C* was important for ARA production. Moreover, the transformants expressing *epa-AD* with *ara-BC* produced ARA as major products. These results indicated both Ara-B and Ara-C were important for ARA production.

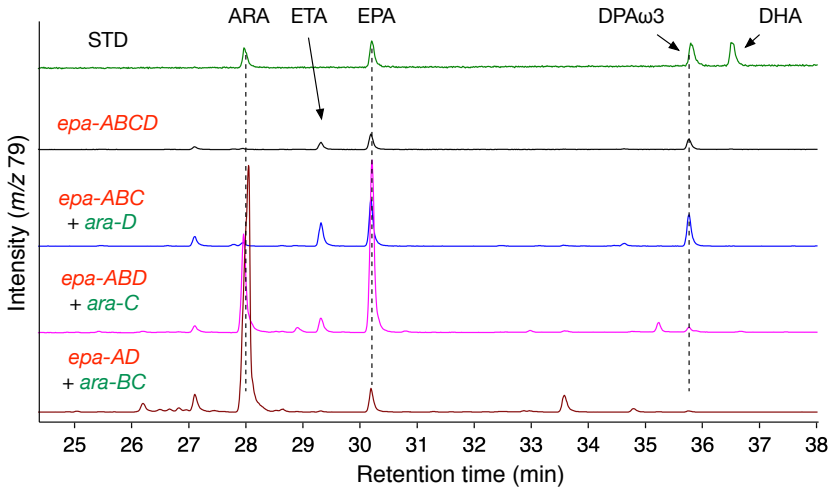

Figure 3-2-1-2. GC-MS analysis traced at *m/z* 79 by gene replacement of *epa* gene with *ara* gene. Top: authentic standard of methyl ester of ARA, EPA, DPA, and DHA.

I next examined which domain in Ara-C is essential for ARA production. The *ara-C* encoded KS, CLF, AT, and two DH_{FabA} domains. I first constructed *ara-C-AT*^{0}, in which the catalytic Ser residue estimated by sequence alignments of AT domains[5] (Figure 3-2-1-3) was mutated to Ala, and co-expressed it with *epa-ABD*. Although PUFA productivity of the AT mutant was decreased compared with parental construct, the PUFA profile of the AT mutants was the same as that of parental construct (Figure 3-2-1-3). Thus, I concluded that the AT domain in Ara-C was unrelated to ARA production and the function was complemented by the AT domain in Epa-B.

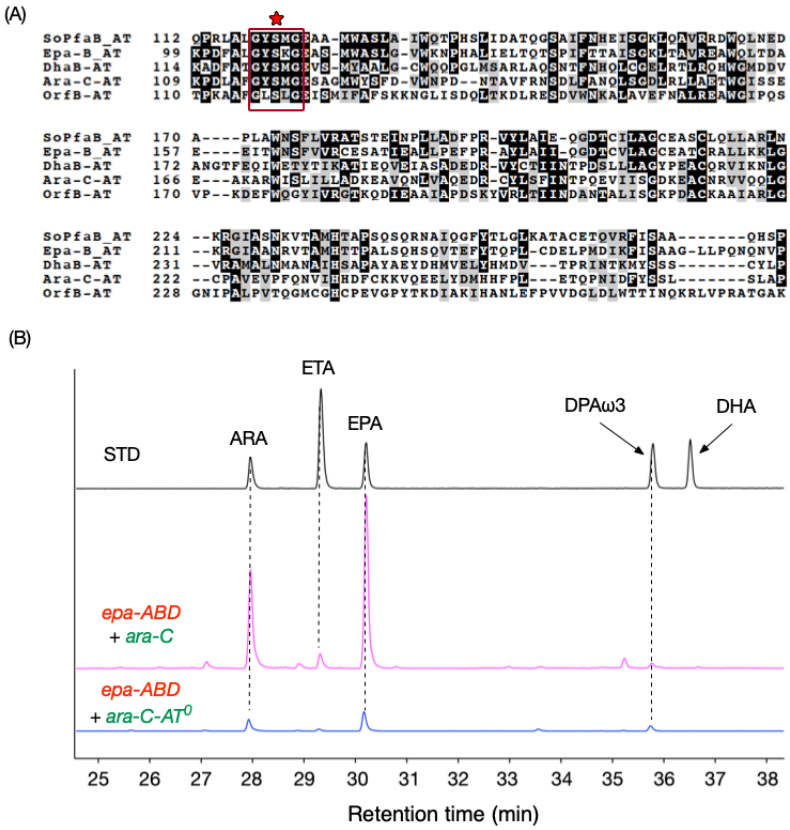

Figure 3-2-1-3. (A) Sequence alignment of the AT domains in PUFA synthases. The red box and star show the catalytic GxSxG motif and the catalytic Ser residue, respectively. SoPfaB-AT: SoPfaB of *Shewanella oneidensis* MR-1, Epa-B-AT: Epa-B of *P. profundum* SS9, Dha-B-AT: Dha-B of *M. marina*, Ara-C-AT: Ara-C of *A. marina*, OrfB-AT: OrfB of *Schizochytrium* sp. ATCC 20888. (B) GC-MS analysis traced at *m/z* 79 of the AT domain mutant (bottom).

I next constructed chimeric genes, *epa-C-ara-DH*$_{FabA}$*-chimera1* and *ara-C-epa-DH*$_{FabA}$*-chimera2,* in which the DH$_{FabA}$ domains in Epa-C and Ara-C were swapped (Figure 3-2-1-4). When *epa-C-ara-DH*$_{FabA}$*-chimera1* was co-expressed with *epa-ABD*, almost the same amounts of ARA and EPA were produced (Figure 3-2-1-4), suggesting that the DH$_{FabA}$ domains in Ara-C are important for ARA production. Unexpectedly, *ara-C-epa-DH*$_{FabA}$*-chimera2* predominantly yielded ARA when co-expressed with *epa-AD* and *ara-B* (Figure 3-2-1-4), suggesting that the KS$_C$/CLF domains in Ara-C are also important. I then constructed dozens of chimeric genes fused at different points in the KS$_C$ and CLF domains but none of the constructs showed activity.

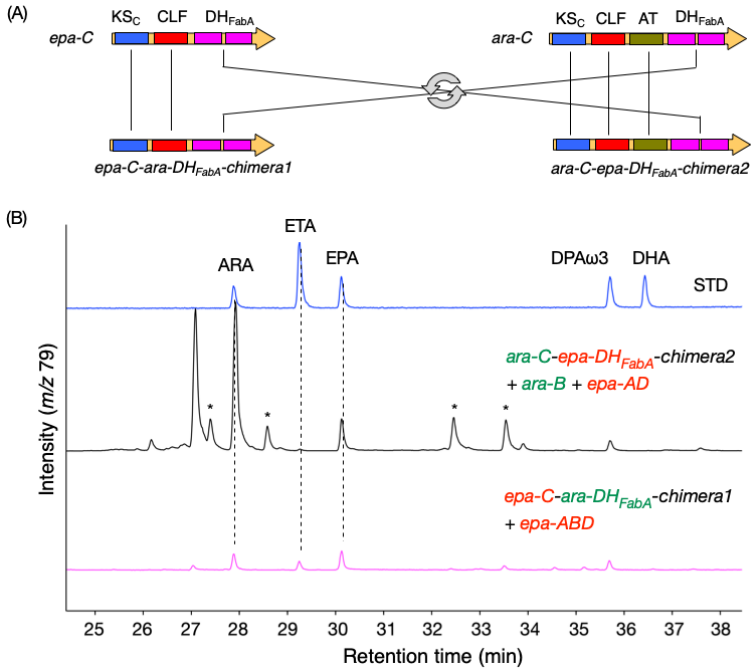

Figure 3-2-1-4. (A) Domain organization of two chimeric genes. (B) GC-MS analysis traced at *m/z* 79 of the products by co-expressions of *ara-C-epa-DH$_{FabA}$-chimera2* with *ara-B* and *epa-AD* (middle) and of *epa-C-ara-DH$_{FabA}$-chimera1* with *epa-ABD* (bottom). Asterisk showed minor uncharacterized PUFA products.

To investigate the essential domain in Ara-B for ARA production, I constructed mutated enzymes. Tyr in the KR domain and His in the DH$_{PKS}$ domain, which are plausibly catalytically essential amino acid residues[6-9] estimated by sequence alignments (Figure 3-2-1-5), were mutated to Phe to construct *ARA-B-KR^0* and *ARA-B-DH^0* by site-directed mutagenesis. The transformant expressing *ara-B-KR^0* with *epa-AD* and *ara-C* produced ARA (Figure 3-2-1-6), plausibly because the function of Ara-B-KR^0 was complemented by the KR domain in Epa-A, while ARA production was drastically decreased by expressing *ara-B-DH^0* with *epa-AD* and *ara-C* (Figure 3-2-1-6). These results showed that the DH$_{PKS}$ domain in Ara-B is important for ARA production. Taking these results together, I concluded that the KS$_C$/CLF and DH$_{FabA}$ domains in Ara-C and the DH$_{PKS}$ domain in Ara-B were responsible for ARA production.

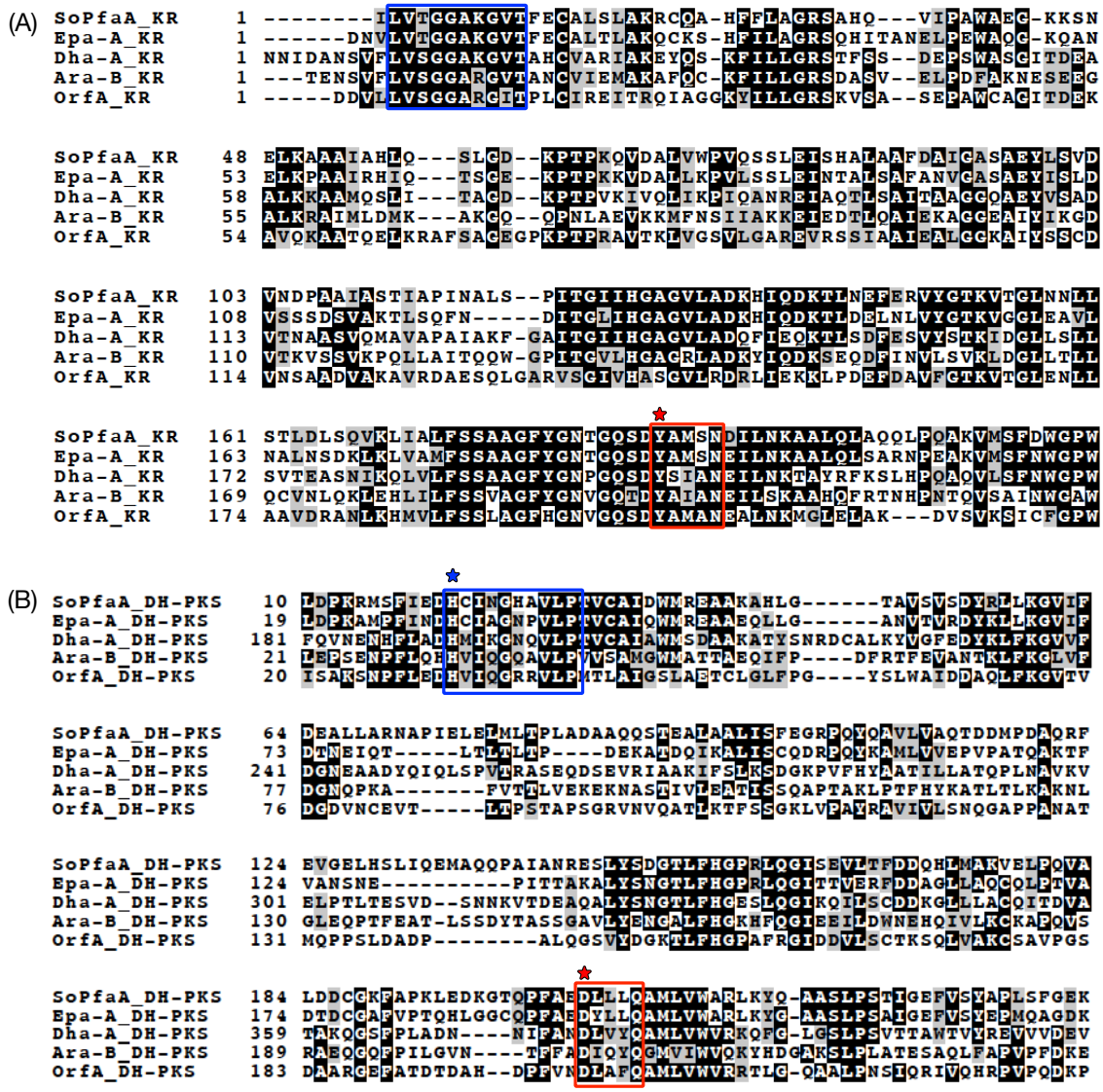

Figure 3-2-1-5. Sequence alignments of KR (A) and DH_{PKS} (B) in PUFA synthases. (A) The blue box shows the NADPH binding motif. The red square and star show the catalytic YxxxN motif and the catalytic Tyr residue, respectively. (B) The blue box and star show the HxxxGxxxxP motif and the catalytic His residue, respectively. The red square and star show the catalytic DxxxQ motif and the catalytic Asp residue, respectively. From top to bottom; SoPfaA of *S. oneidensis* MR-1, Epa-A of *P. profundum* SS9, Dha-A of *M. marina*, Ara-B of *A. marina*, and OrfA of *Schizochytrium* sp. ATCC 20888.

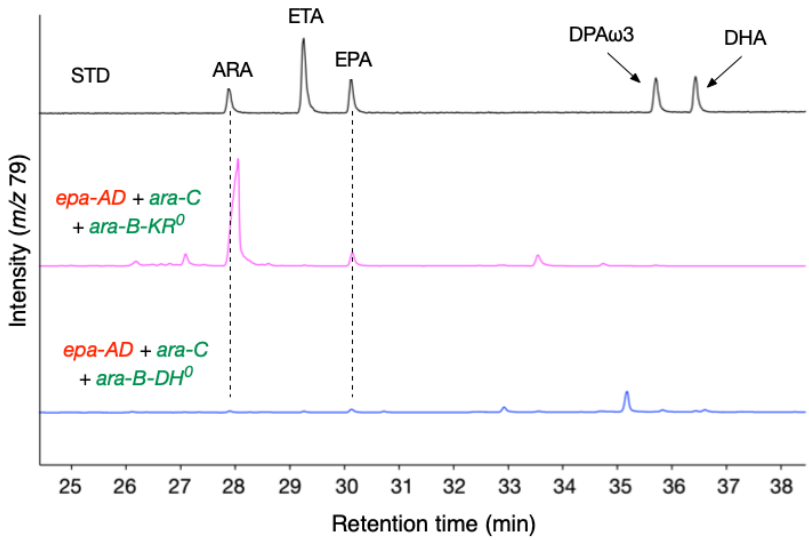

Figure 3-2-1-6. GC-MS analysis traced at *m/z* 79 of the products by co-expression of *ara-B-KR*^{0} (middle) or *ara-B-DH*^{0} (bottom) with *epa-AD* and *ara-C*.

3.2.2. Mechanism for control of first *cis* double bonds positions in PUFA synthases

In vivo experiments suggested that the two type DH domains, DH_{PKS} and DH_{FabA}, were important for ARA production. While the DH_{PKS} showed a similarity to DH domain in modular type I PKS, the DH_{FabA} showed 30-40 % identity to FabA, β-hydroxyacyl-ACP dehydratase in type II FAS. It is known that the FabA catalyzes β,γ-isomerization of 2-*trans* decaenoyl-ACP to form 3-*cis* decaenoyl-ACP besides α,β-dehydration and is responsible for unsaturated fatty acid biosynthesis[10-12] (Figure 3-2-2-1). As mentioned, the branching point between EPA and ARA biosynthesis would be brought by reactions during the carbon elongation from a C_6- to a C_8-ACP intermediate. A saturation reaction of 2-*trans* hexenoyl-ACP would occur in ARA biosynthesis while a β,γ-isomerization reaction from 2-*trans* to 3-*cis* hexenoyl-ACP would take place in EPA biosynthesis. Taken together the information, I estimated that the DH_{FabA} would catalyze dehydration and isomerization reactions of 3-hydroxyhexanoyl-ACP in EPA biosynthesis while the DH_{PKS} catalyze dehydration and the ER domain catalyze enoyl reduction in ARA biosynthesis. To investigate the probability, I carried out *in vitro* experiments using acyl-ACP substrates and truncated recombinant enzymes.

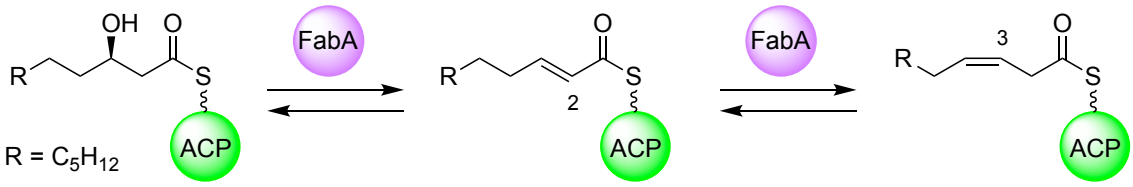

Figure 3-2-2-1. The reaction catalyzed by β-hydroxyacyl-ACP dehydratase FabA in type II FAS

Acyl-ACP substrates were prepared by enzymatic reactions using *apo*-ACP of *S. oneidensis* and phosphopantetheinyl transferase Sfp of *Bacillus subtilis* because the Sfp is known to show promiscuous substrate specificity[13] and could load various acyl-CoAs on *apo*-ACP to form acyl-ACPs. Recombinant *apo*-ACP and Sfp were obtained by expression of their genes in BL21(DE3) and purified as described in Experimental section. I also prepared recombinant DH enzymes, DH_{PKS} and DH_{FabA} of EPA and ARA synthases, but truncated enzymes containing only the DH_{PKS} domain were insoluble. Thus, Epa-A-KR-DH_{PKS} (Epa-KR-DH_{PKS}) and Ara-B-KR-DH_{PKS} (Ara-KR-DH_{PKS}) were prepared as the DH_{PKS} domain (Figure 3-2-2-2).

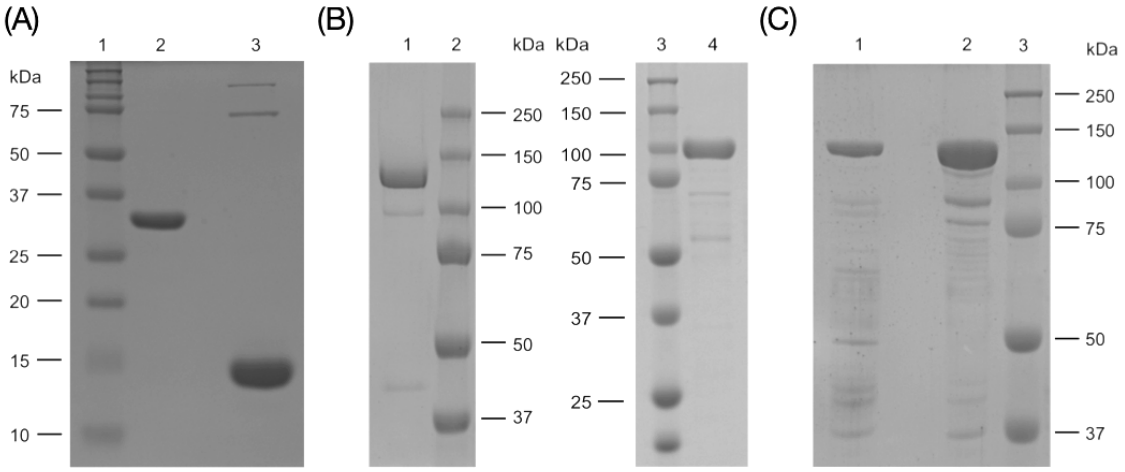

Figure 3-2-2-2. SDS-PAGE analysis of recombinant enzymes. (A) 1, Marker; 2, Sfp (29 kDa); 3, *apo*-ACP (15 kDa). (B) 1, Epa-KR-DH_{PKS} (135 kDa); 2 and 3, marker; 4, Epa-DH_{FabA} (99 kDa). (C) 1; Ara-DH_{FabA} (134 kDa); 2, Ara-KR-DH_{PKS} (130 kDa); 3, Marker.

I measured a hydration activity of the DH domains instead of the forward reactions because 3-hydroxyacyl-ACP was more thermodynamically stable than 2-*trans* acyl-ACP under *in vitro*

reaction conditions[10]. Crotonyl-ACP, 2-*trans* hexenoyl-ACP, and 2-*trans* octenoyl-ACP were enzymatically synthesized, and the formation of the substrates were checked by HPLC-ESI-TOF-MS analysis (Figure 3-2-2-3).

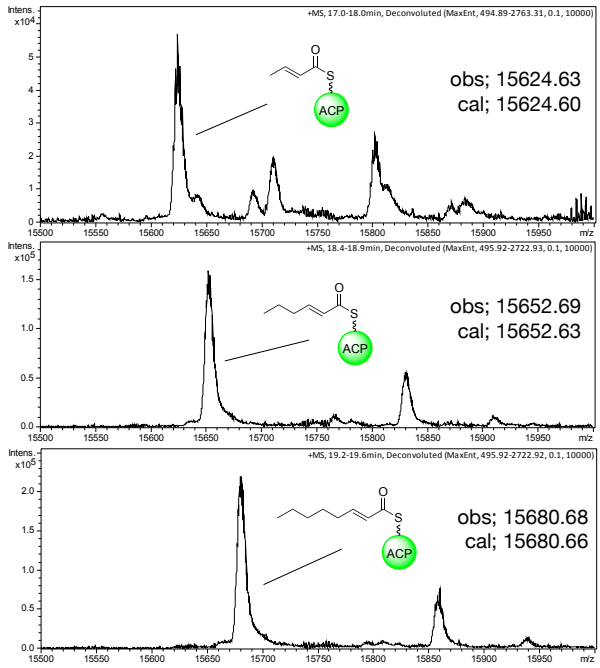

Figure 3-2-2-3. Deconvoluted MS spectra of crotonyl-ACP (top), 2-*trans* hexenoyl-ACP (middle), and 2-*trans* octenoyl-ACP (bottom).

Then, crotonyl-ACP, a C_4 substrate, was incubated with the Epa-KR-DH_{PKS} or Epa-DH_{FabA}. 3-Hydroxybutyryl-ACP was detected in both reaction mixture but the Epa-KR-DH_{PKS} exhibited higher hydration activity than the Epa-DH_{FabA} (Figure 3-2-2-4). The same tendency was also observed with the Ara-KR-DH_{PKS} and Ara-DH_{FabA} (Figure 3-2-2-4). In contrast, in the case of 2-*trans* hexenoyl-ACP, a C_6 substrate, the Epa-KR-DH_{PKS} and Ara-DH_{FabA} showed very weak activities while the EPA-DH_{FabA} and ARA-KR-DH_{PKS} showed high hydration activities (Figure 3-2-2-5). These results suggested that the two different DH domains strictly recognized different intermediates to create ω3 or ω6 PUFAs. I also checked whether the same trends were observed in DHA synthase. Recombinant Dha-KR-DH_{PKS} and Dha-DH_{FabA} enzymes were prepared and used for *in vitro* assays. Both the enzymes showed the

same substrate specificities as the Epa enzymes (Figure 3-2-2-6).

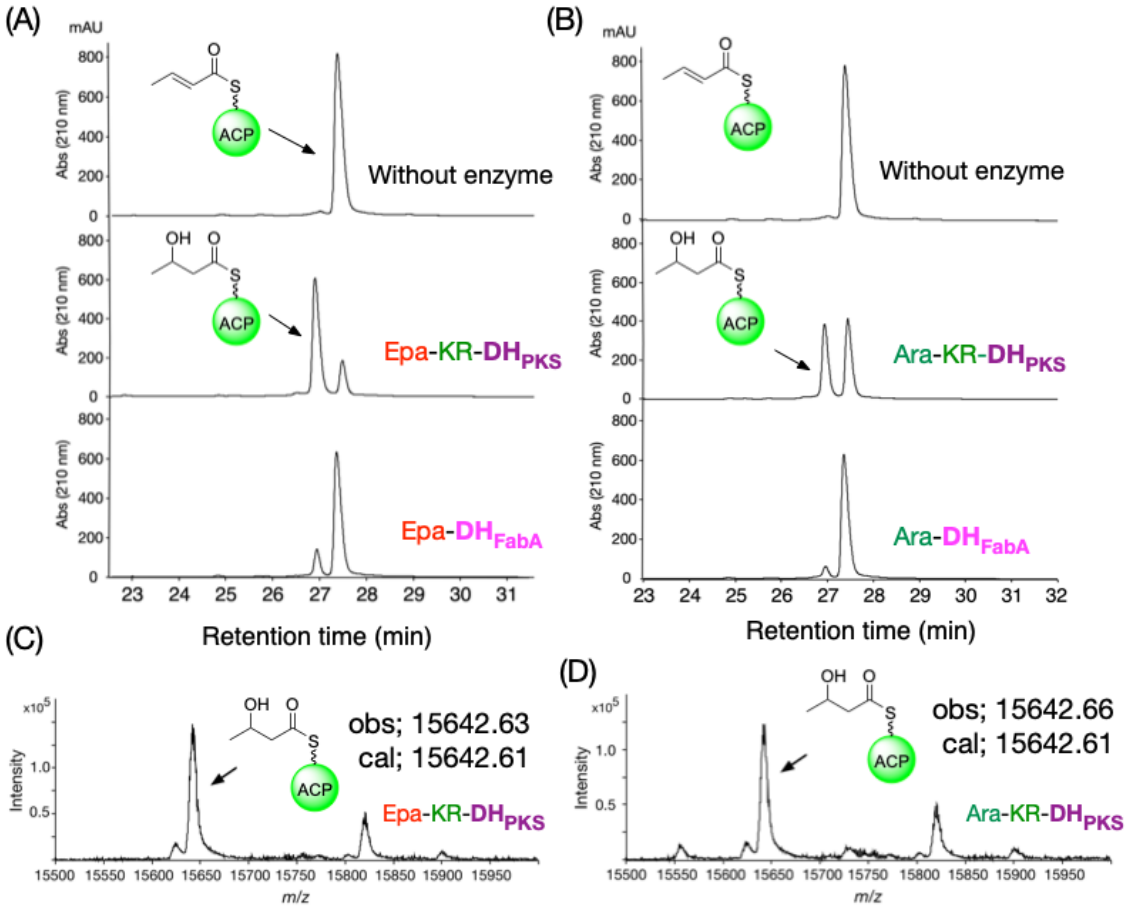

Figure 3-2-2-4. HPLC traces (210 nm) of *in vitro* hydration reactions of crotonyl-ACP with Epa enzymes (A) or Ara enzymes (B). Without enzyme (top), with KR-DH$_{PKS}$ (middle), or with DH$_{FabA}$ (bottom). Deconvoluted MS spectra obtained by HPLC-ESI-TOF-MS analysis of *in vitro* reaction mixtures with crotonyl-ACP and Epa-KR-DH$_{PKS}$ (C) or Ara-KR-DH$_{PKS}$ (D).

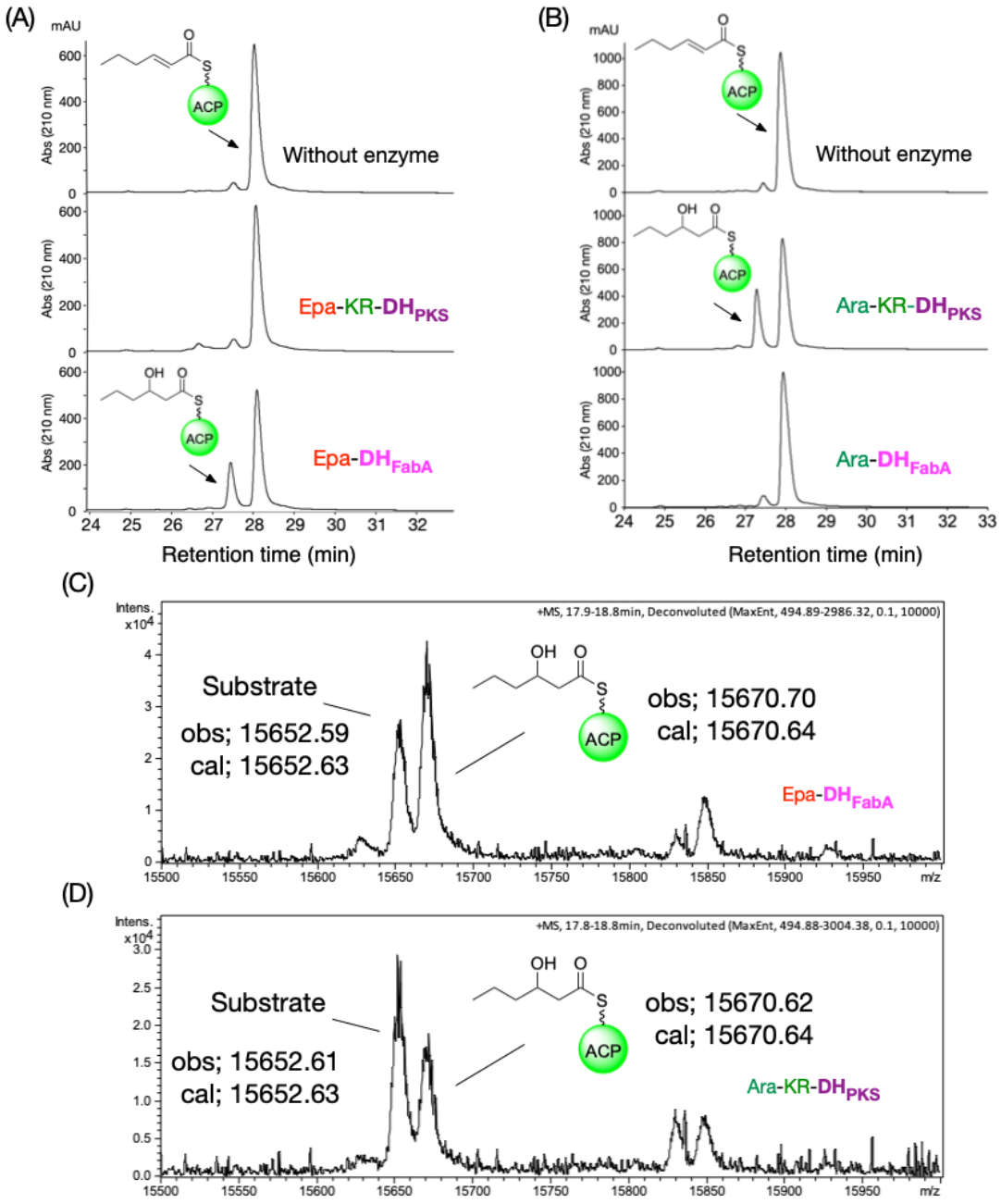

Figure 3-2-2-5. HPLC traces (210 nm) of *in vitro* hydration reactions of 2-*trans* hexenoyl-ACP with Epa enzymes (A) or Ara enzymes (B). Without enzyme (top), with KR-DH_{PKS} (middle), or with DH_{FabA} (bottom). Deconvoluted MS spectra obtained by HPLC-ESI-TOF-MS analysis of *in vitro* reaction mixtures with 2-*trans* hexenoyl -ACP and Epa-DH_{FabA} (C) or Ara-KR-DH_{PKS} (D).

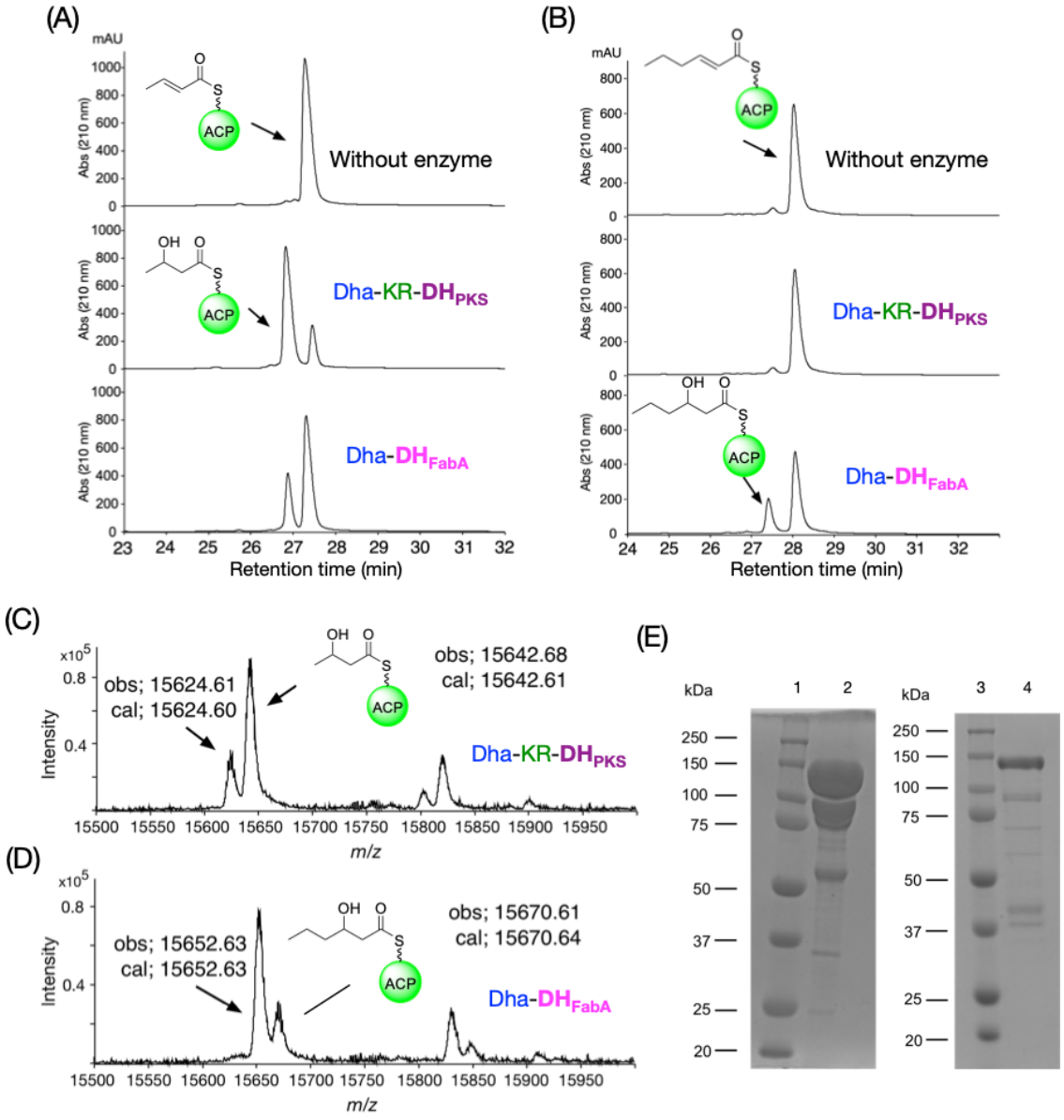

Figure 3-2-2-6. HPLC traces (210 nm) of *in vitro* hydration reactions of crotonyl- (A) or 2-*trans* hexenoyl-ACP (B) with Dha enzymes. Without enzyme (top), with KR-DH_{PKS} (middle), or with DH_{FabA} (bottom). Deconvoluted MS spectra obtained by HPLC-ESI-TOF-MS analysis of *in vitro* reaction mixtures with Dha-KR-DH_{PKS} (C) or Dha-DH_{FabA} (D). SDS-PAGE analysis of recombinants Dha enzymes, 1 and 3, Marker; 2, Dha-KR-DH_{PKS} (136 kDa); 4, Dha-DH_{FabA} (142 kDa).

I also carried out *in vitro* reactions with 2-*trans* octenoyl-ACP, a C_8 substrate, and Ara-enzymes. However, both the ARA-KR-DH_{PKS} and Ara-DH_{FabA} showed almost no hydration activity

when 2-*trans* octenoyl-ACP was used as the substrate (Figure 3-2-2-7). I next prepared, 3-hydroxyoctanoyl-ACP, a substrate for forward reaction and carried out *in vitro* reactions with the Ara enzymes. As shown in Figure 3-2-2-7, a dehydration product was detected in Ara-DH_{FabA} reaction mixture and no products was detected in Ara-KR-DH_{PKS} reaction mixture. As geometry determination of the ACP-product is very difficult because of its high molecular weight, I used *N*-acetylcysteamine (SNAC) derivatives as substrates, widely used as mimics of acyl-ACPs substrates for *in vitro* experiments. When 3-hydroxyoctanoyl-SNAC was incubated with the Ara-DH_{FabA}, a dehydrated product was detected, and the retention time of product was consistent with that of 2-*trans* octenoyl-SNAC but not of 2-*cis* octenoyl-SNAC (Figure 3-2-2-8). Taken together, these results suggested that the DH_{PKS} domain of EPA synthase recognized the C_4 substrate while that of ARA synthase recognized both the C_4 and C_6 substrates for full reduction in the early biosynthetic stage. Moreover, the DH_{FabA} domain acted on substrates to which a *cis* double bond was introduced (C_6 and C_8 intermediates in EPA while C_8 intermediate in ARA biosynthesis).

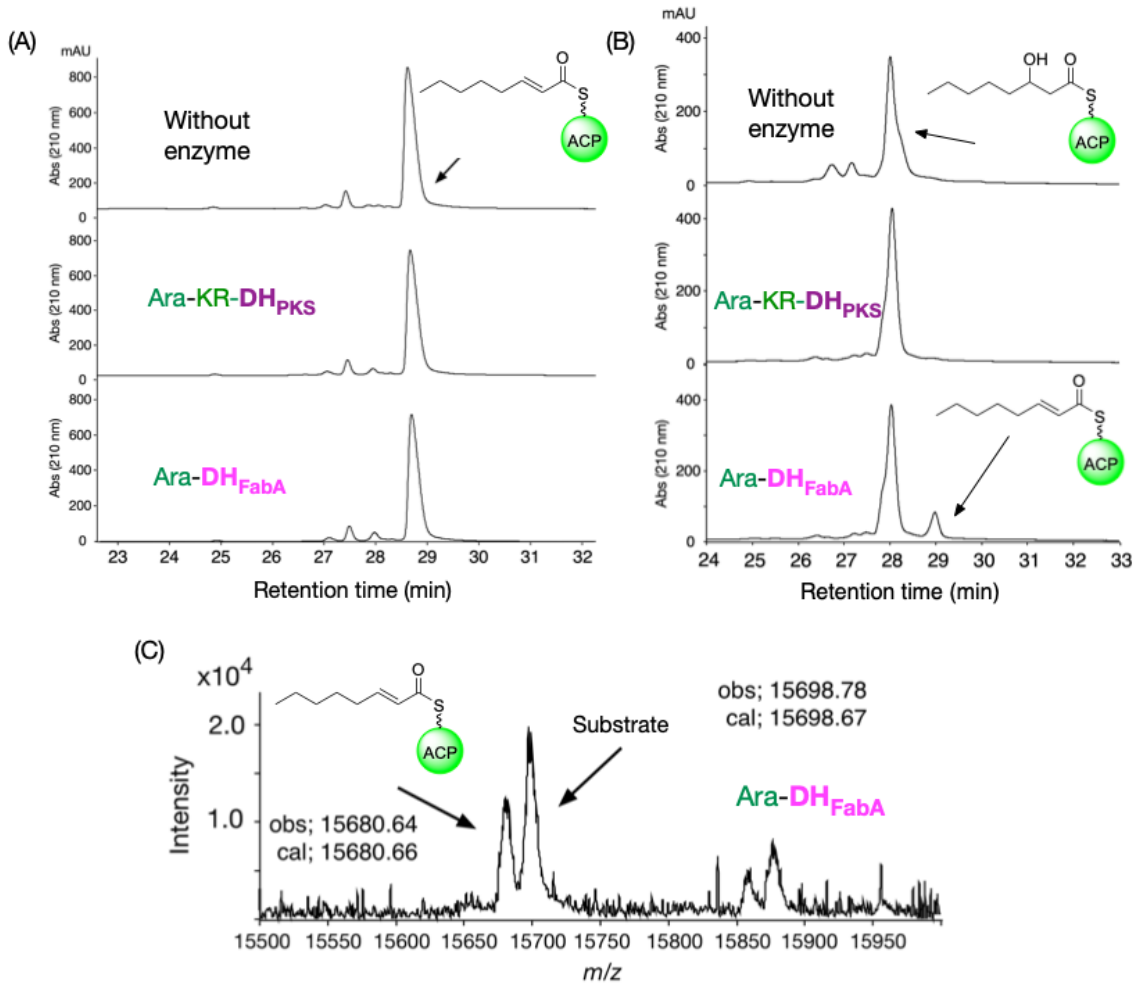

Figure 3-2-2-7. (A) HPLC traces (UV 210 nm) of *in vitro* reaction products with 2-*trans* octenoyl-ACP and Ara-KR-DH$_{PKS}$ or Ara-DH$_{FabA}$. Without enzyme (top), with Ara-KR-DH$_{PKS}$ (middle), or with Ara-DH$_{FabA}$ domain (bottom). (B) HPLC traces (210 nm) of *in vitro* dehydration reactions of 3-hydroxyoctanoyl-ACP with Ara-KR-DH$_{PKS}$ (middle), Ara-DH$_{FabA}$ (bottom), or without enzyme (top). (C) Deconvoluted MS spectra obtained by HPLC-ESI-TOF-MS analysis of *in vitro* reaction mixtures with Ara-DH$_{FabA}$.

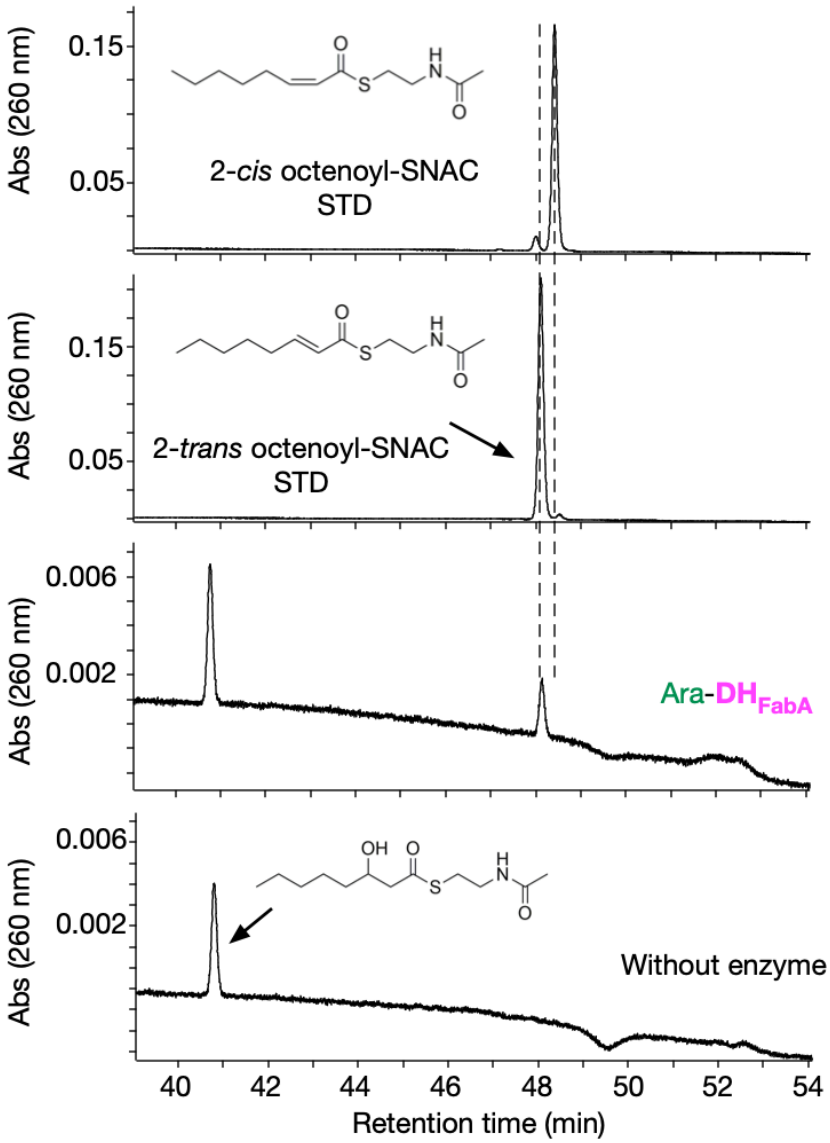

Figure 3-2-2-8. UPLC traces (260 nm) of *in vitro* reaction products with Ara-DH_{FabA} and 3-hydroxyoctanoyl-SNAC. Standards (top and 2nd) and without enzyme (bottom).

I next examined whether *trans* to *cis* isomerization occurs after the dehydration reaction by the DH_{FabA}. However, detection of isomerization with *trans*-substrates was reported to be difficult[10]. I therefore examined whether the DH_{FabA} domains catalyzed the reverse β,γ- and α,β-isomerization reactions with *cis*-acyl-SNAC substrates. When 3-*cis* hexenoyl-SNAC was incubated with the Epa-DH_{FabA}, 2-*trans* hexenoyl-SNAC was clearly detected (Figure 3-2-2-9). Moreover, the Ara-DH_{FabA}

catalyzed the conversion of 2-*cis* octenoyl-SNAC to 2-*trans* octenoyl-SNAC although the activity was very weak compared with the β,γ-isomerization activity of EPA enzyme (Figure 3-2-2-9). These results suggested that the DH_{FabA} domains catalyze *trans* to *cis* isomerization besides dehydration reactions. Although the reaction mechanisms of β,γ- and α,β-isomerization were unclear, β,γ-isomerization might occur by the same reaction mechanism as that of FabA in type II FAS[11,12]. First, the FabA abstracts a C-2 proton of 3-hydroxy acyl-ACP concomitant with the C-3 hydroxyl group elimination from the same face and then isomerizes to generate β,γ double bond with *cis* configuration by abstracting the *pro-R* proton from C_4 of the substrate (Figure 3-2-2-10).

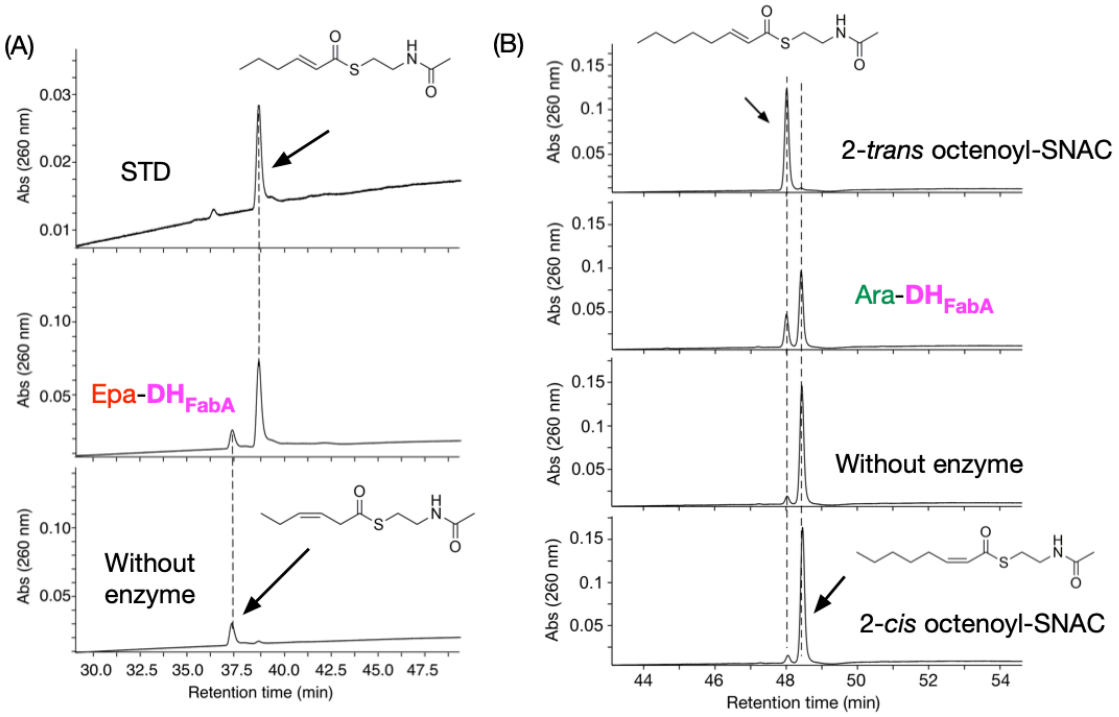

Figure 3-2-2-9. UPLC analysis of *in vitro* isomerization reaction mixtures. (A) UPLC traces (260 nm) of the β,γ-isomerization reaction of 3-*cis* hexenoyl-SNAC with Epa-DH_{FabA}. Standard (top) and without enzyme (bottom). (B) UPLC traces (260 nm) of the α,β-isomerization reaction of 2-*cis* octenoyl-SNAC with Ara-DH_{FabA} (2^{nd}). Standard (top and bottom) and without enzyme (3^{rd}).

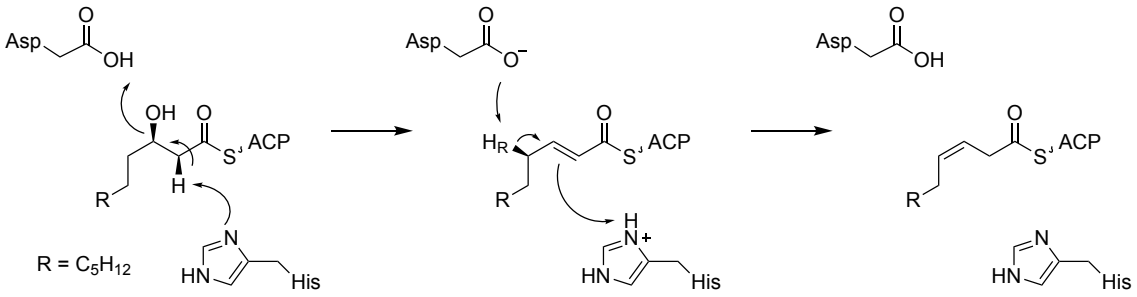

Figure 3-2-2-10. Reaction mechanisms of β-hydroxyacyl-ACP dehydratase FabA.

To deepen understanding of reaction mechanism, I also carried out the geometrical analysis of a product by KR domain in PUFA synthases. Because chiral analysis of 3-hydroxyacyl-ACP products was unsuccessful, I utilized SNAC thioester derivatives, 3-oxobutyryl-SNAC, 3-oxohexanoyl-SNAC, and 3-oxooctanoyl-SNAC as substrates. When 3-oxobutyryl-SNAC was incubated with the Epa-KR-DH_{PKS} and NADPH, 3-hydroxybutyryl-SNAC was clearly detected by UPLC-ESI-MS analysis (Figure 3-2-2-11). Chiral analysis showed that the retention time of the reaction product was consistent with that of the product produced by β-ketoacyl reductase EcFabG of *E. coli* (Figure 3-2-2-12), suggesting the formation of (*3R*)-hydroxybutyryl-SNAC. Furthermore, I also confirmed that the Epa-KR-DH_{PKS} products from 3-oxohexanoyl-SNAC and 3-oxooctanoyl-SNAC were (*3R*)-hydroxyhexanoyl-SNAC and (*3R*)-hydroxyoctanoyl-SNAC, respectively. These results suggested that the KR domain in PUFA synthase catalyzed the formation of (*3R*)-hydroxy forms regardless of the carbon chain lengths of the substrates in the same manner as FAS.

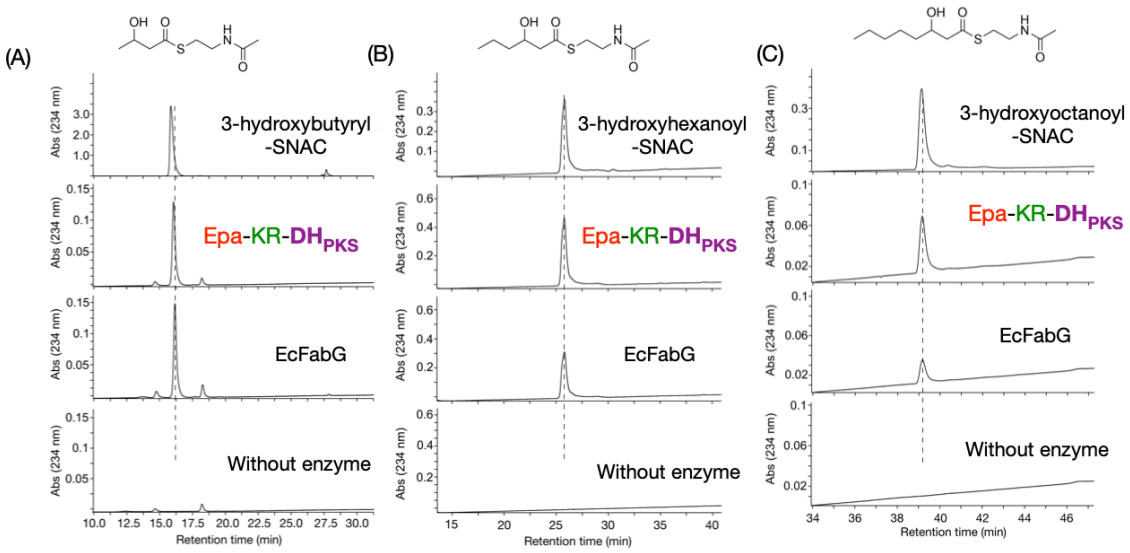

Figure 3-2-2-11. UPLC traces (UV 234 nm) of reaction products with the KR domain in Epa-A and 3-oxobutyryl-SNAC (A), 3-oxohexanoyl-SNAC (B), or 3-oxooctanoyl-SNAC (C). Standards (top), with the KR domain in Epa-A (2nd), with EcFabG (*E. coli*) (3rd), or without enzyme (bottom).

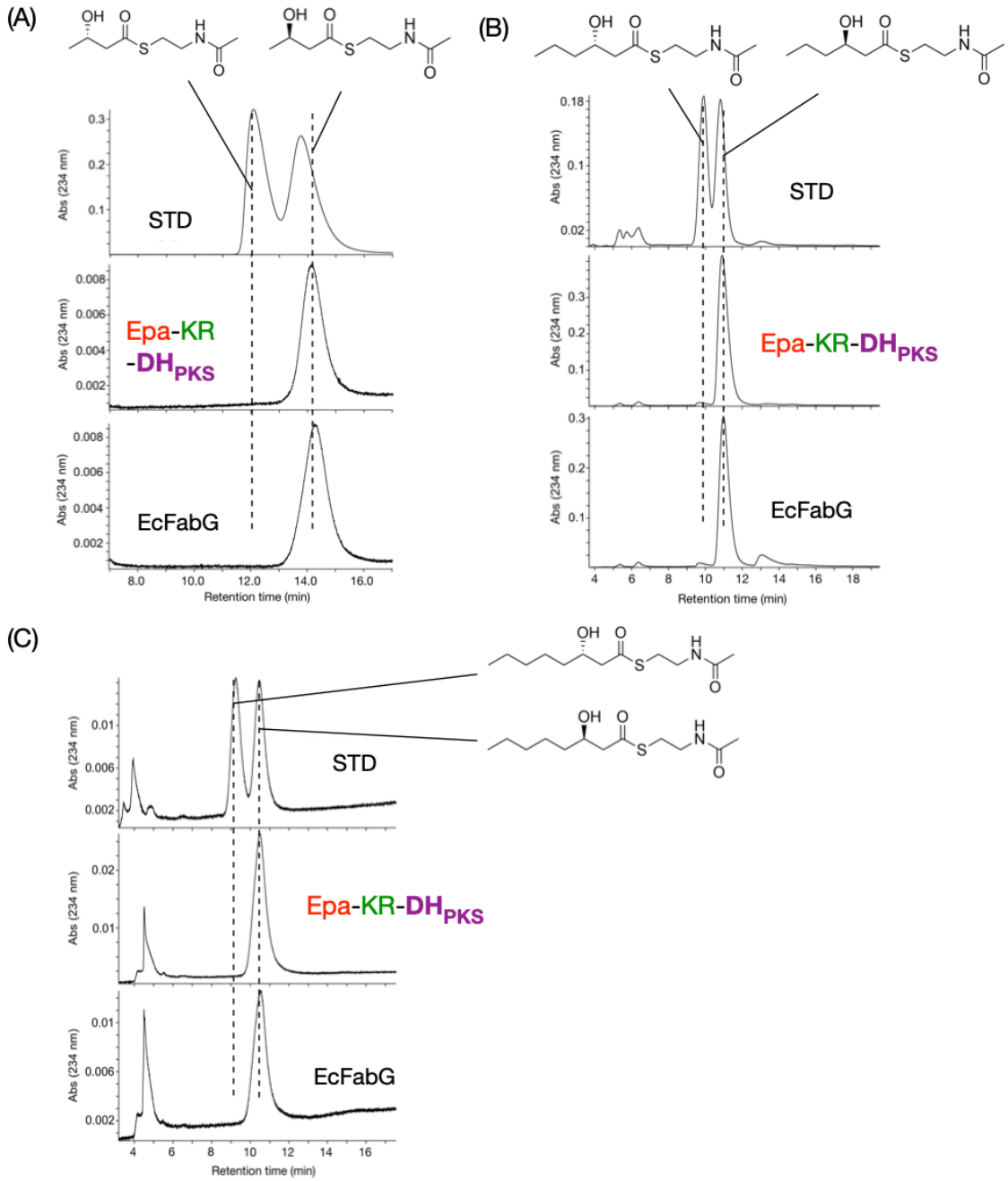

Figure 3-2-2-12. Chiral analysis (UV 234 nm) of reaction products with the KR domain in Epa-A and 3-oxobutyryl-SNAC (A), 3-oxohexanoyl-SNAC (B), or 3-oxooctanoyl-SNAC (C). (*3R*) and (*3S*)-hydroxyacyl-SNAC standards (top), with the KR domain in Epa-A (middle), or with EcFabG (*E. coli*) (bottom)

3.3. Discussion

In this chapter, I studied the mechanism for the formation of the first *cis* double bond by PUFA synthases through *in vivo* and *in vitro* experiments. PUFA synthases utilize the two types of DH domains, DH_{PKS} and DH_{FabA}, depending on the carbon chain length to introduce saturation or *cis* double bonds to growing acyl chains (Figure 3-3-1). In ARA biosynthesis, dehydration by the DH_{PKS} and subsequent enoyl reduction by the ER domain would occur to form hexanoyl-ACP from (*3R*)-hydroxyhexanoyl-ACP. Then, condensation of hexanoyl-ACP with malonyl-ACP by the KS domain, reduction by the KR domain, and dehydration and α,β-isomerization of the C_8 intermediate by the DH_{FabA} would occur (Figure 3-3-1). In contrast, in EPA biosynthesis, dehydration and β,γ-isomerization of a C_6 intermediate would be catalyzed by the DH_{FabA} to form 3-*cis* hexenoyl-ACP. The KS domains would strictly recognize 3-*cis* form and catalyze a condensation of 3-*cis* hexenoyl-ACP with malonyl-ACP to form 5-*cis* 3-oxooctenoyl-ACP (Figure 3-3-1). The DH_{FabA} catalyzes the interconversion of 3-hydroxyacyl-ACP, 2-*trans* acyl-ACP, and 3-*cis* or 2-*cis* acyl-ACP. Therefore, condensation reactions catalyzed by the KS domains is the driving force for the forward reactions and selection of the appropriate intermediates by the KS domains is also important for controlling *cis* double position of PUFA products.

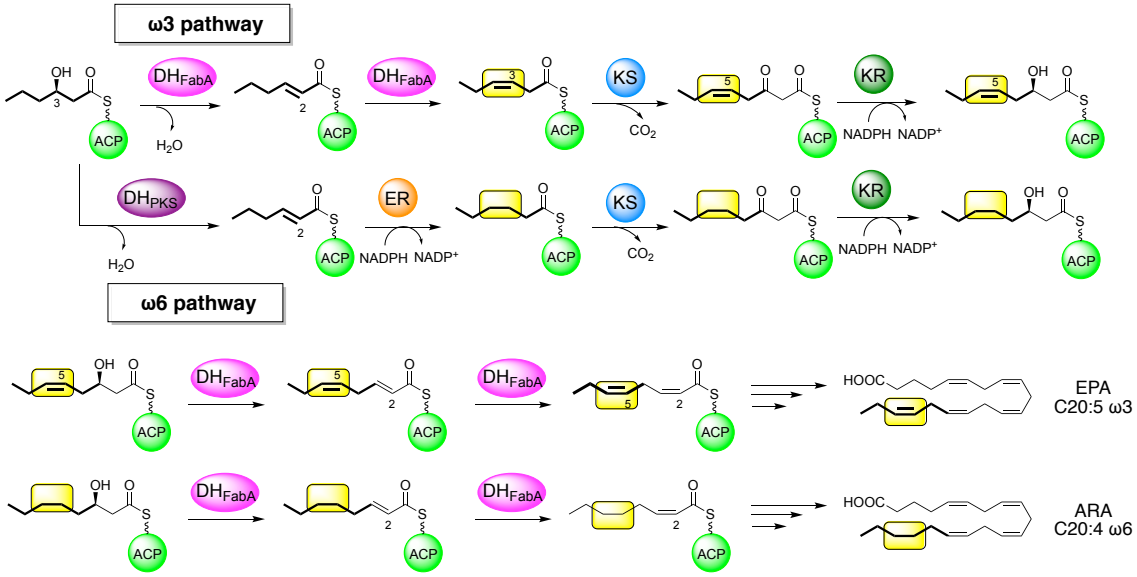

Figure 3-3-1. Proposed biosynthetic pathway of ω3 and ω6 PUFAs on C_6 to C_8 intermediates

There are a few examples of α,β-isomerization of double bond in natural products biosynthesis. In 11-*cis* retinol biosynthesis, all-*trans* retinol is first esterified to create leaving group. Nucleophilic attack of the active site residue of isomerohydrolase on C-11 position of substrate followed by elimination of ester group would allow a rotation of C-C bond. Then, nucleophilic attack of water molecule gives 11-*cis* retinol[14] (Figure 3-3-2). Although a α,β-isomerization was proposed to go through radical mechanisms induced by sunlight in coumarins biosynthesis[15], the coumarin derivatives were synthesized in darkness environments[16]. Kai *et al.*, proposed a mechanism that deprotonation of hydroxy group of CoA thioester intermediate would proceed to form enolate and then lactonization reaction occurs after α,β-isomerization[16] (Figure 3-3-3). The DH_{FabA} catalyzed both β,γ- and α,β-isomerization of double bond of acyl-ACPs. The reaction mechanism of β,γ-isomerization was speculated to be same mechanism of FabA in type II FAS. α,β-Isomerization mechanism might be also similar to that of FabA as mentioned above. However, in this case, a rotation of C-C bond in transition state may be necessary for the formation of 2-*cis* acyl-ACP from 2-*trans* acyl-ACP in the similar manner to the coumarin biosynthesis (Figure 3-3-4).

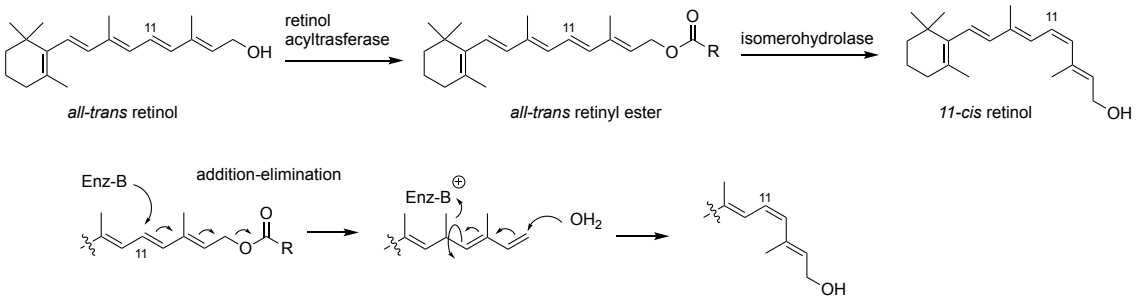

Figure 3-3-2. Reaction mechanisms of α,β-isomerization in 11-*cis* retinol biosynthesis.

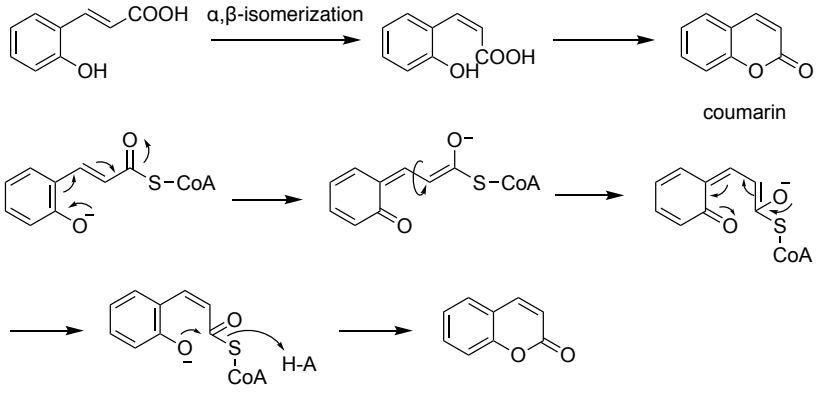

Figure 3-3-3. Reaction mechanisms of α,β-isomerization in coumarin biosynthesis.

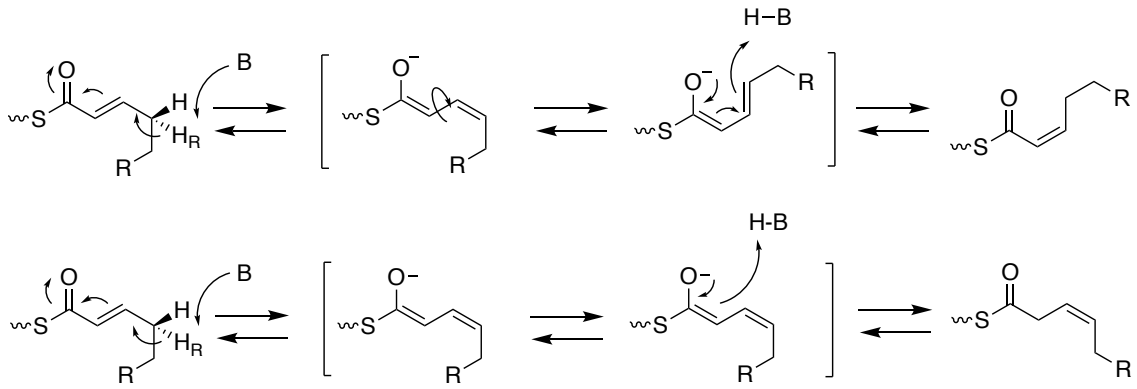

Figure 3-3-4. Proposed mechanisms of α,β- (top) and β,γ- (bottom) isomerization catalyzed by DH_{FabA} in PUFA biosynthesis

References

1. J. G. Metz, P. Roessler, D. Facciotti, C. Levering, F. Dittrich, M. Lassner, R. Valentine, K. Lardizabal, F. Domergue, A. Yamada, K. Yazawa, V. Knauf, J. Browse, Production of polyunsaturated fatty acids by polyketide synthases in both prokaryotes and eukaryotes. *Science* **293**, 290–293 (2001).
2. E. E. Allen, H. D. Bartlett, Structure and regulation of the omega-3 polyunsaturated fatty acid synthase genes from the deep-sea bacterium *Photobacterium profundum* strain SS9. *Microbiology* **148**, 1903–1913 (2002).
3. N. Morita, M. Tanaka, H. Okuyama, Biosynthesis of fatty acids in the docosahexaenoic acid-producing bacterium *Moritella marina* strain MP-1. *Biochem. Soc. Trans*. **28**, 943–945 (2000).
4. T. Ujihara, M. Nagano, H. Wada, S. Mitsuhashi, Identification of a novel type of polyunsaturated fatty acid synthase involved in arachidonic acid biosynthesis. *FEBS Lett.* **588**, 4032–4036 (2014).
5. S. Poust, I. Yoon, P. D. Adams, L. Katz, C. J. Petzold, J. D. Keasling, Understanding the Role of Histidine in the GHSxG Acyltransferase Active Site Motif: Evidence for Histidine Stabilization of the Malonyl-Enzyme Intermediate. *PLoS ONE* **9**, e109421. (2014)
6. R. Reid, M. Piagentini, E. Rodriguez, G. Ashley, N. Viswanathan, J. Carney, D. V. Santi, C. R. Hutchinson, R. McDaniel, A model of structure and catalysis for ketoreductase domains in modular polyketide synthases. *Biochemistry* **42**, 72–79 (2003).
7. A. T. Keatinge-Clay, A tylosin ketoreductase reveals how chirality is determined in polyketides. *Chem. Biol.,* **14**, 898–908 (2007).
8. A. T. Keatinge-Clay, Crystal structure of the erythromycin polyketide synthase dehydratase. *J. Mol. Biol*., **384**, 941–953 (2008).
9. D. L. Akey, J. R. Razelun, J. Tehranisa, D. H. Sherman, W. H. Gerwick, J. L. Smith, Crystal structure of dehydratase domains from the curacin polyketide biosynthetic pathway. *Structure* **18**, 94–105 (2010).
10. R. J. Heath, C. O. Rock, Roles of the FabA and FabZ β-hydroxyacyl-acyl carrier protein dehydratases in *Escherichia coli* fatty acid biosynthesis. *J. Biol. Chem.* **1996**, 271, 27795–27801.
11. J. M. Schwab, J. B. Klassen, Steric course of the allylic rearrangement catalysed by β-hydroxydecanoylthioester dehydrase. Mechanistic implications. *J. Am. Chem. Soc.* **106**, 7217–7227 (1984).
12. L. Moynie, S. M. Leckie, S. A. McMahon, F. G. Duthie, A. Koehnke, J. W. Taylor, M. S. Alphey, R. Brenk, A. D. Smith, J. H. Naismith, Structural insights into the mechanism and inhibition of

the β-hydroxydecanoyl-acyl carrier protein dehydratase from *Pseudomonas aeruginosa*. *J. Mol. Biol.,* **425**, 365–377 (2013).

13. M. R. Mofid, R. Finking, L. O. Essen, M. A. Marahiel, Structure-based mutational analysis of the 4'-phosphopantatheinyl transferases Sfp from Bacillus subtilis: Carrier protein recognition and reaction mechanism. *Biochemistry* **43**, 4128–4136 (2004).
14. G. Moiseyev, R. K. Crouch, P. Goletz, J. Oatis, Jr., T. M. Redmond, J. X. Ma, Retinyl esters are the substrate for isomerohydrolase. *Biochemistry* **42**, 2229–2238 (2003).
15. F. A. Haskins, L. G. Williams, H. J. Gorz, Light-induced *trans* to *cis* conversion of β-D-Glucosyl *o*-hydroxycinnamic acid in *Melilotus alba* leaves. *Plant Physiol.,* **39**, 777–781 (1964).
16. K. Kai, M. Mizutani, N. Kawamura, R. Yamamoto, M. Tamai, H. Yamaguchi, K. Sakata, B. Shimizu, Scopoletin is biosynthesized via ortho-hydroxylation of feruloyl CoA by a 2-oxoglutarate-dependent dioxygenase in *Arabidopsis thaliana*. *The Plant Journal* **55**, 989–999 (2008).

Chapter 4

Mechanism for control of carbon chain length of final products in PUFA synthases

4.1. Introduction

In chapter 3, I studied the mechanism for control of the first *cis* double bond position in PUFA products, and showed that the two type DH domains, DH_{PKS} and DH_{FabA}, were responsible for the control through *in vivo* and *in vitro* experiments. I next examined how the enzymes control carbon chain length (C_{22} or C_{20}) of the products using DHA and EPA synthases (Figure 4-1-1).

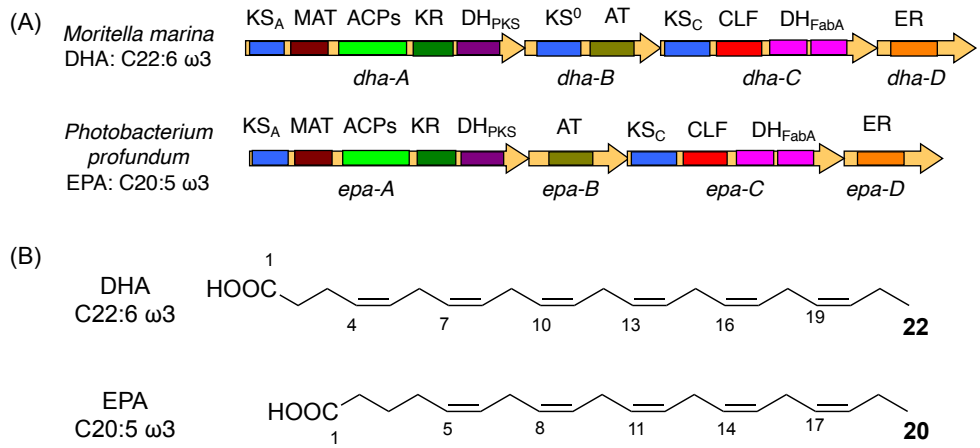

Figure 4-1-1. (A) Domain organizations of DHA and EPA synthase genes (B) Chemical structures of DHA and EPA

In 2009, Orikasa *et al*. suggested that subunit B gene encoding AT domain would be responsible for control of EPA and DHA production through gene knockout and complementation experiments[1]. However, detail role of the AT domain was still unclear (the role of AT domain was examined in chapter 5). Furthermore, the branching point would be brought by reactions during C_{20} and C_{22} intermediates considering the later stage of putative DHA and EPA biosynthetic pathways (Figure 4-1-2). In the pathways, a reaction catalyzed by the AT domain is unnecessary. Thus, the mechanism for control of carbon chain length remained obscure. In this chapter, I investigated important genes and domains responsible for controlling EPA and DHA production using the heterologous expression system and *in vitro* experiments.

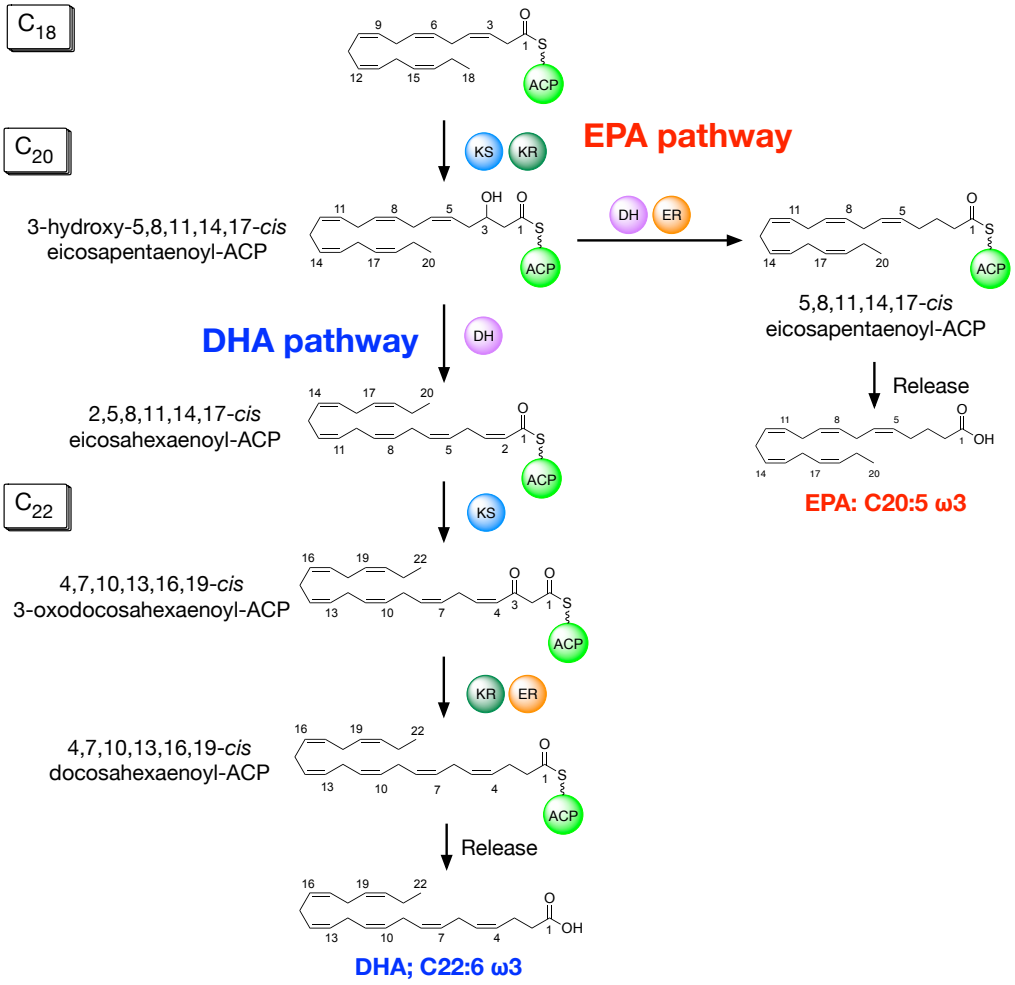

Figure 4-1-2. Putative DHA and EPA biosynthetic pathway of C_{20} to C_{22} intermediates

4.2. Results

4.2.1. Important domains for control of EPA or DHA production

I first carried out gene exchange experiments to identify important gene(s) responsible for EPA and DHA productions. The EPA synthase genes (*epa*) of *P. profundum* and DHA synthase genes (*dha*) of *M. marina*, both of which comprise four genes (A to D) were used in the experiments. Because EPA genes had already been cloned as mentioned above, the *dha* genes were cloned into vectors with T7 promoters and introduced into *E. coli* (Figure 4-2-1-1). I confirmed that the transformant harboring *dha-ABCDE* genes produced DHA as the main product concomitant with small amounts of ETA (Figure 4-2-1-2).

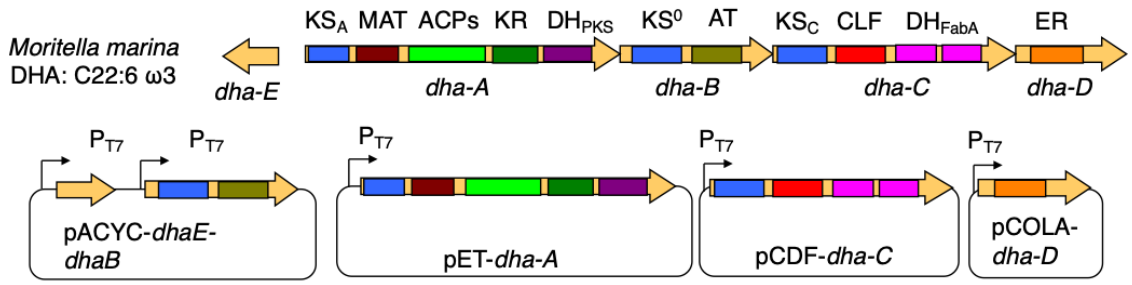

Figure 4-2-1-1. The plasmids set for expression of DHA synthase genes of *M. marina.*

Then, each EPA synthase gene was replaced with the corresponding DHA synthase gene. When *epa-A*, *-B* or *-D* was replaced with the corresponding DHA gene, the PUFA profiles (EPA production) were almost the same as that of the transformant expressing *epa-ABCD*, although the PUFA productivities tended to decrease. By replacing *epa-C* with *dha-C*, however, the major product was changed to DHA (Figure 4-2-1-2). Similarly, by replacing *dha-C* with *epa-C*, EPA was produced and DHA production was lost. However, PUFA profiles were almost same as that of the transformant expressing *dha-ABCD* when *dha-A*, *-B* or *-D* was replaced with the corresponding EPA gene (Figure 4-2-1-2). The same result was also obtained with the EPA synthase genes (*SopfaABCD*) of *Shewanella oneidensis* (Figure 4-2-1-3). These results suggested that the "C" gene is the important subunit gene for controlling the carbon

chain length of final products.

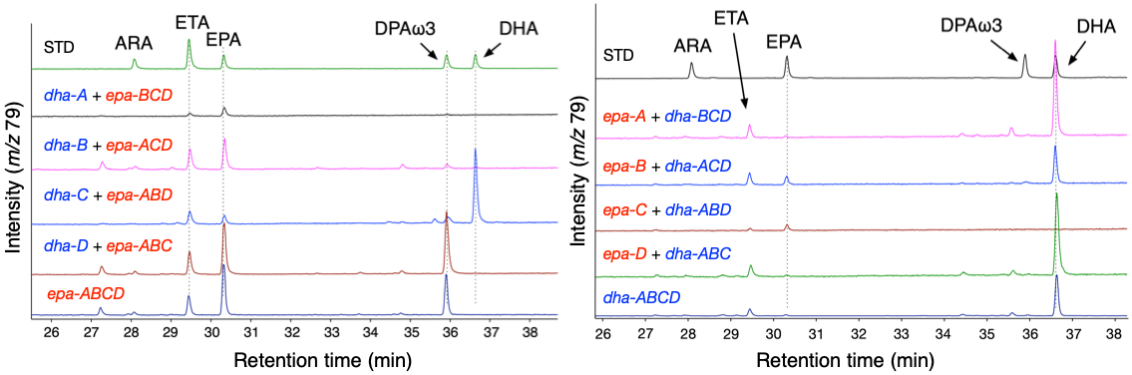

Figure 4-2-1-2. GC/MS analysis traced at *m/z* 79 of products produced in the gene exchange assay. (left) Gene replacement of *epa* genes with *dha* genes (from 2nd to 5th). Standards (top) and *epa-ABCD* (bottom). (right) Gene replacement of *dha* genes with *epa* genes (from 2nd to 5th). Standards (top) and *dha-ABCD* (bottom).

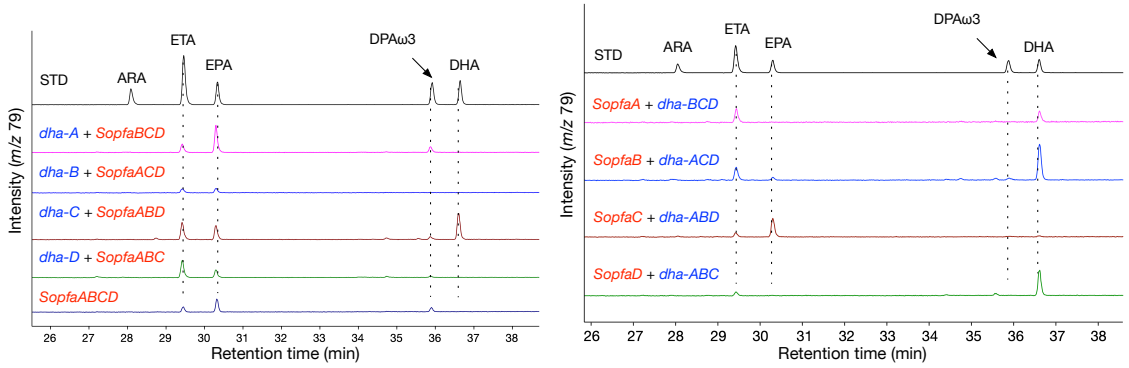

Figure 4-2-1-3. GC/MS analysis traced at *m/z* 79 of products produced in the gene exchange assay. (left) Gene replacement of *Sopfa* genes with *dha* genes (from 2nd to 5th). Standards (top) and *SopfaABCD* (bottom). (right) Gene replacement of *dha* genes with *Sopfa* genes (from 2nd to 5th). Standards (top).

I next constructed chimeric "C" genes to narrow down the chain length control domain. Based on the sequence alignment of C genes, I constructed two chimeric genes, *epa-C-dha-C-chimera1* and *dha-C-epa-C-chimera2*, as shown in Figure 4-2-1-4. In the case of *epa-C-dha-C-chimera1*, EPA was produced by co-expression with *dha-ABD* or *epa-ABD* (Figure 4-2-1-5). The transformant expressing *dha-C-epa-C-chimera2* together with *epa-ABD* or *dha-ABD* produced both

EPA and DHA (Figure 4-2-1-6). These results clearly indicated that the KS_C or CLF-like domain controlled the carbon chain length. To examine which domain is responsible for this control, I constructed dozens of chimeric genes in which the *dha-C* gene and *epa-C* gene were fused at different points between the KS_C domain and CLF-like domain. However, all the constructs lost PUFA productivity, suggesting that the quaternary structure of KS_C/CLF-like domains are important. Indeed, the recent study showed that the KS_C was interacted with the CLF-like domain and formed as a heteromultimer[2]. Thus, I concluded that both the KS_C and CLF-like domains were important for control of DHA and EPA productions.

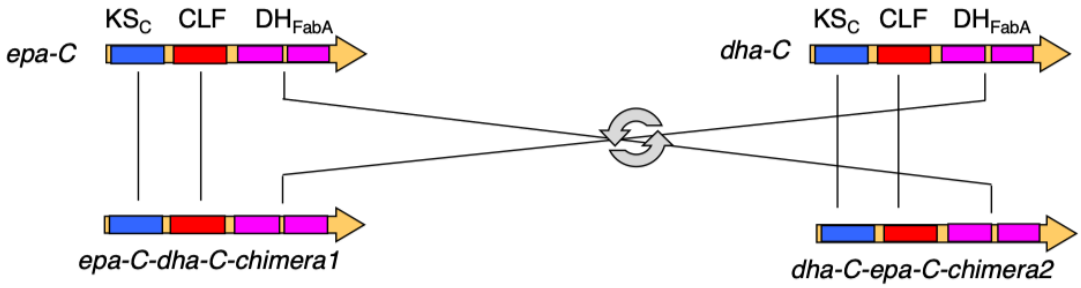

Figure 4-2-1-4. Domain organizations of chimeric "C" genes.

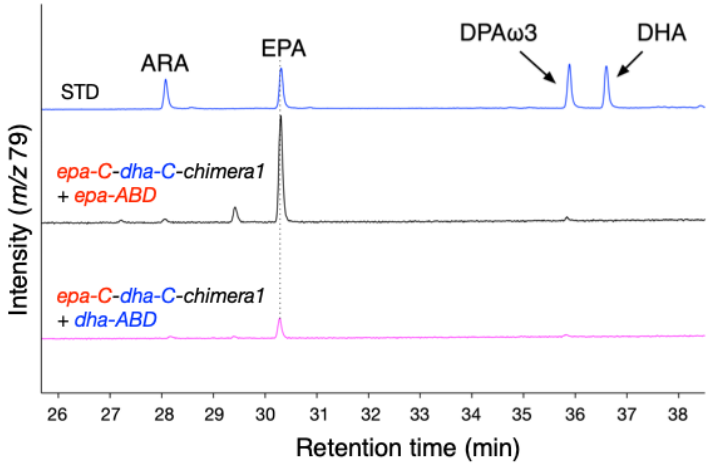

Figure 4-2-1-5. GC/MS analysis trace at *m/z* 79 of products produced by expressing chimeric "C" gene with *epa-ABD* (middle) or *dha-ABD* (bottom).

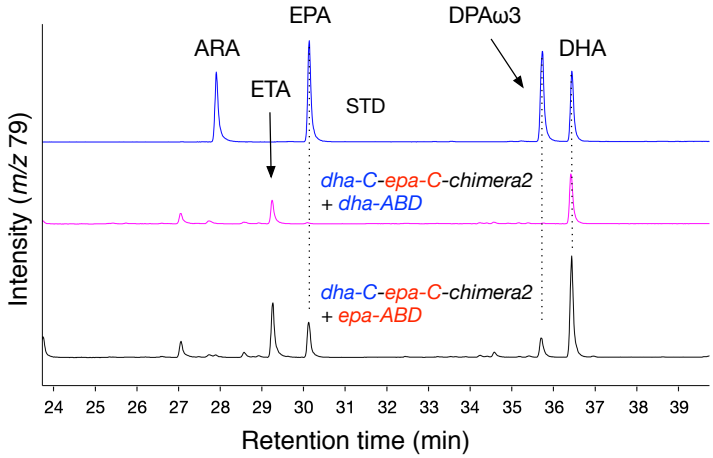

Figure 4-2-1-6. GC/MS analysis trace at *m/z* 79 of products produced by expressing chimeric "C" gene with *dha-ABD* (middle) or *epa-ABD* (bottom).

4.2.2. Mechanism for control of carbon chain length of final products in PUFA synthases

I next carried out *in vitro* experiments using recombinant KS_C/CLF-like domains with acyl-ACPs. Because the functions of the KS_A domain in the "A" subunit were also still unclear, I prepared both truncated KS enzymes to investigate their roles in PUFA biosynthesis. I tried to express a truncated enzyme containing only the KS_A domains in EPA and DHA enzymes, but no soluble protein was obtained. Instead, I prepared truncated KS_A-MAT domains as soluble proteins (Figure 4-2-2-1). I also enzymatically prepared various acyl-ACPs as substrates by the same method in chapter 3. Then, I carried out *in vitro* condensation reactions with each four truncated enzymes, Epa-KS_A-MAT (Epa-KS_A), Epa-KS_C-CLF (Epa-KS_C), Dha-KS_A-MAT (Dha-KS_A), and Dha-KS_C-CLF (Dha-KS_C).

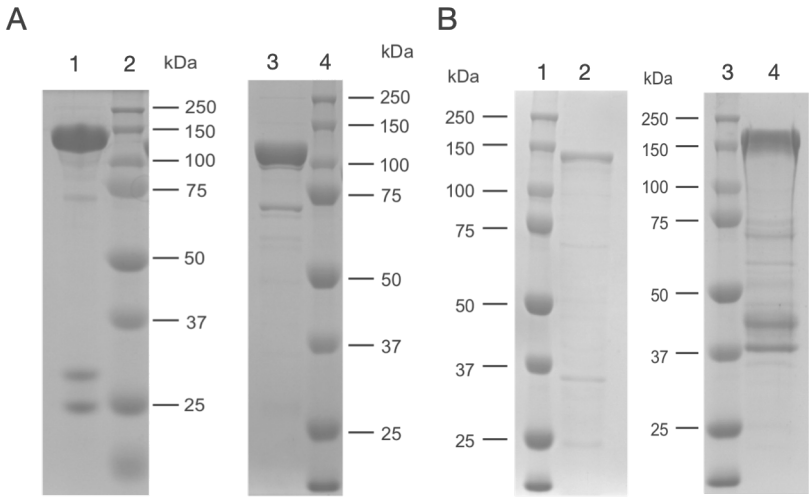

Figure 4-2-2-1. SDS-PAGE analysis of recombinant enzymes. (A) 1, Epa-KS_A-MAT (128 kDa); 2 and 4, Marker; 3, Epa-KS_C-CLF (108 kDa). (B) 1 and 3, Marker; 2, Dha-KS_A-MAT (133 kDa); 4, Dha-KS_C-CLF (160 kDa).

When acetyl-ACP and malonyl-ACP were incubated with the Epa-KS_A or Dha-KS_A, 3-oxobutyryl-ACP was clearly detected by LC-MS, while no product was formed with the KS_C enzymes (Figure 4-2-2-2). The results indicated that the KS_A domain was responsible for the first condensation reactions in EPA and DHA biosynthesis. Then, I examined the subsequent elongation steps. When malonyl-ACP and butyryl-ACP or 3-*cis* hexenoyl-ACP were used as substrates, the KS_A enzymes showed high activities to form 3-oxohexanoyl-ACP and 5-*cis* 3-oxooctenoyl-ACP (Figure 4-2-2-3) while the KS_C enzymes weakly catalyzed these reactions. In contrast, a condensation reaction was not observed when 2-*trans* hexenoyl-ACP was used as substrate (data not shown). These results suggested that the KS_A accepted the short acyl chains and functioned in early biosynthesis steps, and the KS_A strictly recognized geometry of double bonds in substrates.

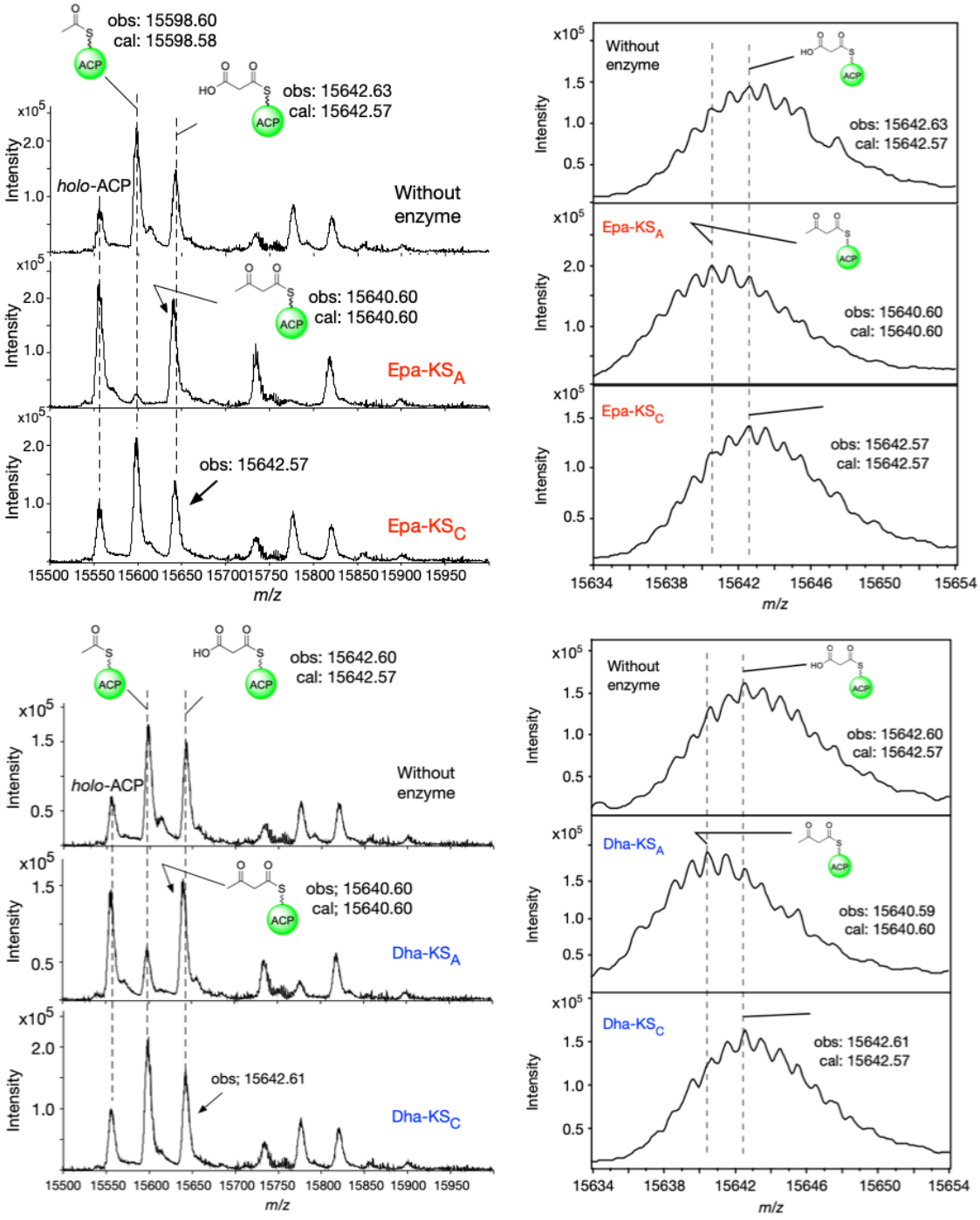

Figure 4-2-2-2. Deconvoluted MS spectra obtained by HPLC-ESI-TOF-MS analysis (left) and their enlarged spectra from *m/z* 15634 to 15654 (right) of reaction mixtures with acetyl-ACP/malonyl-ACP and KS_A (middle), KS_C (bottom) or without enzyme (top).

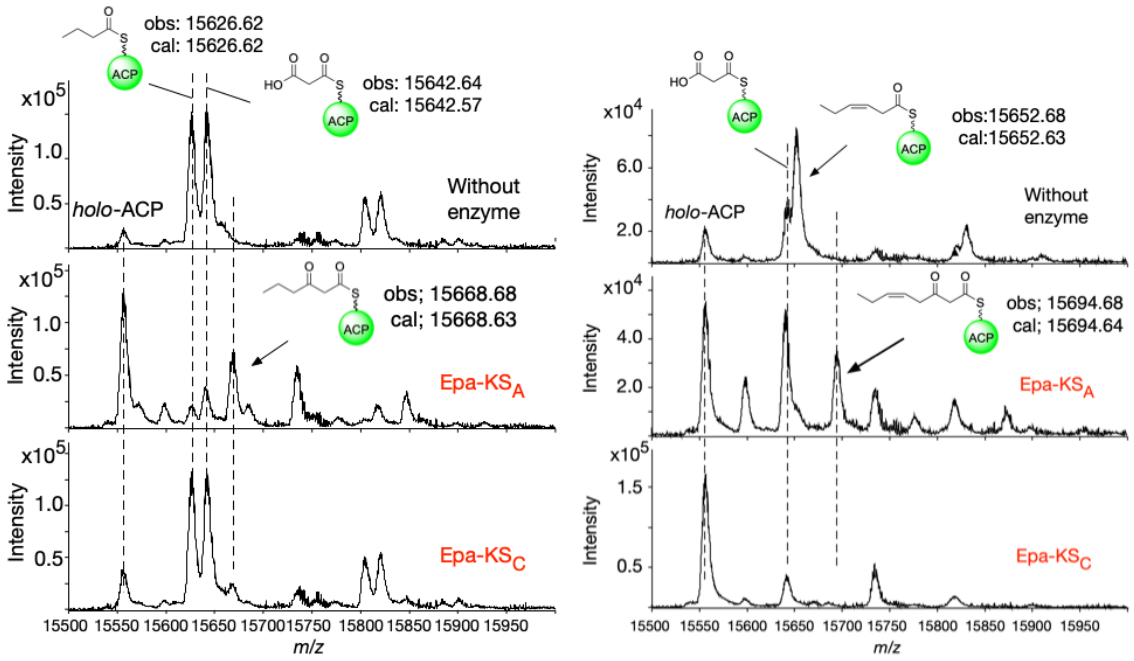

Figure 4-2-2-3. Deconvoluted MS spectra obtained by HPLC-ESI-TOF-MS analysis of reaction mixtures with butyryl-ACP/malonyl-ACP (left) or 3-*cis* hexenoyl-ACP/malonyl-ACP (right) and Epa-KS_A (middle), Epa-KS_C (bottom) or without enzyme (top).

I next examined the functions of the two KS domains during middle to late biosynthetic stages. However, none of the predicted fatty acid substrates were commercially available and their chemical synthesis was also difficult. 4,7-*Cis* decadienoyl-ACP and 3,6,9,12,15-*cis* octadecapentaenoyl-ACP were the only substrates that I could chemically synthesize. I performed *in vivo* analysis for functional analysis of KS_C domains besides the *in vitro* assay. When 4,7-*cis* decadienoyl-ACP and malonyl-ACP were used as the substrates, the Epa-KS_A and Epa-KS_C showed almost the same activities and formed 6,9-*cis* 3-oxododecadienoyl-ACP (Figure 4-2-2-4). Similarly, both the Dha-KS_A and Dha-KS_C showed the same activities (Figure 4-2-2-4).

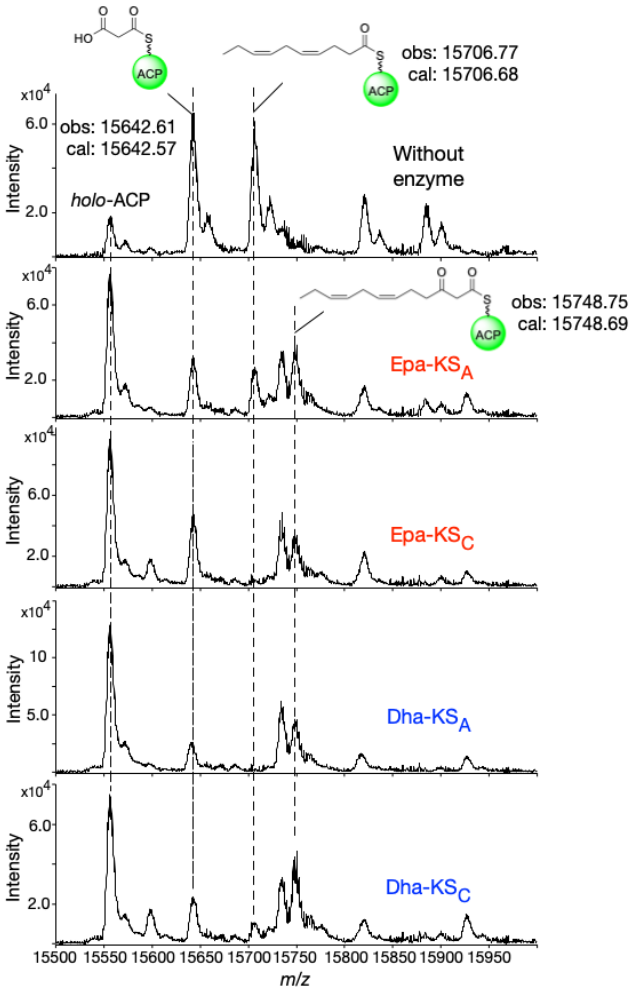

Figure 4-2-2-4. Deconvoluted MS spectra obtained by HPLC-ESI-TOF-MS analysis of reaction mixtures with 4,7-*cis* decadienoyl-ACP/malonyl-ACP and Epa-KS$_A$ (2nd), Epa-KS$_C$ (3rd), Dha-KS$_A$ (4th), or Dha-KS$_C$ (5th). Without enzyme (top).

To get more insight about the role of the KS$_C$ domain, I then constructed two mutated enzymes, Epa-C-KS^0 and Dha-C-KS^0, in which the catalytic Cys residues estimated by the sequence alignments (Figure 4-2-2-5) in the KS$_C$ domains were mutated to Ala, and were co-expressed with *epa-ABD*. In the case of *epa-C-KS^0* expression, α-linoleic acid (ALA; C18:3 ω3) and 7,10,13-*cis* hexadecatrienoic acid (C16:3 ω3) were produced as major and minor products, respectively (Figure 4-2-2-6). Similarly, DHA production was completely abolished and ALA was produced as the major product with *dha-C-KS^0* (Figure 4-2-2-6). Considering that ALA was produced as the major product

in both cases, the products including ALA were shunt products probably formed by chain elongation from C12:3 ω3 intermediate. Therefore, the KS_C domain was suggested to catalyze the intrinsic chain elongation during the middle biosynthetic stage.

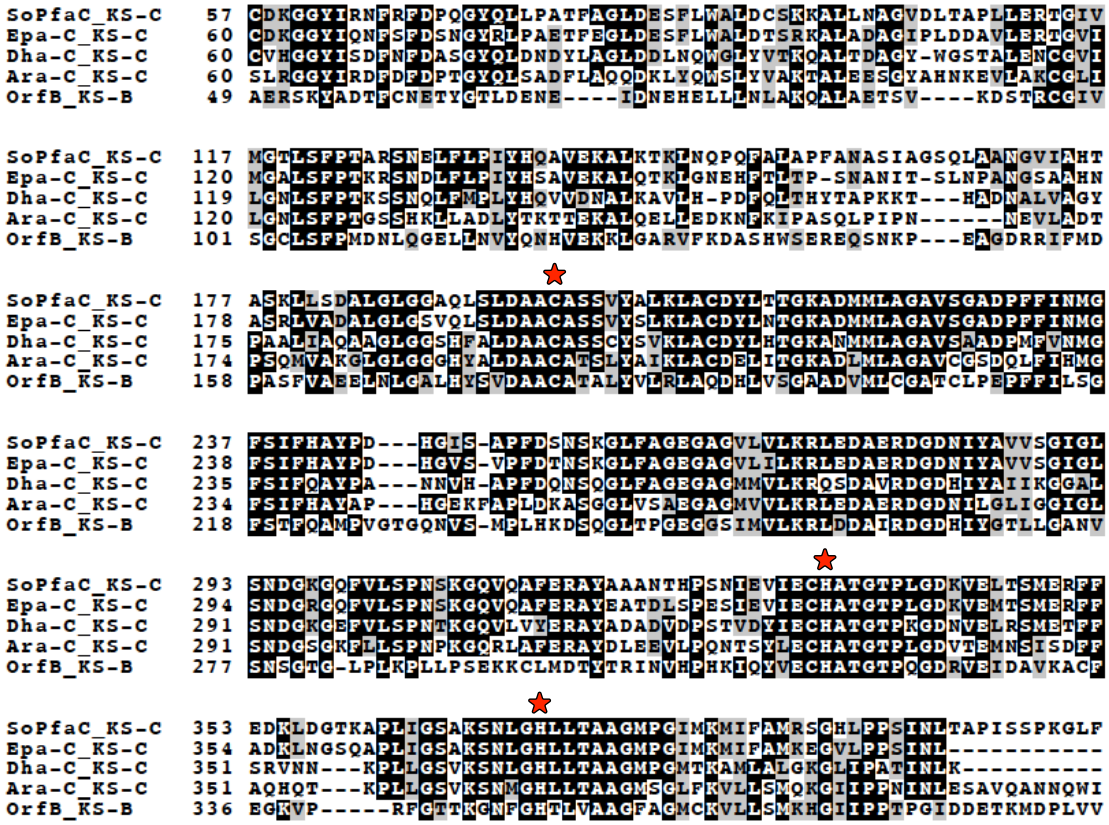

Figure 4-2-2-5. Sequence alignments of KS_C domains in PUFA synthases. Red stars show catalytic Cys/His residues. From top to bottom, KS_C domain of SoPfaC in EPA synthase of *S. oneidensis* MR-1, KS_C domain of Epa-C of *P. profundum* SS9, KS_C domain of Dha-C of *M. marina*, KS_C domain of Ara-C of *A. marina*., and KS_B domain of OrfB of *Schizochytrium* sp.

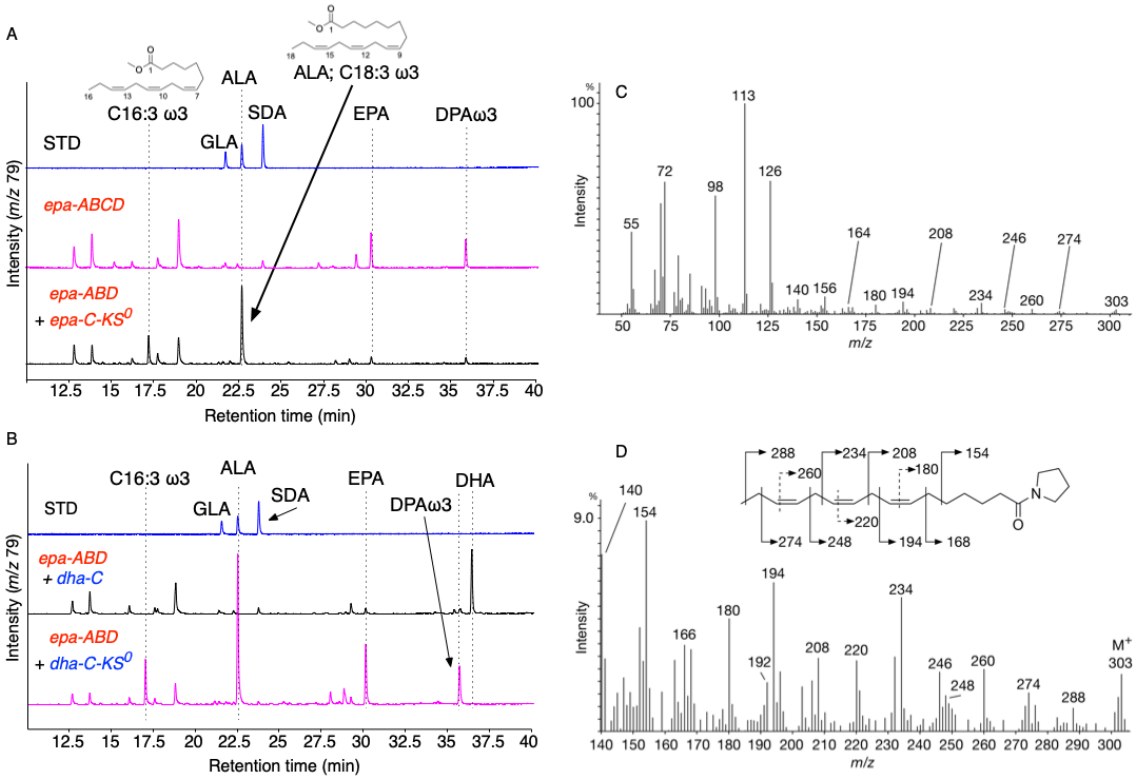

Figure 4-2-2-6. GC-MS analysis traced at *m/z* 79 of products produced by co-expression of e*pa-C-KS*^{0} or *dha-C-KS*^{0} with *epa-ABD*. (A) co-expression of *epa-C* (wild type) (middle) or *epa-C-KS*^{0} (KS mutant) (bottom) with *epa-ABD.* (B) co-expression of *dha-C* (wild type) (middle) or *dha-C-KS*^{0} (KS mutant) (bottom) with e*pa-ABD*. Authentic standards of methyl esters of GLA (C18:3 ω6), ALA (C18:3 ω3), and SDA (C18:4 ω3) (top). GC-MS analysis of the pyrrolidine derivative of 7,10,13-*cis* hexadecatrienoic acid. MS spectrum ranging from 50 to 310 *m/z* of the pyrrolidine derivative of 7,10,13-cis hexadecatrienoic acid (C) and enlarged MS spectrum from 140 to 310 *m/z* (D).

I next carried out *in vitro* reactions with 3,6,9,12,15-*cis* octadecapentaenoyl-ACP as the substrate to investigate the final condensation reaction of EPA. Surprisingly, when the Epa-KS$_A$ and Dha-KS$_A$ were used as catalysts, the estimated 5,8,11,14,17-*cis* 3-oxoeicosapentaenoyl-ACP was detected by LC-MS while no product was observed when the Epa-KS$_C$ and Dha-KS$_C$ were used (Figure 4-2-2-7), indicating that the KS$_A$ domain again participated in the last chain elongation in EPA biosynthesis (from C_{18} to C_{20}).

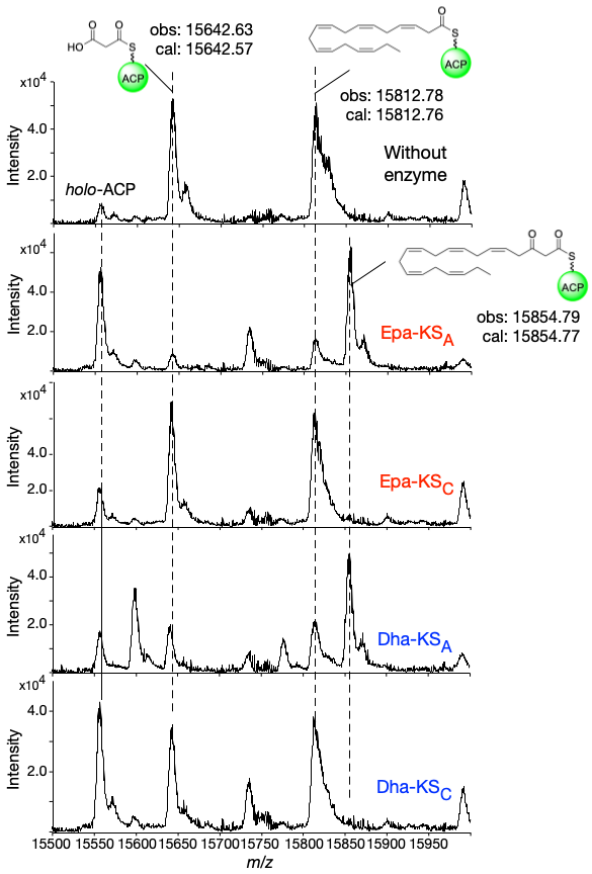

Figure 4-2-2-7. Deconvoluted MS spectra obtained by HPLC-ESI-TOF-MS analysis of reaction mixtures with 3,6,9,12,15-*cis* octadecapentaenoyl-ACP/malonyl-ACP and Epa-KS_A (2^{nd}), Epa-KS_C (3^{rd}), Dha-KS_A (4^{th}), Dha-KS_C (5^{th}) . Without enzyme (top).

To investigate the final chain elongation in DHA biosynthesis (from C_{20} to C_{22}), I employed a combination enzyme assay (Figure 4-2-2-9) because preparation of the predicted substrate, 2,5,8,11,14,17-*cis* eicosahexaenoyl-ACP, was difficult. After addition of the Epa-KR-DH_{PKS} into the abovementioned reaction mixture using 3,6,9,12,15-*cis* octadecapentaenoyl-ACP and the Dha-KS_A, a product whose molecular weight was identical to the estimated product, 3-hydroxy-5,8,11,14,17-*cis* eicosapentaenoyl-ACP, was detected. By further addition of the Epa-DH_{FabA} and Dha-KS_C, a plausible 2,4,7,10,13,16,19-docosaheptaenoyl-ACP (Figure 4-2-2-9) was also detected, suggesting that the KS_C domain in Dha-C catalyzed the chain elongation from C_{20} to C_{22}. Taken these results together, I proposed EPA and DHA biosynthesis pathway as shown in Figure 4-2-2-10. The KS_A accepted short

acyl chains while the KS_C did middle acyl chains in the early and middle biosynthetic stage, respectively. In the late stage, the condensation of 3,6,9,12,15-*cis* octadecapentaenoyl-ACP (from C_{18} to C_{20}), the last condensation in EPA biosynthesis, was catalyzed by the KS_A domain in both DHA and EPA biosynthesis. In EPA biosynthesis, a 5,8,11,14,17-*cis* 3-oxoeicosapentaenoyl-ACP intermediate would be hydrolyzed after the reactions catalyzed by the KR, DH_{PKS}, and ER domains. In contrast, 2,5,8,11,14,17-*cis* eicosahexaenoyl-ACP formed by the KR and DH_{FabA} domains would be used as the substrate of the KS_C domain to form 4,7,10,13,16,19-*cis* docosahexaenoyl-ACP in DHA biosynthesis. After reduction, dehydration, and enoyl reduction of the intermediate, the product would be released.

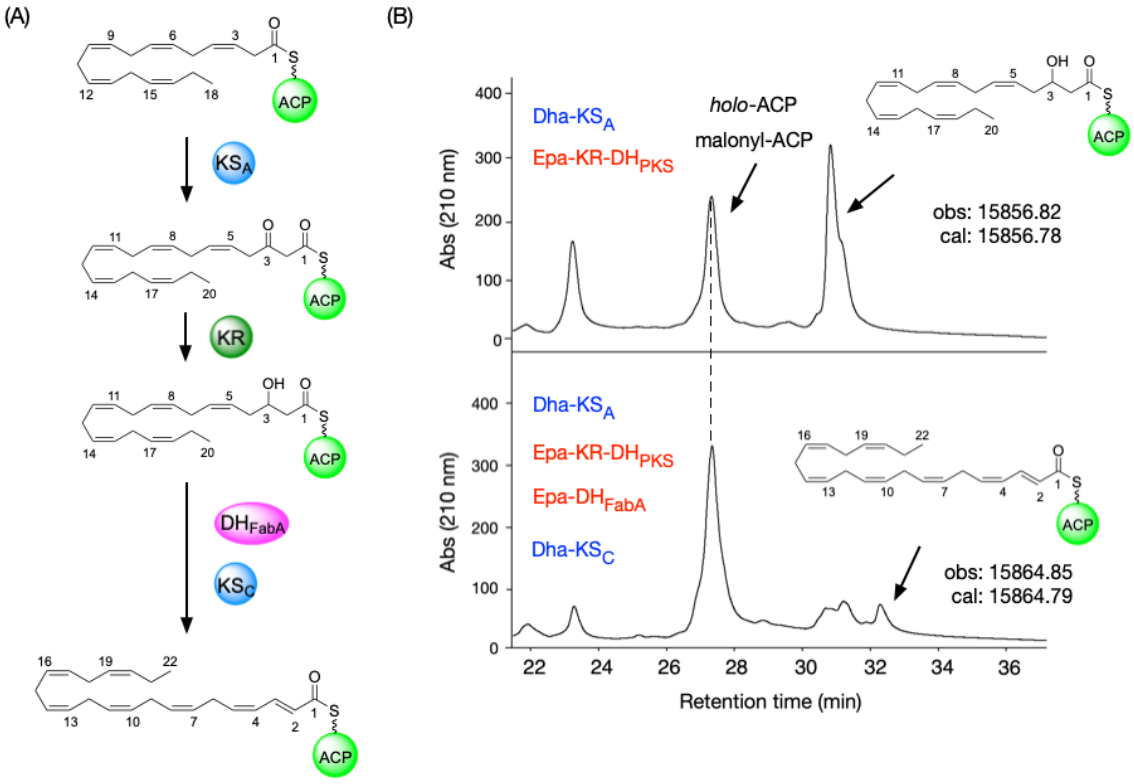

Figure 4-2-2-9. *In vitro* combination reactions. (A) Reaction scheme of *in vitro* combination reactions. (B) HPLC analysis (UV 210 nm) of *in vitro* combination reactions using 3,6,9,12,15-*cis* octadecapentaenoyl-ACP, Dha-KS_A, and Epa-KR-DH_{PKS} (top), plus Epa-DH_{FabA} and Dha-KS_C (bottom).

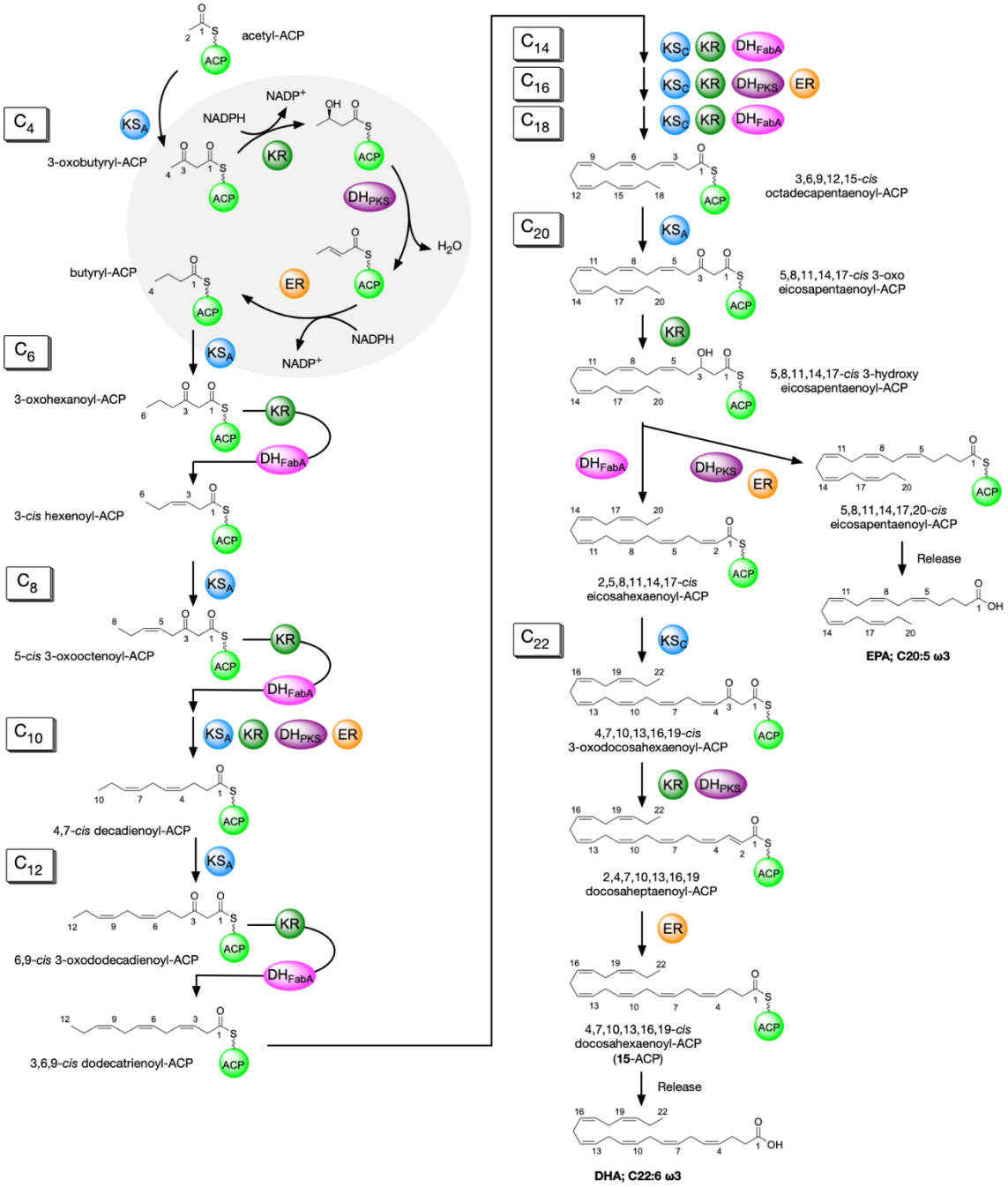

Figure 4-2-2-10. Proposed DHA and EPA biosynthetic pathway from acetyl- (C_2) to C_{20} or C_{22} products

4.3. Discussion

In this chapter, I studied the mechanism for controlling carbon chain length of the products, EPA (C_{20}) and DHA (C_{22}), through *in vivo* and *in vitro* experiments. The *in vitro* reactions with various acyl-ACPs showed that PUFA synthases used the two KS domains depending on carbon chain length of acyl-ACPs for chain elongation reactions. In the early biosynthetic stage, the KS_A was responsible for chain elongation reactions to form elongated β-oxoacyl-ACPs. Then, as described in chapter 3, the KR, DH_{PKS}, DH_{FabA}, ER domains catalyze the proper reactions depending on carbon chain length to form saturated or *cis* double bond form. In the middle biosynthetic stage, the elongation domain responsible was switched to the KS_C. In the late biosynthetic stage, surprisingly, the elongation domain responsible was switched again to the KS_A at C_{18} to C_{20} step. The difference between EPA and DHA biosynthesis was the elongation reaction from C_{20} to C_{22} catalyzed by the KS_C domain (Figure 4-2-2-10). The facts that a substrate with *trans* double bond was not accepted by the KS domains as a substrate suggested the KSs recognized geometry and position of double bond of intermediates for appropriate PUFA productions.

When PUFA synthase genes were identified in 2001, a domain located at next to KS_C domain was called as "CLF" domains because it showed a similarity to β-ketoacyl synthase but had no active residue Cys like a CLF in Type II PKS. In type II PKS system, active KS and CLF showed a heterodimeric structure and biosynthesized poly-β-keto chains (Figure 4-3-1). One of the roles of the CLF was priming reaction, decarboxylation of malonyl unit to form acetyl unit[3,4]. Another role of the CLF was determination of chain length of polyketide products[3,5-7]. It was proposed that the chain length of polyketides is controlled by the size of the catalytic pocket in a KS/CLF interface (Figure 4-3-2). Recent studies showed that highly reducing polyketide polyene was also produced by type II PKS enzymes (Figure 4-3-1)[8,9]. The intermediates were modified by discrete KR and DH in this type II PKS system. The chemical structures of the products would be strictly controlled by KS/CLF during

elongation reactions. In other words, the KS/CLF functioned as gatekeeper and selected an appropriate intermediate for next elongation reaction (Figure 4-3-3). I proposed that the role of CLF-like domain in PUFA synthase is a gatekeeper and the KS_C/CLF strictly select the intermediate for next elongation.

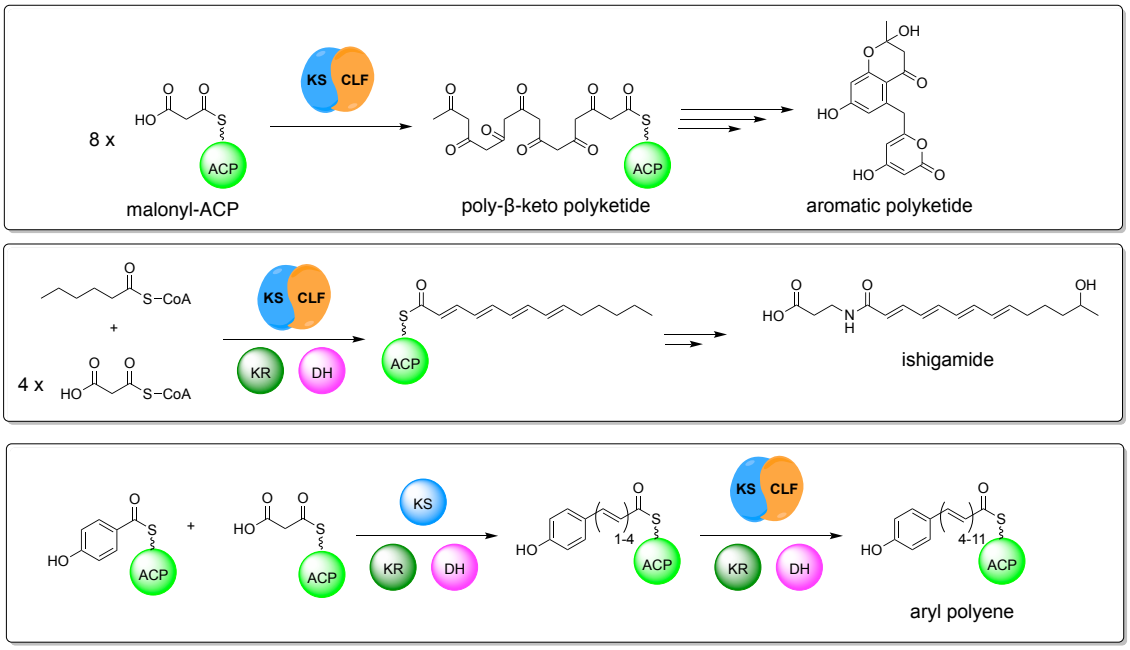

Figure 4-3-1. Biosynthetic pathway of aromatic and high reducing polyketides by type II PKS enzymes

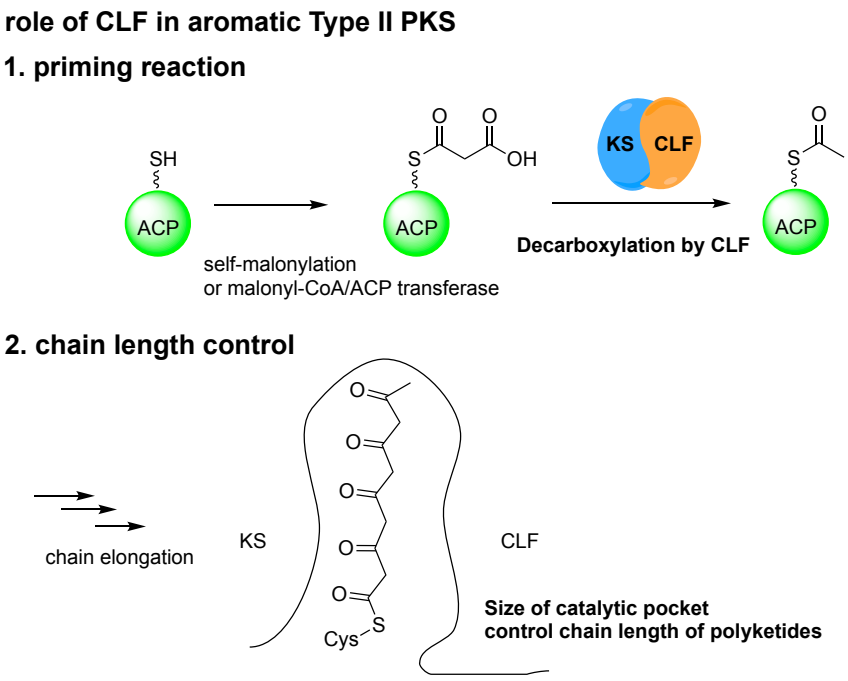

Figure 4-3-2. Roles of CLF in aromatic type II PKS system.

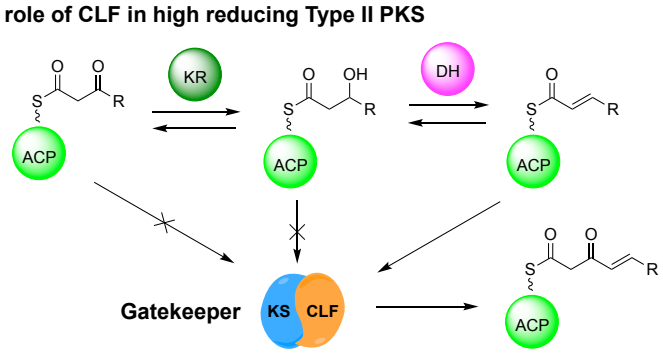

Figure 4-3-3. Putative role of CLF in high reducing type II PKS system

As mentioned in introduction, Orikasa *et al*. suggested that the AT domain in subunit B was important for EPA and DHA production[1] although the detailed function was unclear. Recently, Santin *et al*. carried out *in vitro* experiments for analysis of function of MAT and AT domains[10]. They showed MAT domains expectedly showed loading activity against malonyl-CoA to form malonyl-ACP while AT domains showed no and weak loading activities against acetyl-CoA and malonyl-CoA, respectively. These evidences indicated that the AT domain was not involved in an initiation step in PUFA biosynthesis and suggested that it would be important for termination steps. Thus, I next examined the role of the AT domain in as described chapter 5.

References

1. Y. Orikasa, M. Tanaka, S. Sugihara, R. Hori, T. Nishida, A. Ueno, N. Morita, Y. Yano, K. Yamamoto, A. Shibahara, H. Hayashi, Y. Yamada, A. Yamada, R. Yu, A. Watanabe, H. Okuyama, pfaB products determine the molecular species produced in bacterial polyunsaturated fatty acid biosynthesis. *FEMS Microbiology Letters* **295**, 170–176 (2009).
2. M. Naka, K. Ikeuchi, S. Hayashi, Y. Satoh, Y. Ogasawara, T. Dairi. Subtle control of carbon chain length in polyunsaturated fatty acid synthases. *ACS Chem. Biol.* doi.org/10.1021/acschembio.9b00803.
3. C. Hertweck, A. Luzhetskyy, Y. Rebets, A. Bechthold, Type II polyketide synthases: gaining a deeper insight into enzymatic teamwork. *Nat. Prod. Rep*., **24**, 162–190 (2007).
4. C. Bisang, P. F. Long, J. Cortes, J. Westcott, J. Crosby, A. L. Matharu, R. J. Cox, T. J. Simpson, J. Staunton, P. F. Leadlay. A chain initiation factor common to both modular and aromatic polyketide synthases. *Nature* **401**, 502–505 (1999).
5. Y. Tang, S. C. Tsai, C. Khosla, Polyketide chain length control by chain length factor. *J. Am. Chem. Soc*., **125**, 12708–12709 (2003).
6. K. K. Burson, C. Khosla, Dissecting the chain length specificity in bacterial aromatic polyketide synthases using chimeric genes. *Tetrahedron* **56**, 9401–9408 (2000).
7. R. McDaniel, S. E. Khosla, D. A. Hopwood, C. Khosla, Engineered biosynthesis of novel polyketides: Manipulation and analysis of an aromatic polyketide synthase with unproven catalytic specificities. *J. Am. Chem. Soc.,* **115**, 11671–11675 (1993).
8. G. L. C. Grammbitter, M. Schmalhofer, K. Karimi, Y. Shi, T. A. Schoner, N. J. Tobias, N. Morgner, M. Groll, H. B. Bode, An uncommon type II PKS catalyzes biosynthesis of aryl polyene pigments. *J. Am. Chem. Soc*., **141**, 16615–16623 (2019).
9. D. Du, Y. Katsuyama, K. Shin-ya, Y. Ohnishi, Reconstitution of a type II polyketide synthase that catalyzes polyene formation. *Angew. Chem. Int. Ed.,* **57**, 1954–1957 (2018).
10. O. Santin, G. Moncalian, Loading of malonyl-CoA onto tandem acyl carrier protein domains of polyunsaturated fatty acid synthases. *J. Biol. Chem.*, **293**, 12491–12501 (2018).

Chapter 5
Off-loading mechanism of products in PUFA synthases

5.1. Introduction

In chapter 4, I studied the mechanism for control of carbon chain length of PUFA products and showed that PUFA synthase utilized the two KS domains, KS_A and KS_C, for elongation reactions depending on carbon chain length of acyl-ACPs. The substrate specificity of the KS_C/CLF was important for controlling EPA and DHA productions. After condensation and modification reactions catalyzed by KSs, KR, DHs, and ER domains, PUFA-intermediates believed to be released from ACP to produce final products. However, PUFA synthases had no TE domain and the off-loading mechanism was unclear. In this chapter, I examined the mechanism.

All PUFA synthases have two AT domains in subunit A and B/C. Both AT domains showed similarity to malonyl-CoA/ACP transacylases. As discussed in chapter 4, the AT domain in subunit A showed an efficient loading activity of malonyl-CoA onto *holo*-ACP but the AT domain in subunit B/C showed weak and no loading activity to malonyl-CoA and acetyl-CoA[1], respectively. The results suggested that the AT domain in subunit B was not involved in the initiation step in PUFA biosynthesis. Considering the results, which KS_A catalyzed condensation of acetyl-ACP with malonyl-ACP, I proposed that acetyl-ACP is generated by decarboxylation of malonyl-ACP and condensed with malonyl-ACP to form 3-oxobutyryl-ACP by the KS_A domain in the initiation step. Thus, I carried out *in vitro* reactions using the KS_A and malonyl-ACP as preliminary experiments. As the results, 3-oxobutyryl-ACP were detected when malonyl-ACP was used as the sole substrate, indicating that an initiation reaction in PUFA synthase was decarboxylation catalyzed by the KS_A domain and that C_2 unit, acetyl-ACP, was generated (Figure 5-1-1 and -2).

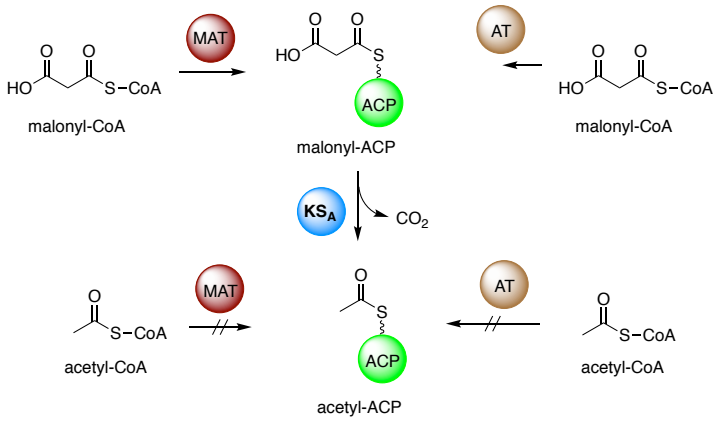

Figure 5-1-1. Proposed priming reactions in PUFA biosynthesis pathway by PUFA synthases.

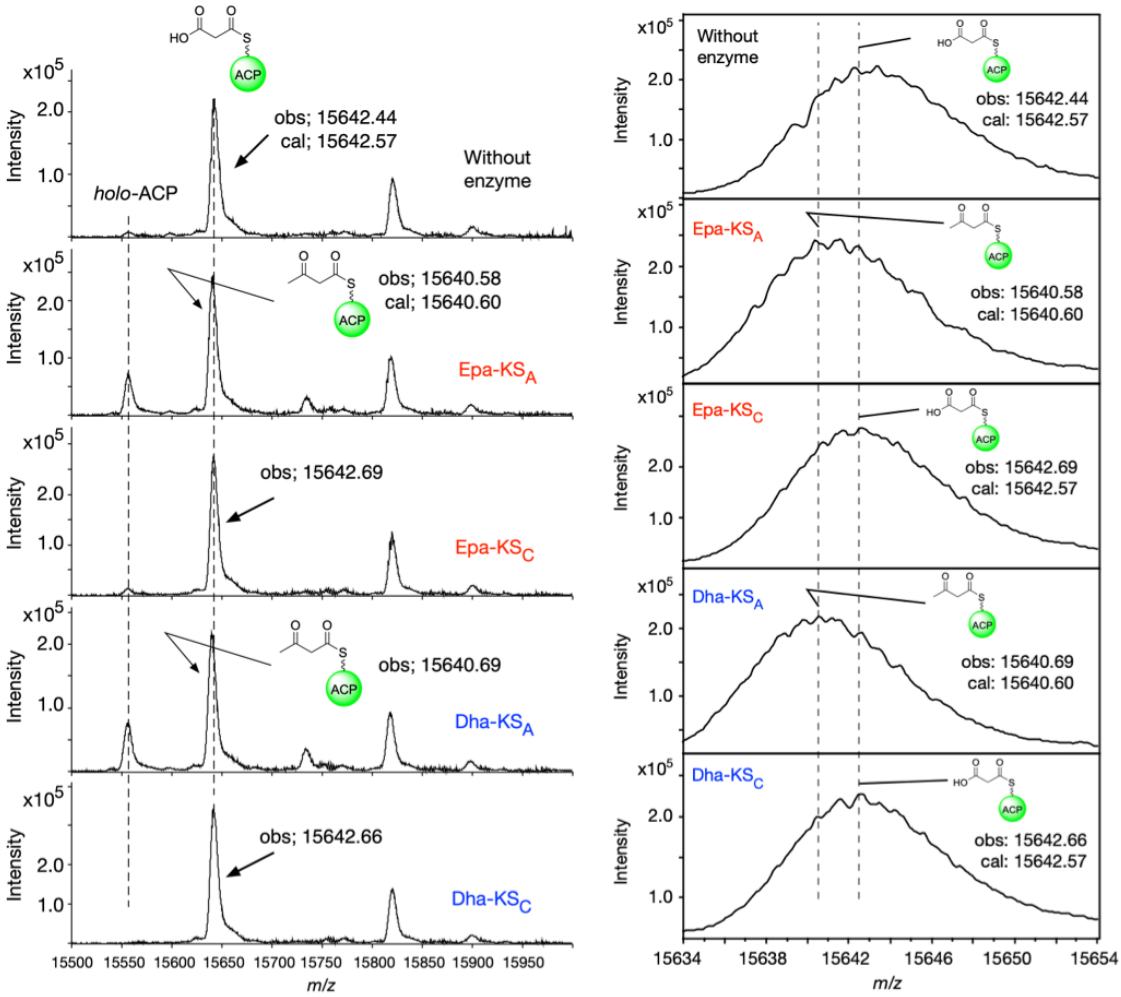

Figure 5-1-2. Deconvoluted MS spectra obtained by HPLC-ESI-TOF-MS analysis (left) and their enlarged spectra from m/z 15634 to 15654 (right) of reaction mixtures with enzymes and malonyl-ACP. Without enzyme (top), with Epa-KS$_A$ (2nd), with Epa-KS$_C$ (3rd), with Dha-KS$_A$ (4th), or with Dha-KS$_C$ (bottom).

As for the termination step in PUFA synthases, it was reported that DHA synthase of microalgae *Schizochytrium* sp. produced DHA as free fatty acids[2], suggesting that a catalytic domain encoded in subunit gene would be responsible for hydrolysis of final products. Other group identified a discrete gene *orf6* encoding TE homologous upstream of PUFA synthase of *P. profundum* gene operon and showed that Orf6 had a hydrolytic activity on long-chain acyl-CoA[3]. However, disruption of the gene effected on a decrease of PUFA productivity in native strains, but no effect on the productivity and PUFA profiles was observed when the gene was co-expressed with PUFA synthase genes in *E. coli*[4]. Therefore, they proposed it as the Orf6 was functioned as type II TE, which was accessory enzyme and could be used to enhance product yields[5]. Therefore, a gene and domain responsible for off-loading of products from ACP is not identified. As mentioned in chapter 4, the AT domain in subunit B was important for EPA and DHA production[6]. Furthermore, the AT domain belongs to α/β-hydrolase superfamily, which includes α/β-hydrolase TE. Thus, I proposed the AT domain catalyze hydrolysis reaction of acyl-ACPs and is involved in the off-loading of final products.

5.2. Results

5.2.1. The effect of site-directed mutagenesis on AT domains

I first confirmed whether the AT domain was essential in PUFA biosynthesis. As described in chapter 2 and 3, I have already cloned the DHA synthase genes *orfA, B, C* of *Schizochytrium* sp., EPA synthase genes, *epa-A, B, C, D* of *P. profundum*, and DHA synthase genes *dha-A, -B, -C, -D* of *M. marina* and succeeded in PUFA productions using *E. coli* as the heterologous host. Thus, I carried out *in vivo* inactivation experiments. Based on the sequence alignment of the AT domains as described in chapter 3, the active residue Ser in GxSxG motif was mutated to Ala by sire-directed mutagenesis to construct AT mutant genes, *orfB-AT^0*, *epa-B-AT^0*, and *dha-B-AT^0*. Each mutant gene was co-expressed with corresponding gene sets in *E. coli*, and PUFA products were analyzed by GC-MS. The GC-MS analysis showed that the DHA productivity of transformants expressing *orfB-AT^0* was drastically decreased by about 90% compared with that of wild type (Figure 5-2-1-1). The similar results were obtained using the mutant gene of EPA synthase of *P. profundum* and DHA synthase of *M. marina*, indicating that the AT domain was important for PUFA biosynthesis (Figure 5-2-1-2).

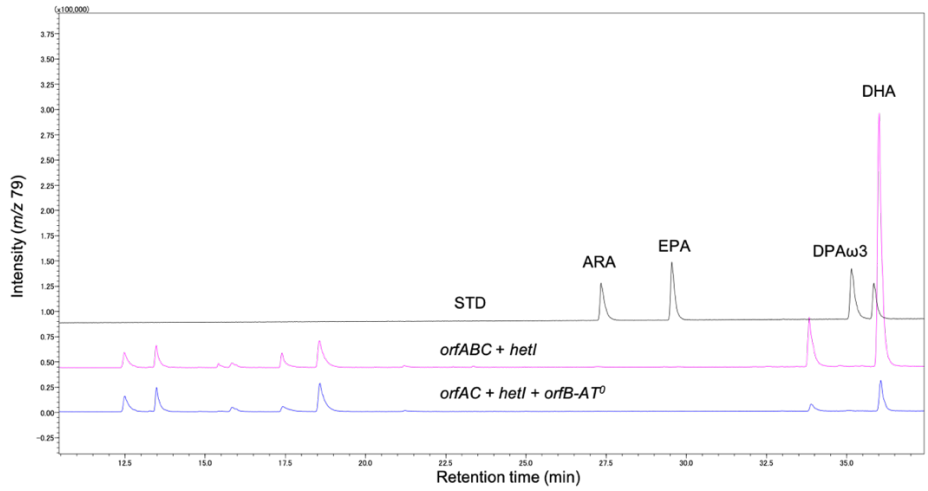

Figure 5-2-1-1. GC/MS analysis traced at *m/z 79* of the products produced by the transformants expressing *orfAC, hetI,* and *orfB* (middle) or *orfB-AT^0* (bottom), authentic standards (top).

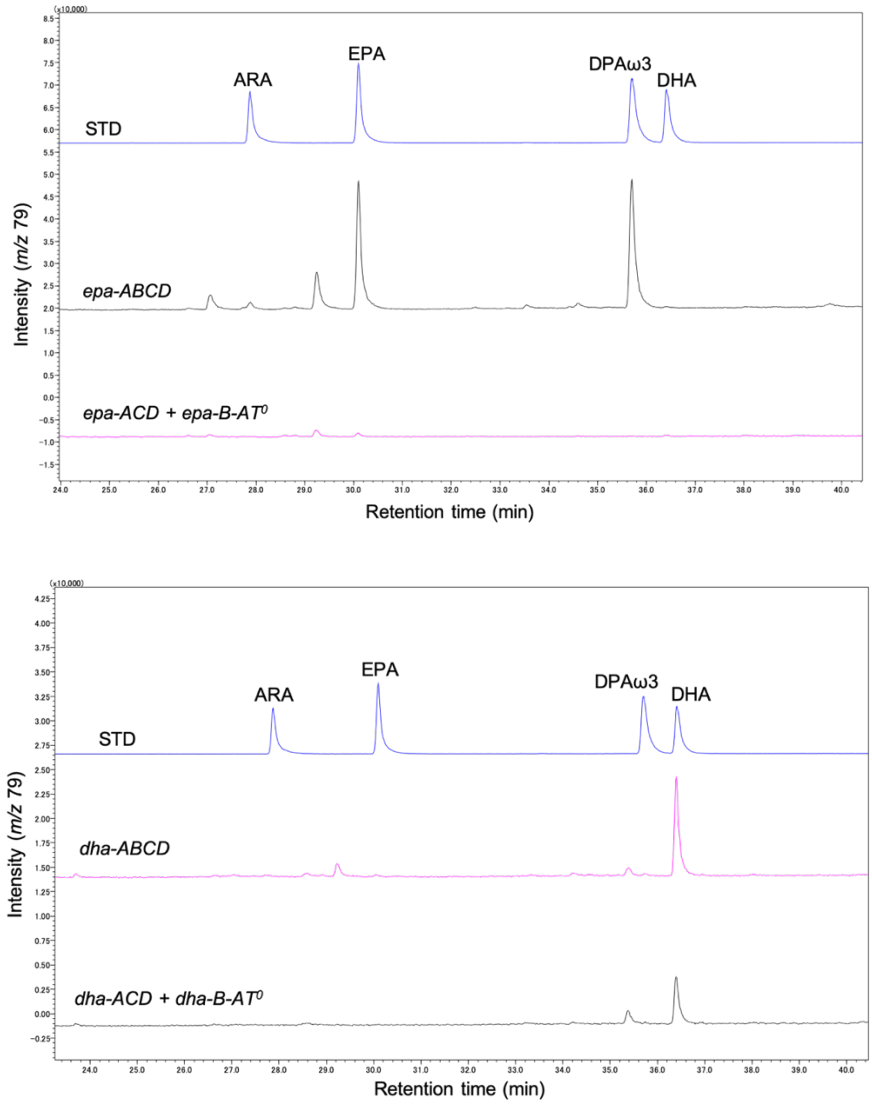

Figure 5-2-1-2. GC/MS analysis traced at *m/z 79* of the products produced by the transformants expressing *epa* genes (top) or *dha* genes (bottom), authentic standards (top trace).

5.2.2. Off-loading reactions catalyzed by AT domains

I next carried out *in vitro* hydrolytic reactions of the AT domain with acyl-ACP substrates. The AT domain was encoded in middle of *orfB* gene between the CLF-like and ER domain. I first tried to obtain a truncated recombinant AT protein using *E. coli* BL21(DE3). But any of trial failed because all the truncated proteins were insoluble. Thus, whole OrfB fused with maltose-binding protein was obtained as a soluble protein and used for *in vitro* reactions (Figure 5-2-2-1). I prepared

docosahexaenoyl-CoA by organic synthesis and docosahexaenoyl-ACP was enzymatically synthesized as the same method described in chapters 3 and 4. The formation of docosahexaenoyl-ACP was confirmed by HPLC-ESI-MS analysis (Figure 5-2-2-2). After docosahexaenoyl-ACP was incubated with 1 μM OrfB for 1 h at 30℃, the reaction mixture was analyzed by HPLC. The HPLC analysis showed that docosahexaenoyl-ACP was mostly hydrolyzed to *holo*-ACP, indicating that the OrfB catalyzed the release reaction of the final product (Figure 5-2-2-2). Furthermore, free fatty acids of DHA was observed in the reaction mixture (Figure 5-2-2-2). Then, I prepared recombinant OrfB-AT^0, in which the active residue Ser in the AT domain was mutated to Ala, and the enzyme was incubated with docosahexaenoyl-ACP under the same conditions. HPLC analysis showed that no hydrolytic reactions were observed in the AT mutant reaction mixture. Thus, the AT domain in OrfB catalyzed a hydrolysis reaction and functioned as TE domain in microalgal PUFA synthase.

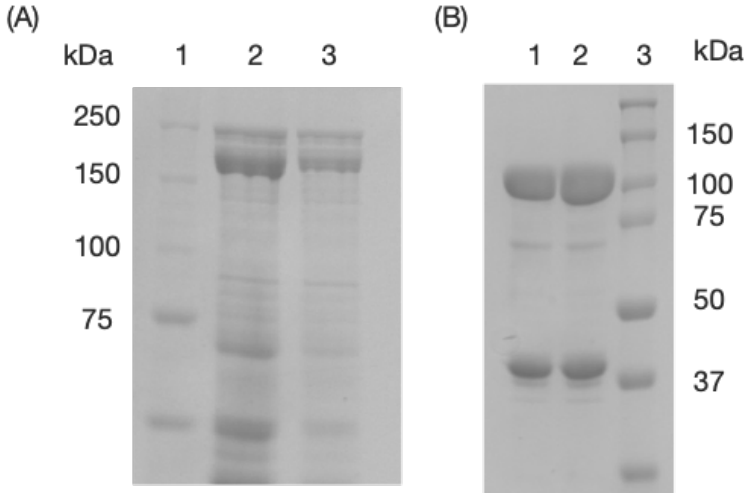

Figure 5-2-2-1. SDS-PAGE analysis of OrfB enzymes (A) and Epa-B enzymes (B). Left, 1: Epa-B (117 kDa), 2: Epa-B-AT^0 (117 kDa), 3: Markers. Right, 1: Markers, 2: OrfB (260 kDa), 3: OrfB-AT^0 (260 kDa).

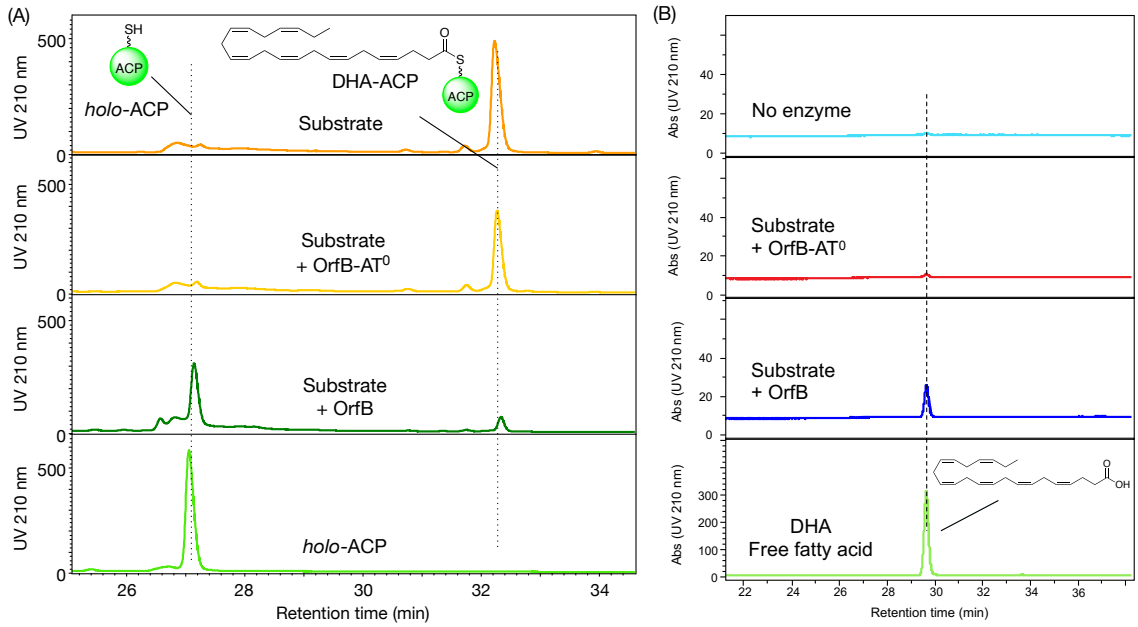

Figure 5-2-2-2. (A) HPLC analysis (UV 210 nm) of *in vitro* reactions using DHA-ACP and OrfB-AT^0 (2nd) or OrfB (3rd). Substrate (top) and *holo*-ACP (bottom). (B) HPLC analysis (UV 210 nm) of *in vitro* reactions using DHA-ACP and OrfB-AT^0 (2nd) or OrfB (3rd). No enzyme (top) and standards of free fatty acids of DHA (bottom)

To confirm the role of the AT domain, I carried out the same experiments using AT domain in EpaB of the EPA synthase of *P. profundum*. I successfully obtained recombinant EpaB fused with MBP as a soluble protein and enzymatically synthesized eicosapentaenoyl-ACP from eicosapentaenoyl-CoA (Figure 5-2-2-3). The hydrolytic reaction was carried out with 5 μM EpaB for 1 h at 20°C. HPLC analysis showed *holo*-ACP and free fatty acids of EPA were clearly detected in the reaction mixture. When EpaB-AT^0, in which the Ser residue was mutated to Ala, was used, no hydrolysis reaction was observed (Figure 5-2-2-3).

As mentioned in chapter 1, acyltransferases in FASs were reported to catalyze the direct acyl transfer of fatty acids to accepter molecules. To examine the possibility of direct transfer from acyl-ACP to CoA or glycerol-3-phosohate in bacterial PUFA synthases, these acceptors were added into the reaction mixtures. No effects on reaction activities were observed (Figure 5-2-2-4), suggesting that

PUFAs were transferred on phospholipids via re-activation by acyl-CoA synthetases after *de novo* synthesis.

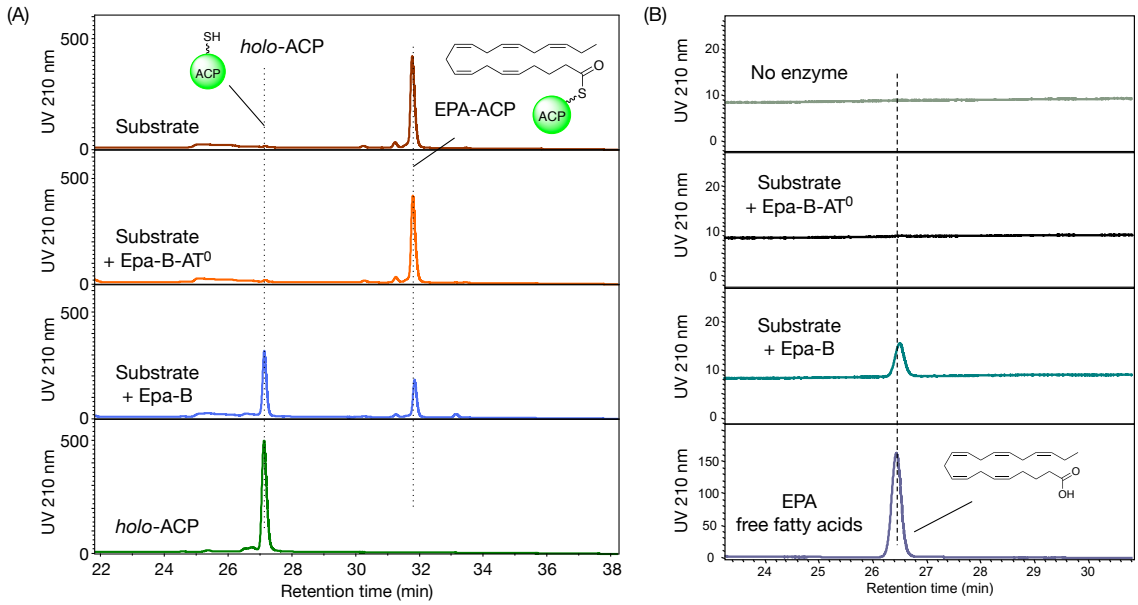

Figure 5-2-2-3. (A) HPLC analysis (UV 210 nm) of *in vitro* reactions using EPA-ACP and Epa-B-AT^0 (2nd) or Epa-B (3rd). Substrate (top) and *holo*-ACP (bottom). (B) HPLC analysis (UV 210 nm) of *in vitro* reactions using EPA-ACP and Epa-B-AT^0 (2nd) or Epa-B (3rd). No enzyme (top) and standards of free fatty acids of EPA (bottom)

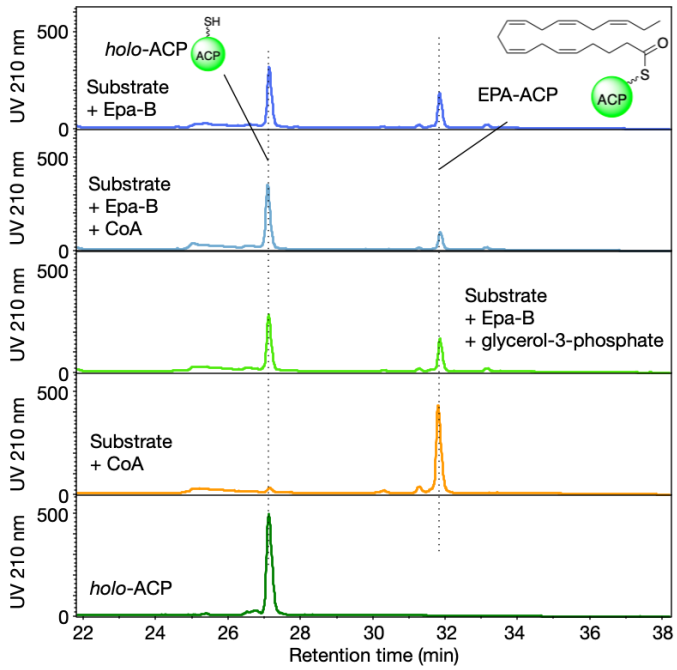

Figure 5-2-2-4. HPLC analysis (UV 210 nm) of *in vitro* reactions using EPA-ACP and Epa-B (top), Epa-B/CoA (2nd), Epa-B/glycerol-3-phosphate (3rd), or CoA (4th). *holo*-ACP (bottom).

Using various acyl-ACPs as substrates, I examined the substrate specificity of the AT domain in OrfB. When short chain length substrates, butyryl-ACP and hexanoyl-ACP, were used, almost no hydrolytic activities were observed. As for middle chain length substrates, 4,7-*cis* decadienoyl-ACP, myristoyl-ACP (C_{14}), and palmitoyl-ACP (C_{16}) were also not hydrolyzed (Figure 5-2-2-5). In the case of long acyl chain length substrates, saturated substrate, stearoyl-ACP (C_{18}) was accepted by the AT domain in OrfB as substrate but unsaturated substrate, 3,6,9,12,15-*cis* octadecapentaenoyl-ACP (C_{18}), was not. The AT domain also catalyzed hydrolysis of eicosapentaenoyl-ACP (Figure 5-2-2-5). In case of the AT domain in Epa-B, weak hydrolytic activities were detected when butyryl-, hexanoyl-, myristoyl-, palmitoyl-, stealoyl-ACP were used as substrates. In contrast, when 3,6,9,12,15-*cis* octadecapentaenoyl- and docosahexaenoyl-ACP were used as substrates, *holo*-ACP were clearly detected (Figure 5-2-2-6). The Epa-B showed promiscuous substrate specificity although the activities were weak compared with the intrinsic substrate. This

broad substrate specificity would allow the transformants expressing *epa-ABCD* to produce ETA and DPAω3 besides intrinsic product EPA as described in chapter 3 and 4. Taken these results together, the AT domain recognized long chain length (C_{18} to C_{22}) acyl-ACP with *cis* double bonds as substrates. From view points of the product profiles of PUFA synthases, PUFA synthases showed high product specificity and produced specific products without undesired by-products. These facts suggested that the condensation and modification reactions at the late biosynthetic steps would be much faster than the release reaction catalyzed by the AT domain in PUFA biosynthetic process.

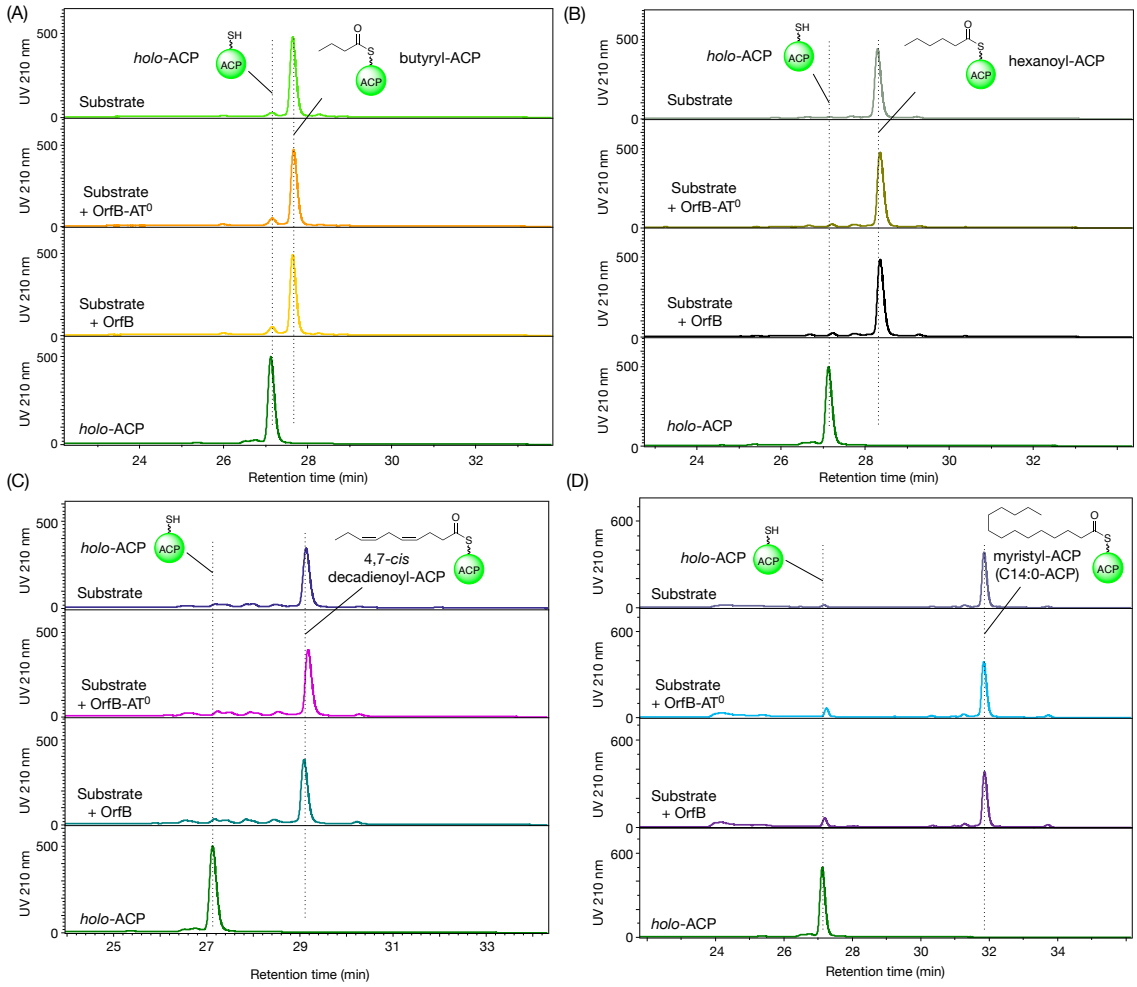

Figure 5-2-2-5. HPLC analysis (UV 210 nm) of *in vitro* reactions using butyryl- (A), hexanoyl- (B), 4,7-cis decadienoyl- (C), myristoyl- (D), palmitoyl- (E), stearoyl- (F), 3,6,9,12,15-cis octadecapentaenoyl- (G), or EPA-ACP (H) and OrfB-AT^0 (2^{nd}) or OrfB (3^{rd}). Substrate (top) and *holo*-ACP (bottom).

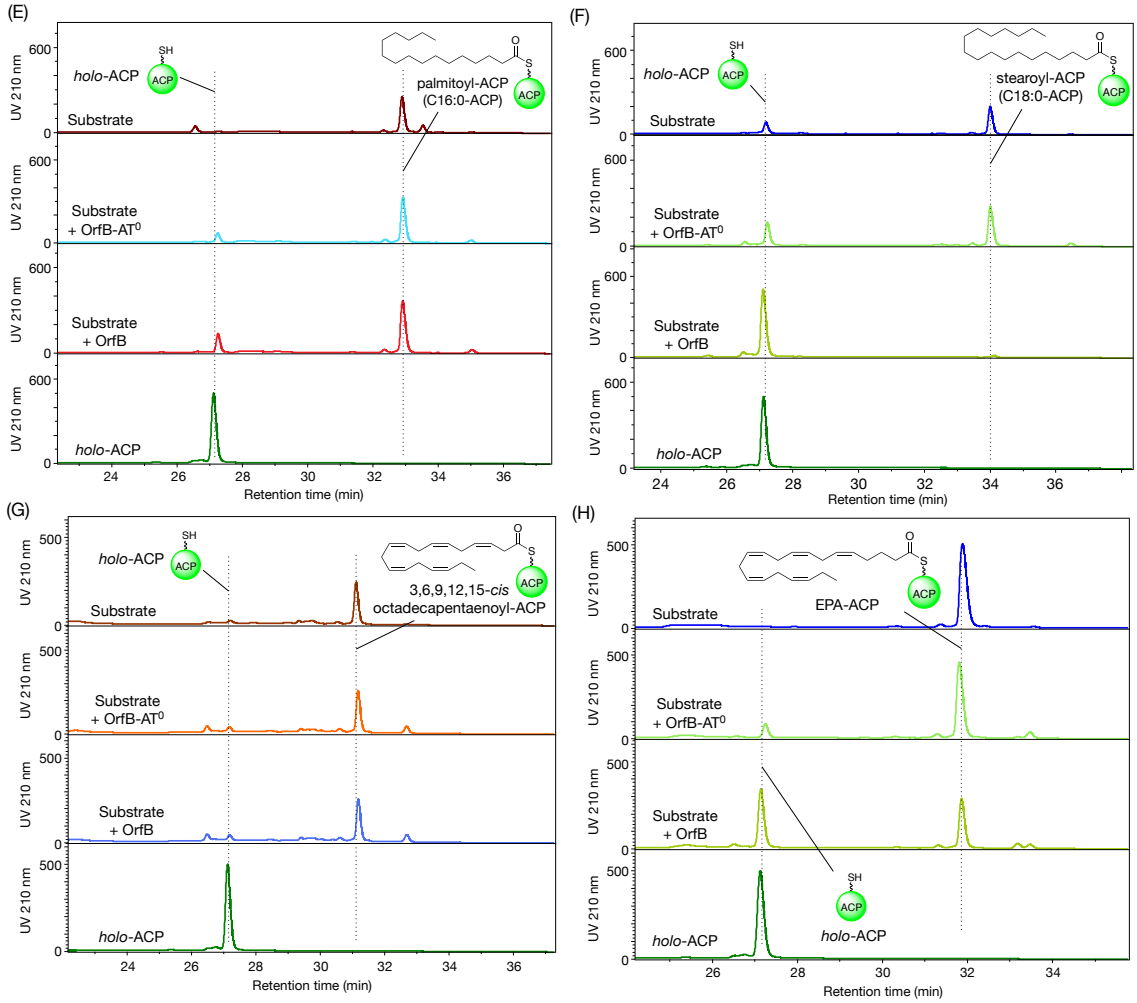

Figure 5-2-2-5. Continued.

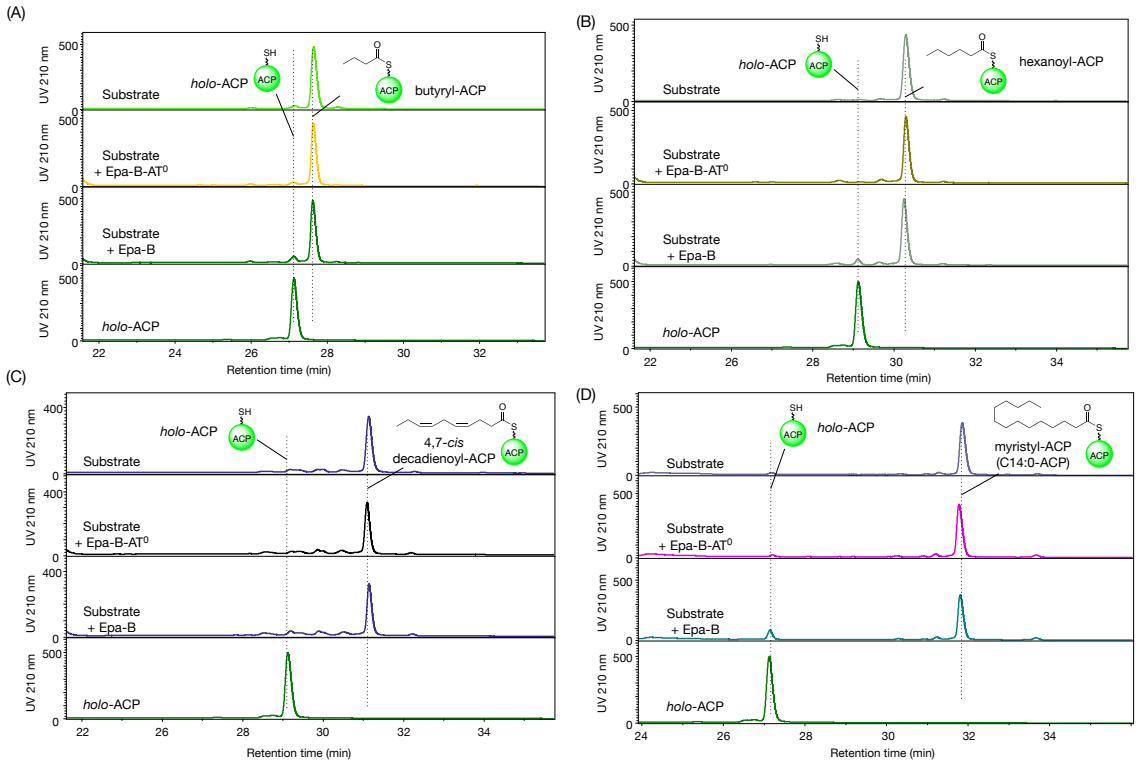

Figure 5-2-2-6. HPLC analysis (UV 210 nm) of *in vitro* reactions using butyryl- (A), hexanoyl- (B), 4,7-cis decadienoyl- (C), myristoyl- (D), palmitoyl- (E), stearoyl- (F), 3,6,9,12,15-*cis* octadecapentaenoyl- (G), or DHA-ACP (H) and Epa-B-AT^0 (2nd) or Epa-B (3rd). Substrate (top) and *holo*-ACP (bottom).

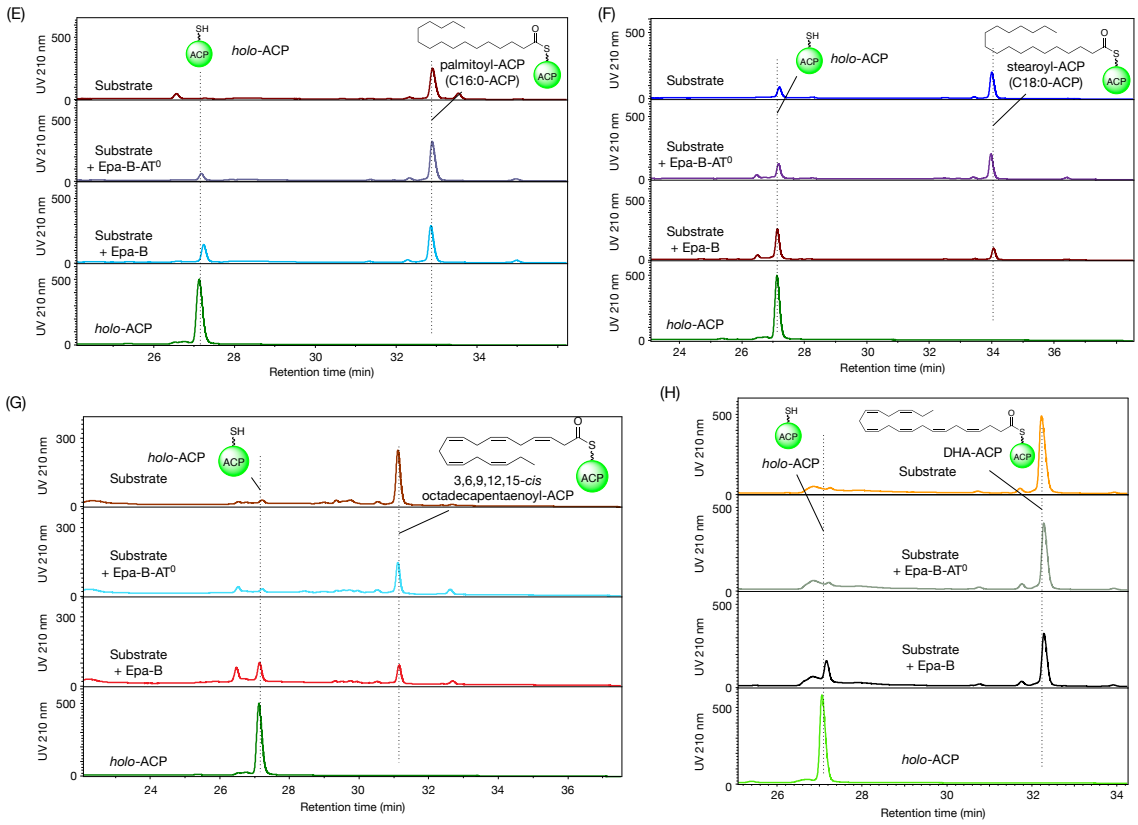

Figure 5-2-2-6. Continued.

5.3. Discussion

In this chapter, I showed that the AT domain in PUFA synthases had hydrolytic activities on long chain fatty acyl-ACP through *in vitro* experiments and concluded that the AT domain was responsible for an off-leading reaction in both eukaryotic and prokaryotic PUFA biosynthesis systems. The termination step in PUFA biosynthesis was shown in Figure 5-3-1. Although the AT domain showed a similarity to malonyl-CoA/ACP transacylase, the domain utilized water molecule as acyl accepter and the hydrolytic reaction proceeded in a similar manner to that of α/β-hydrolase type thioesterase[7]. Once acyl-ACP product was transferred on the Ser residue in the AT domain for the formation of thioester, the nucleophilic attack of a water molecule would occur to form a carboxylic acid.

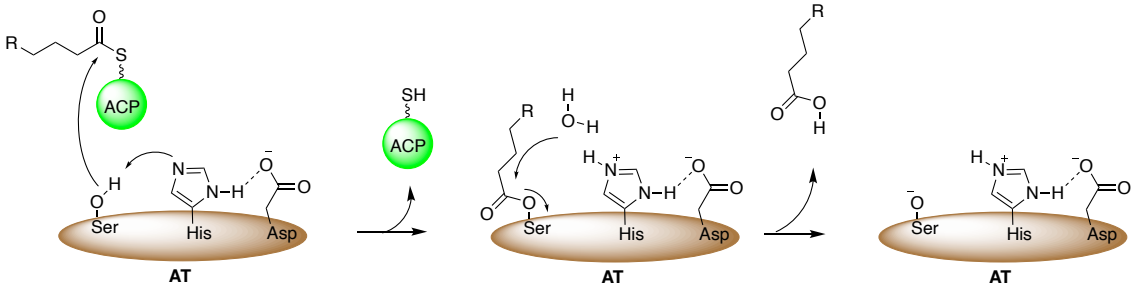

Figure 5-3-1. Proposed mechanism of hydrolysis reaction catalyzed by AT domain.

Most off-loading reactions are TE domain-mediated hydrolysis or macrolactamization reactions in FASs, PKSs, and nonribosomal peptide synthetases. However, some of other types of chain release mechanisms were reported in secondary metabolites biosynthetic system (Figure 5-3-2), such as reductive release[8], condensation release[9,10], and dehydratase domain-mediated hydrolytic release[11]. Furthermore, acyltransferase-mediated off-loading system has also been reported. In rifamycin biosynthesis, RifF, homologue of arylamine: acetyl-CoA transferase, was involved in the off-loading reaction to generate intramolecular amide bond in its macrocyclic structure[12]. A discrete

acyltransferase, LovD, catalyzed a release reaction of the product and transferred the product to monacolin J acid as accepted molecule in lovastatin biosynthesis system[13]. In the case of FAS, malonyl/palmitoyl transferase domain mediated the direct acyl transfer of fatty acids to acyl acceptor CoA[14] (Yeast FAS system as described in chapter 1). In this chapter, I showed that the AT domain mediated the off-loading reaction using water molecule as the acyl accepter in PUFA synthase biosynthetic system.

Interestingly, Gemperlein *et al*. recently suggested a different off-loading reaction in terrestrial myxobacterium PUFA synthase[15]. 1-Acylglycerol-3-phosphate *O*-acyltransferase (AGPAT) domain encoded in its PUFA synthase gene catalyzed the direct acyl transfer of PUFAs on 1-acylglycerol-3-phosphate as acceptor molecule (Figure 5-3-3), suggesting that phospholipids with PUFAs would be biosynthesized by this domain in the strains. In contrast, the biosynthesis pathway of the phospholipids is probably different in marine eukaryotic and prokaryotic microorganisms. The facts that microalgae DHA synthase produced DHA as free fatty acids[2] suggest that free acid DHA would be re-activated by acyl-CoA synthetases and transferred on glycerides and phospholipids. In bacterial PUFA synthase, the results obtained in this chapter and the report that one of *plsC* gene was responsible for incorporation of EPA into phospholipids in *Shewanella* sp[16]., suggested the same mechanisms for its biosynthesis pathway.

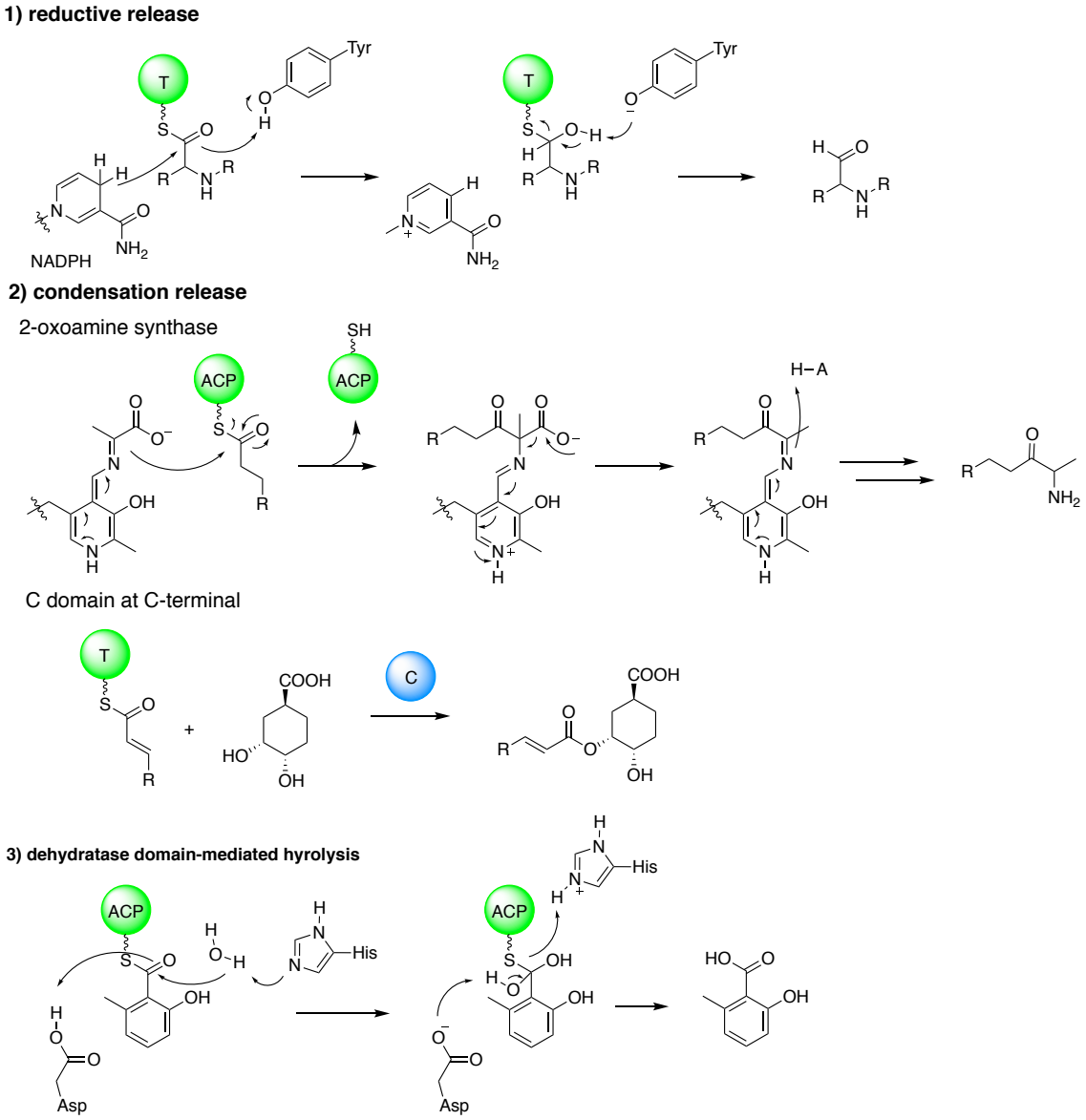

Figure 5-3-2. Various chain release mechanisms in secondary metabolite biosynthesis

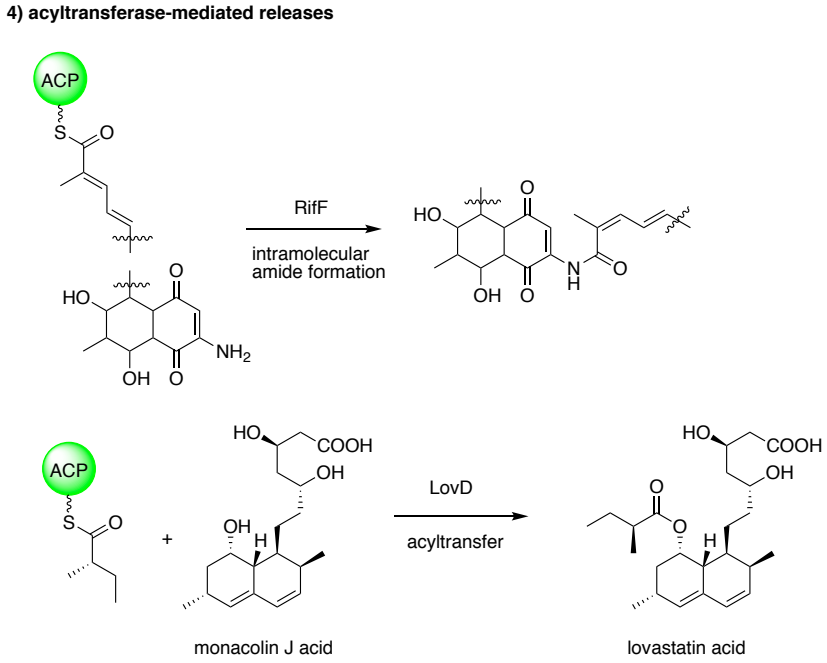

Figure 5-3-2. Continued.

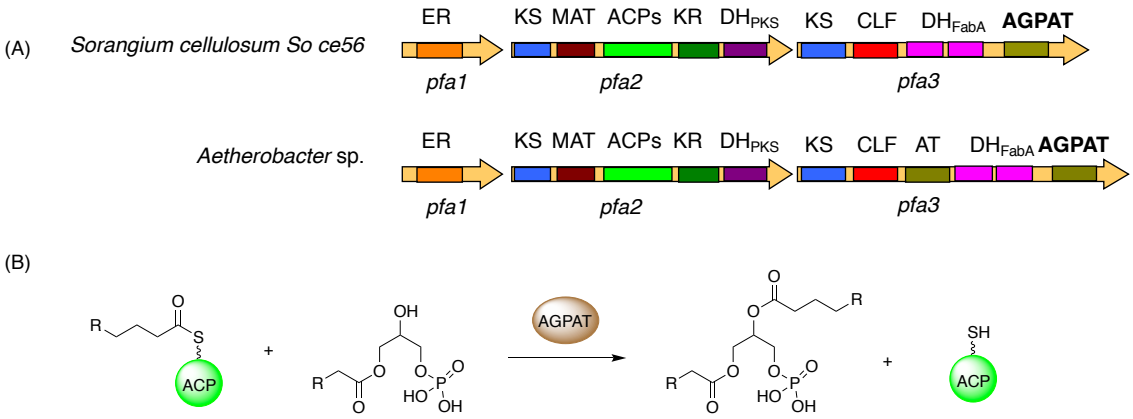

Figure 5-3-3. (A) Domain organizations of PUFA synthases in myxobacterium. (B) Proposed reaction catalyzed by AGPAT domain in myxobacterium PUFA synthases.

References

1. O. Santin, G. Moncalian, Loading of malonyl-CoA onto tandem acyl carrier protein domains of polyunsaturated fatty acid synthases. *J. Biol. Chem.*, **293**, 12491–12501 (2018).
2. J. G. Metz, J. Kuner, B. Rosenzweig, J. C. Lippmeier, P. Roessler, R. Zirkle, Biochemical characterization of polyunsaturated fatty acid synthesis in *Schizochytrium*: Release of the products as free fatty acids. *Plant Physiology and Biochemistry* **47**, 472–478 (2009).
3. M. Rodriguez-Guilbe, D. Oyola-Robles, E. R. Schreiter, A. Baerga-Ortiz, Structure, activity, and substrate selectivity of the Orf6 thioesterase from *Photobacterium profundum*. *J. Biol. Chem.*, **288**, 10841–10848 (2013).
4. M. N. Allemann, C. N. Shulse, E. E. Allen, Linkage of marine bacterial polyunsaturated fatty acid and long-chain hydrocarbon biosynthesis. *Front. Microbiol*., **10**, 702 (2019)
5. M. Kotowska, K. Pawlik, Roles of type II thioesterases and their application for secondary metabolite yield improvement. *Appl. Microbiol. Biotechnol.* **98**, 7735–7746 (2014).
6. Y. Orikasa, M. Tanaka, S. Sugihara, R. Hori, T. Nishida, A. Ueno, N. Morita, Y. Yano, K. Yamamoto, A. Shibahara, H. Hayashi, Y. Yamada, A. Yamada, R. Yu, A. Watanabe, H. Okuyama, pfaB products determine the molecular species produced in bacterial polyunsaturated fatty acid biosynthesis. *FEMS Microbiology Letters* **295**, 170–176 (2009).
7. K. Finzel, D. J. Lee, M. D. Burkart., Using modern tools to probe the structure-function relationship of fatty acid synthases., *ChemBioChem*. **16**, 528–547 (2015).
8. M. W. Mullowney, R. A. McClure, M. T. Robey, N. L. Kelleher, R. J. Thomson, Natural products from thioester reductase containing biosynthetic pathways. *Nat. Proc. Rep.*, **35**, 847–878 (2018)
9. R. Gerber, L. Lou, L. Du, A PLP-dependent polyketide chain releasing mechanism in the biosynthesis of mycotoxin fumonisins in Fusarium verticillioides. *J. Am. Chem. Soc*., **131**, 3148-3149 (2009).
10. J. Masschelein, P. K. Sydor, C. Hobson, R. Howe, C. Jones, D. M. Roberts, Z. L. Yap, J. Parkhill, E. Mahenthiralingam, G. L. Challis, A dual transacylation mechanism for polyketide synthase chain release in enacyloxin antibiotic biosynthesis. *Nat. Chem.,* **11**, 906–912 (2019).
11. T. Moriguchi, Y. Kezuka, T. Nonaka, Y. Ebizuka, I. Fujii, Hidden function of catalytic domain in 6-methylsalicylic acid synthase for product release. *J. Biol. Chem.,* **285**, 15637-15643 (2010)
12. T. Yu, Y. Shen, Y. Doi-Katayama, L. Tang, C. Park, B. S. Moore, C. R. Hutchinson, H. G. Floss, Direct evidence that the rifamycin polyketide synthase assembles polyketide chains processively. *PNAS*, **96**, 9051–9056 (1999).
13. X. Xie, M. J. Meehan, W. Xu, P. C. Dorrestein, Y. Tang, Acyltransferase mediated polyketide release from a fungal megasynthase. *J. Am. Chem. Soc.,* **131**, 8388–8389 (2009).
14. F. Lynen., On the structure of fatty acid synthetase of yeast., *Eur. J. Biochem.*, **112**, 431–442 (1980).

15. K. Gemperlein, S. Rachid, O. R. Garcia, C. S. Wenzel, R. Müller, Polyunsaturated fatty acid biosynthesis in myxobacteria: different PUFA synthases and their product diversity. *Chem. Sci.* **5**, 1733–1741 (2014).
16. T. Ogawa, A. Tanaka, J. Kawamoto, T. Kurihara, Purification and characterization of 1-acyl-*sn*-glycerol-3-phosphate acyltransferase with a substrate preference for polyunsaturated fatty acyl donors from the eicosapentaenoic acid-producing bacterium *Shewanella livingstonensis* Ac10. *J. Biochem*., **164**, 33–39 (2018).

Chapter 6

Conclusion

PUFAs such as DHA and EPA are typically synthesized from saturated fatty acids by elongase and desaturase enzymes in plants, fungi, bacteria. However, PUFA synthase enzyme complex composed of three or four polypeptides with catalytic domains like structure of Type I FAS synthesized *de novo* PUFAs using malonyl-CoA in some marine microorganisms and terrestrial myxobacteria. After discovery of this biosynthetic pathway in 2001, detailed biosynthetic machineries of PUFA synthase are still obscure.

In this study, I investigated the biosynthetic machinery in PUFA synthases of marine microorganisms. In chapter 2, I first examined the role of multi-tandem ACP domains in the enzymes. Typically, FAS and PKS system employed single ACP domain whereas all PUFA synthases identified had tandem ACP domains ranging from 3 to 9. I showed that the number of ACP domains impacted on PUFA productivities without the PUFA profile change and the structure of the domains were also important for its productivity through *in vivo* experiments.

In chapter 3, I examined the mechanism for controlling *cis* double bond position, ω3 or ω6, of PUFA products using EPA and ARA synthases. Gene exchange and domain swapping experiments showed that the two type DH domains, DH_{PKS} and DH_{FabA}, were important for the control. Therefore, I carried out *in vitro* reactions with the DH domains and various acyl-ACP to get further information. It was demonstrated that PUFA synthase utilized the two type DH domains depending on carbon chain length of acyl-ACP intermediates to construct *cis* double bond or saturation and the DH_{FabA} catalyzed double bond isomerization reactions besides the dehydration reaction.

In chapter 4, I investigated the mechanism for controlling carbon chain length, C_{20} or C_{22}, of PUFA products using EPA and DHA synthases. I showed that the KS_C/CLF domains in subunit C were important for DHA and EPA production through the gene exchange and domain swapping

experiments. I carried out the *in vitro* reactions using the KS_A/KS_C and acyl-ACP substrates with wide range of chain length. These experiments showed that PUFA synthases utilized the two KS domains depending on carbon chain length of acyl-ACP intermediates and the substrate specificity of the KS_C domain against C_{20} intermediate was important for controlling carbon chain length, C_{20} or C_{22}, of PUFA products.

Finally, I showed the initiation and termination steps in PUFA biosynthetic machinery through the *in vitro* experiments in chapter 5. The decarboxylation reaction of malonyl-ACP catalyzed by the KS_A domain was initiation step to form acetyl-ACP in the system. As for the termination reaction, it was demonstrated that the AT domain catalyzed hydrolytic reactions of acyl-ACPs in both microalgae and marine bacteria PUFA synthases and accepted the long chain acyl-ACPs with *cis* double bonds as substrates.

Taken together all the results, I proposed the PUFA synthase biosynthetic machinery as shown in Figure 7-1. First, malonyl-CoA were loaded on the tandem ACP domains catalyzed by the MAT domain and acetyl-ACP was generated via decarboxylation of malonyl-ACP catalyzed by the KS_A domain. Acyl-ACPs were elongated by the KS_A and KS_C/CLF domains. While the KS_A domain accepted short (from C_2 to C_{12}) and long (from C_{18} to C_{20}) acyl chains, the KS_C/CLF domains accepted middle (from C_{12} to C_{16}) and very long acyl chains (from C_{20} to C_{22}, specific pathway in DHA biosynthesis). The single KR domain catalyzed β-ketoreduction of elongated acyl-ACPs to form (*3R*)-hydroxyacyl-ACPs regardless of carbon chain lengths. Then, the DH_{PKS} recognized hydroxyacyl-ACPs and catalyzed α,β-dehydration reactions, followed by enoyl reduction catalyzed by the ER domain to form α,β-saturated acyl-ACPs. Conversely, the DH_{FabA} accepted hydroxyacyl-ACPs and catalyzed α,β-dehydration reactions, α,β- or β,γ-isomerization of *trans* double bond to form *cis* double bond. After formation of EPA- or DHA-ACP, the AT domain catalyzed off-loading reactions,

hydrolytic reactions of PUFA-ACP, to produce PUFAs as free fatty acids. Based on the proposed pathway, it will be possible to perform molecular engineering for desired PUFA production in PUFA synthases.

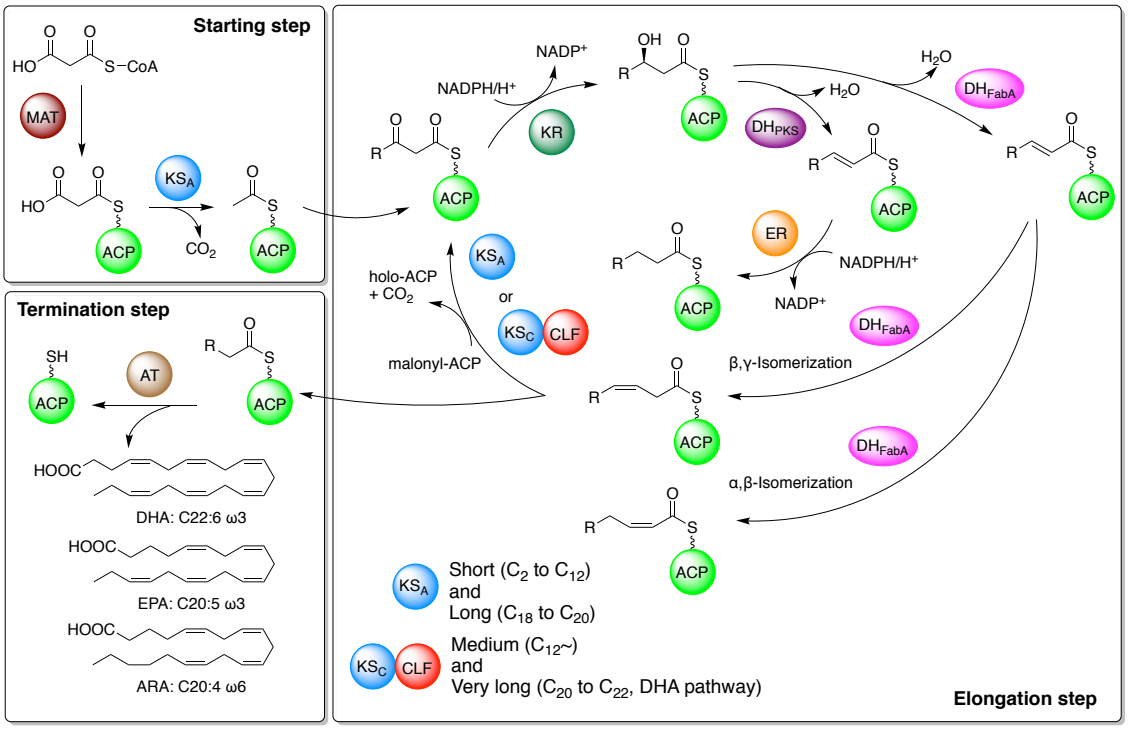

Figure 7-1. Proposed PUFA biosynthetic machinery in PUFA synthases.

Experimental section

1. General

Authentic standards, methyl esters of DHA (C22:6 ω3), docosapentaenoic acid ω3 (DPAω3, C22:5 ω3), EPA (C20:5 ω3), eicosatetraenoic acids (ETA, C20:4 ω3), vaccenic acid (C18:1 ω7), palmitic acid (C16:0), α-linoleic acids (ALA, C18:3 ω3), gamma-linoleic acids (GLA, C18:3 ω6), stearidonic acids (SDA, C18:4 ω3), were purchased from Sigma-Aldrich Japan K.K. (Tokyo, Japan) or Cayman Chemical Company (Ann Arbor, MI, USA). Free fatty acids, DHA (C22:6 ω3), EPA (C20:5 ω3) and heptadecanoic acids (C17:0), were purchased from Cayman Chemical Company and Tokyo Chemical Industry Co. Ltd. (Tokyo, Japan). Acyl-CoAs, crotonyl-CoA, acetyl-CoA, butyryl-CoA, hexanoyl-CoA, malonyl-CoA, myristoyl-CoA, palmitoyl-CoA, stearoyl-CoA, were purchased from Sigma-Aldrich Japan K.K. 3-*cis* Hexenoyl-CoA, 2-*trans* hexenoyl-CoA, 2-*trans* octenoyl-CoA, 3-hydroxyoctanoyl-CoA, 4,7-*cis* decadienoyl-CoA, 3,6,9,12,15-*cis* octadecapentaenoyl-CoA, eicosapentaenoyl-CoA, docosahexaenoyl-CoA were prepared by organic synthesis as shown in synthetic methods. *N*-Acetyl cysteamine (SNAC) thioesters were also prepared by organic synthesis. Other chemicals were purchased from Sigma-Aldrich Japan K.K., Cayman Chemical Company, Tokyo Chemical Industry Co. Ltd., or Wako Pure Chemical Industries, Ltd. (Osaka, Japan). Primers were purchased from FASMAC Co. Ltd. (Kanagawa, Japan). Enzymes and kits for DNA manipulation were purchased from Takara Bio Inc. (Shiga, Japan) or New England Biolabs Japan Inc. (Tokyo, Japan). PCR reactions were carried out using a GeneAmp PCR System 9700 thermal cycler (Thermo Fisher Scientific Inc., Waltham, MA, USA) with Tks Gflex DNA polymerase (Takara Bio). General genetic manipulations of *E. coli* were performed according to standard protocols. NMR spectra were obtained using a JEOL ECS-400 spectrometer. Chemical shifts are reported relative to TMS or the appropriate solvent peak. High-Resolution-MS (HR-MS) data for acyl-CoA were obtained using a Thermo Scientific Exactive mass spectrometer.

2. Bacteria strains and media

The strains used in this study are summarized in Table 2-1. *Escherichia coli* XL1-Blue (Nippon Gene Co. Ltd., Tokyo, Japan) was routinely used for plasmid construction. A β-oxidation-deficient *E. coli* mutant, BLR(DE3)*ΔfadE*, was used as the heterologous host for PUFA production. *E. coli* BL21(DE3) (Nippon Gene Co. Ltd.) was used to prepare recombinant enzymes. The media used were LB broth medium (Sigma-Aldrich Japan) and terrific broth (TB) medium (Becton, Dickinson and Company, NJ, USA). For growth on plates, 1.5% agar was added into the media. Ampicillin (Ap), chloramphenicol (Cm), kanamycin (Km), and streptomycin (Sm), were added to the media at concentrations of 100, 30, 25, and 20 μg/ml, respectively, if necessary.

Table 2-1. The strains used in this study.

Strains	Descriptions	Source
E. coli XL1-Blue	*hsdR*17, *recA*1, *endA*1, *gyrA*96, *thi*-1, *supE*44, *relA*1, *lac*[F', *proAB*, *lacI*^{q}ZΔM15, Tn10(*tet*^{R})]	Nippon Gene Co. Ltd.
E. coli BLR(DE3)	F^{-}, *ompT hsdS*$_{B}$(r_{B}^{-} m_{B}^{-}) *gal dcm* (DE3) Δ(*srl-recA*)306::Tn*10* (*tet*^{R})	Merck
E. coli BLR(DE3) *ΔfadE*	BLR(DE3) derivative, *ΔfadE*	This study
E. coli BL21(DE3)	F^{-}, *dcm*, *ompT*, *hsd*S_{B}(r_{B}^{-} m_{B}^{-}), *gal*, λ(DE3)	Nippon Gene Co. Ltd.
Schizochytrium sp.	*orfABC* (AF378327, AF378328, AF378329), ATCC20888	ATCC
Photobacterium profundum SS9	*epa-ABCD* (CR354531), ATCC BAA-1252	ATCC
Shewanella oneidensis MR-1	*SopfaABCDE* (NC_004347), ATCC BAA-1096	ATCC
Moritella marina MP-1	*dha-ABCDE* (AB025342), ATCC 15381	ATCC
Aureispira marina	*ara-ABCDE* (AB980240), JCM23201	JCM
Nostoc sp. PCC 7120	*hetI* (L22883), ATCC27893	ATCC

ATCC; American Type Culture Collection, JCM; Japan Collection of Microorganisms, RIKEN Bioresource Center.

3. Deletion of the *fadE* gene in *Escherichia coli* BLR(DE3)

To construct a *fadE* disruptant, the Quick & Easy *Escherichia coli* Gene Deletion Kit was used according to the manufacturer's protocol (Figure 3-1). In brief, DNA fragments possessing a Km-resistance gene cassette flanked with FRT sites and 50-bp homologous arms whose sequences were identical to the target regions were amplified by PCR with primers (KO01/KO02). The amplified DNA fragments were used to transform *E. coli* BLR(DE3). Gene disruption in the Km-resistant colonies was confirmed by PCR using appropriate sets of primers that hybridized approximately 300 bp upstream and downstream of the target genes. The sequences of the amplicons were then analysed to confirm the deletion. After that, the selection marker in the obtained mutant was removed with FLP-recombinase and the gene deletion was confirmed by PCR and direct sequencing of the amplicons.

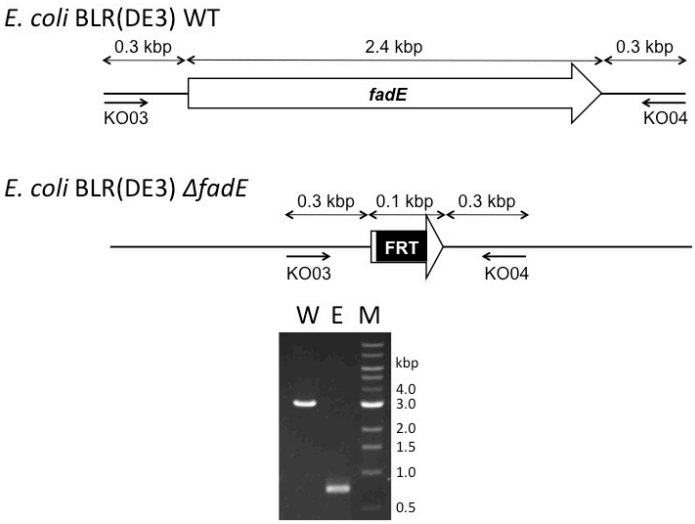

Figure 3-1. Deletion of the *fadE* gene in *Escherichia coli* BLR(DE3). The *fadE* regions of the wild type (upper) and Δ*fadE* strain (middle) are shown schematically. Arrows indicate the primers used for PCR analysis. Disruption was confirmed by PCR (bottom), W, wild type; E, Δ*fadE* disruptant; M, marker

4. PUFA production

To prevent degradation of the synthesized PUFAs, *E. coli* BLR(DE3)Δ*fadE* was used as a host. The PUFA biosynthetic gene sets were co-introduced into the host with the corresponding phosphopantetheinyl transferase gene (*hetI* for *orfA*, *SopfaE* for *SopfaA* and *epa-A*, *ara-E* for *ara-A,* or *dha-E* for *dha-A*). The transformants were cultured at 30 °C in TB broth medium for 24 h, and then 1 mL of the broth was inoculated into 200-mL baffled flasks containing 20 mL of TB medium and 1 mM IPTG. After cultivation for 48 h at 20 °C with agitation (230 rpm), 5 mL of the culture broth were collected and centrifuged. Total lipids were extracted from the pelleted cells following Bligh and Dyer[1]. For methyl esterification, the lipid fraction was dissolved in hexane (1 mL), to which methanol containing 14 wt% boron trifluoride (1 mL, Sigma-Aldrich Japan) was added, and incubated at 60 °C for 10 min. After the reaction mixture was evaporated, the pellet was dissolved with 0.2 mL of hexane and analysed with a Shimadzu GCMS-QP2010 Ultra system (Kyoto, Japan) equipped with a VF-23ms column (0.25 mm × 60 m, film thickness 0.25 μm, Agilent Technologies Inc., Santa Clara, CA, USA). The analytical conditions were as follows; carrier gas, helium with constant flow rate at 1.4 mL min^{-1}; injection temperature, 250 °C; column temperature, 150 °C (5 min)–250 °C (2 °C min^{-1})–250 °C (15 min); ion source temperature, 250 °C; detection, scan mode (*m/z* 50 to 500) for qualitative analysis and selected ion mode (*m/z* 79) for quantitative analysis. Heptadecanoic acid was used as an internal standard for quantitative analysis. To determine the double bond positions of the PUFAs, pyrrolidide derivatives of fatty acid methyl esters were prepared[2] and analysed by GC-MS.

5. Purification of recombinant enzymes.

The transformant BL21(DE3) harboring the expression vector was cultured at 37 °C in LB broth medium containing 25 μg/ml Km for 16 h, and the overnight culture was inoculated into 100 ml LB medium containing 25 μg/ml Km. Protein expression was induced by addition of 0.5 mM IPTG when the optical density at 600 nm reached 0.5 to 1.0. After cultivation for 16 h at 16 °C, the culture broth was collected and centrifuged at 8,000 rpm for 5 min. After the pellet was resuspended with phosphate buffer (50 mM NaH_2PO_4, 300 mM NaCl, 20 mM imidazole, pH 8.0), the cells were disrupted with sonication. Recombinant enzymes were purified using a Ni-NTA agarose column or amylose affinity column with elution buffer (50 mM NaH_2PO_4, 300 mM NaCl, 250 mM imidazole, pH 8.0 for the Ni-NTA agarose column or 50 mM Tris-HCl, 500 mM NaCl, 10 mM maltose, pH 7.5 for the amylose affinity column). The Epa-KR-DH_{PKS} and Dha-KR-DH_{PKS} enzymes were purified by two-step purification using a Ni-NTA agarose column, followed by an amylose affinity column. Enzymes were rebuffered with 100 mM Tris-HCl, 100 mM NaCl, pH 7.5 using an Amicon Ultra 3K, 30K, or 100K (Merck KGaA, Darmstadt, Germany). Enzyme purities were analyzed by SDS-PAGE on 5–12% gels. Enzyme concentration was determined by the Bradford method using bovine serum albumin as a standard.

6. Plasmids constructions

The plasmids used in this study are summarized in Table 6-1. DNA fragments were amplified by PCR with the primers shown in Table 6-2. The amplified fragments were digested with appropriate restriction enzymes and inserted into the corresponding restriction sites of the expression vectors. Detailed processes for plasmid construction are described below.

Table 6-1. Plasmids list used in this study.

Name	Description	Source
pET-21a	protein expression vector, T7 promoter, Ap^r	Merck
pCDF-1b	protein expression vector, T7 promoter, Sm^r	Merck
pCOLADuet-1	protein co-expression vector, T7 promoter, Km^r	Merck
pACYCDuet-1	protein co-expression vector, T7 promoter, Cm^r	Merck
pSTV28	cloning vector, *lac* promoter, Cm^r	Takara Bio
pET-*orfA*	pET-21a derivative with *orfA* from *Schizochytrium* sp.	This study
pCDF-*orfB*	pCDF-1b derivative with *orfB* from *Schizochytrium* sp.	This study
pCOLA-*orfC*	pCOLADuet-1 derivative with *orfC* from *Schizochytrium* sp.	This study

pSTV-*hetI*	pSTV28 derivative with *hetI* from *Nostoc* sp. PCC 7120 whose codons were optimized for expression in *E. coli.*	This study
pET-*orfA4*	pET-*orfA* derivative possessing 4×ACP domains	This study
pET-*orfA5*	pET-*orfA* derivative possessing 5×ACP domains	This study
pET-*orfA6*	pET-*orfA* derivative possessing 6×ACP domains	This study
pET-*orfA7*	pET-*orfA* derivative possessing 7×ACP domains	This study
pET-*orfA8*	pET-*orfA* derivative possessing 8×ACP domains	This study
pET-*orfA10*	pET-*orfA* derivative possessing 10×ACP domains	This study
pET-*orfA11*	pET-*orfA* derivative possessing 11×ACP domains	This study
pET-*SopfaA*	pET-21a derivative with *SopfaA* from *S. oneidensis*	This study
pACYC-*SopfaE-SopfaB*	pACYCDuet-1 derivative with *SopfaE* and *SopfaB* from *S. oneidensis*	This study
pCDF-*SopfaC*	pCDF-1b derivative with *SopfaC* from *S. oneidensis*	This study
pCOLA-*SopfaD*	pCOLADuet-1 derivative with *SopfaD* from *S. oneidensis*	This study
pET-*SopfaA5*	pET-*SopfaA* derivative possessing 5×ACP domains	This study
pET-*SopfaA6*	pET-*SopfaA* derivative possessing 6×ACP domains	This study
pET-*SopfaA7*	pET-*SopfaA* derivative possessing 7×ACP domains	This study
pET-*SopfaA8*	pET-*SopfaA* derivative possessing 8×ACP domains	This study
pET-*SopfaA9*	pET-*SopfaA* derivative possessing 9×ACP domains	This study
pET-*SopfaA5-1M*	pET-*SopfaA* derivative possessing one inactivated ACP domains (1st position) and four active ACP domains (2nd to 5th positions)	This study
pET-*SopfaA5-2M*	pET-*SopfaA* derivative possessing one inactivated ACP domains (2nd) and four active ACP domains (1st and 3rd to 5th)	This study
pET-*SopfaA5-3M*	pET-*SopfaA* derivative possessing one inactivated ACP domains (3rd) and four active ACP domains (1st, 2nd, 4th and 5th)	This study
pET-*SopfaA5-4M*	pET-*SopfaA* derivative possessing one inactivated ACP domains (4th) and four active ACP domains (1st to 3rd and 5th)	This study
pET-*SopfaA5-5M*	pET-*SopfaA* derivative possessing one inactivated ACP domains (5th) and four active ACP domains (1st to 4th)	This study
pET-*SopfaA-araAM*	pET-*SopfaA* derivative possessing one inactivated ACP domains (3rd) of *araA* and four active ACP domains (1st, 2nd, 4th and 5th)	This study
pET-*SopfaA-epaAM*	pET-*SopfaA* derivative possessing one inactivated ACP domains (3rd) of *epaA* and four active ACP domains (1st, 2nd, 4th and 5th)	This study

pET-*SopfaA-dhaAM*	pET-*SopfaA* derivative possessing one inactivated ACP domains (3rd) of *dhaA* and four active ACP domains (1st, 2nd, 4th and 5th)	This study
pET-*SopfaA-orfAM*	pET-*SopfaA* derivative possessing one inactivated ACP domains (3rd) of *orfA* and four active ACP domains (1st, 2nd, 4th and 5th)	This study
pET-*SopfaA-S1*	pET-*SopfaA* derivative possessing four active ACP domains (1st, 2nd, 4th and 5th) and "sequence 1" (between 2nd and 4th ACP domain)	This study
pET-*SopfaA-S2*	pET-*SopfaA* derivative possessing four active ACP domains (1st, 2nd, 4th and 5th) and "sequence 2" (between 2nd and 4th ACP domain)	This study
pET-*araA*	pET-21a derivative with *araA* from *A. marina*	This study
pCDF-*araC*	pCDF-1b derivative with *araC* from *A. marina*	This study
pCOLA-*araD*	pColADuet-1 derivative with *araD* from *A. marina*	This study
pACYC-*araE-araB*	pACYCDuet-1 derivative with *araE* and *araB* from *A. marina*	This study
pACYC-*SopfaE-araB*	pACYCDuet-1 derivative with *SopfaE* and *araB*	This study
pET-*epa-A*	pET-21a derivative carrying *epa-A* from *P. profundum.*	This study
pACYC-*SopfaE-epa-B*	pACYCDuet-1 derivative carrying *epa-B* from *P. profundum* and *SopfaE* from *S. oneidensis*	This study
pCDF-*epa-C*	pCDF-1b derivative carrying *epa-C* from *P. profundum.*	This study
pCOLA-*epa-D*	pCOLADuet-1 derivative carrying *epa-D* from *P. profundum.*	This study
pACYC-*SopfaE-ara-B-KR*^{0}	pACYC-*SopfaE-ara-B* derivative carrying the inactivated KR domain in *ara-B*	This study
pACYC-*SopfaE-ara-B-DH*^{0}	pACYC-*SopfaE-ara-B* derivative carrying the inactivated DH_{PKS} domain in *ara-B*	This study
pCDF-*ara-C-AT*^{0}	pCDF-*ara-C* derivative carrying the inactivated AT domain in *ara-C*	This study
pCDF-*epa-C-ara-DH*$_{FabA}$*-chimera1*	pCDF-*epa-C* derivative carrying the KS and CLF domains from *epa-C* and the double DH_{FabA} domain from *ara-C*	This study
pCDF-*ara-C-epa-DH*$_{FabA}$*-chimera2*	pCDF-*ara-C* derivative carrying the KS, CLF, and AT domains from *ara-C* and the double DH_{FabA} domain from *epa-C*	This study
pET-28a (+)	protein expression vector, T7 promoter, Km^r	Merck
pET28-*epa-A-KR-DH*$_{PKS}$	pET-28a (+) derivative for expression of *C*-terminal *epa-A* encoding the KR and DH_{PKS} domains with *N*-terminal maltose binding protein-fused and *C*-terminal 6×His tags-fused enzyme.	This study

pET28-*epa-C-DH*$_{FabA}$	pET-28a (+) derivative for expression of *C*-terminal *epa-C* encoding the consecutive DH_{FabA} domain with *N*-terminal 6×His tag.	This study
pET28-*dha-A-KR-DH*$_{PKS}$	pET-28a (+) derivative for expression of *C*-terminal *dha-A* encoding the KR and DH_{PKS} domain with *N*-terminal maltose binding protein-fused and *C*-terminal 6×His tags-fused enzyme.	This study
pET28-*dha-C-DH*$_{FabA}$	pET-28a (+) derivative for expression of *C*-terminal *dha-C* encoding the double DH_{FabA} domain was fused with *N*-terminal maltose binding protein tag.	This study
pET28-*ara-B*	pET-28a (+) derivative for expression of *ara-B* with *N*-terminal maltose binding protein tag.	This study
pET28-*ara-C-DH*$_{FabA}$	pET-28a (+) derivative for expression of *C*-terminal *ara-C* encoding the consecutive DH_{FabA} domain with *N*-terminal maltose binding protein tag.	This study
pET28-*sfp*	pET-28a (+) derivative for expression of *sfp* from *Bacillus subtilis* with *N*- and *C*-terminal 6×His tags	This study
pET28-*ACP*	pET-28a (+) derivative for expression of a single *ACP* domain gene from *S. oneidensis* with *N*- and *C*-terminal 6×His tags.	This study
pET28-*EcfabG*	pET-28a (+) derivative for expression of 3-ketoacyl reductase *EcfabG* gene of *E. coli* with *N*-terminal 6×His tag.	This study
pET-*dha-A*	pET-21a derivative carrying *dha-A* from *M. marina.*	This study
pACYC-*dha-E-dha-B*	pACYCDuet-1 derivative carrying *dha-B* and *dha-E* from *M. marina*.	This study
pCDF-*dha-C*	pCDF-1b derivative carrying *dha-C* from *M. marina.*	This study
pCOLA-*dha-D*	pCOLADuet-1 derivative carrying *dha-D* from *M. marina.*	This study
pACYC-*dha-E-SopfaB*	pACYC-*dha-E* derivative carrying *SopfaB* from *S. oneidensis*	This study
pACYC-*SopfaE-dha-B*	pACYC-*SopfaE* derivative carrying *dha-B* from *M. marina*	This study
pACYC-*dha-E-epa-B*	pACYC-*dha-E* derivative carrying *epa-B* from *P. profundum*	This study
pCDF-*epa-C-KS*^{0}	pCDF-*epa-C* derivative carrying the inactivated KS_C domain in *epa-C*	This study
pCDF-*dha-C-KS*^{0}	pCDF-*dha-C* derivative carrying the inactivated KS_C domain in *dha-C*	This study
pCDF-*epa-C-dha-C-chimera1*	pCDF-*epa-C* derivative carrying the KS_C and CLF domains from *epa-C* and the double DH_{FabA} domain from *dha-C*	This study
pCDF-*dha-C-epa-C-chimera2*	pCDF-*dha-C* derivative carrying the KS_C and CLF domains from *dha-C* and double DH_{FabA} domain from *epa-C*	This study

pET28-*epa-A-KS$_A$-MAT*	pET-28a (+) derivative for expression of *N*-terminal *epa-A* encoding the KS$_A$ and MAT domains was fused with *N*-terminal 6×His tag.	This study
pET28-*epa-C-KS$_C$-CLF*	pET-28a (+) derivative for expression of *N*-terminal *epa-C* encoding the KS$_C$ and CLF domains with *N*-terminal 6×His tag.	This study
pET28-*dha-A-KS$_A$-MAT*	pET-28a (+) derivative for expression of *N*-terminal *dha-A* encoding the KS$_A$ and MAT domains with *N*-terminal 6×His tag.	This study
pET28-*dha-C-KS$_C$-CLF*	pET-28a (+) derivative for expression of *N*-terminal *dha-C* encoding the KS$_C$ and CLF domains with *N*-terminal maltose binding tag.	This study
pCDF-*orfB-AT^0*	pCDF-*orfB* derivative carrying the inactivated AT domain in *orfB*	This study
pACYC-*SopfaE-epa-B-AT^0*	pACYC-*SopfaE-epa-B* derivative carrying the inactivated AT domain in *epa-B*	This study
pET28-maltose-*epa-B*	pET28-maltose derivative with *epa-B* from *P. profundum*.	This study
pET28-maltose-*epa-B-AT^0*	pET28-maltose-*epa-B* derivative carrying the inactivated AT domain in *epa-B*	This study
pET28-maltose-*orfB*	pET28-maltose derivative with *orfB* from *Schizochytrium* sp.	This study
pET28-maltose-*orfB-AT^0*	pET28-maltose-*orfB* derivative carrying the inactivated AT domain in *orfB*	This study

Table 6-2. Primers list used in this study.

Name	Sequences (5' to 3')
KO primers	
KO01	TATCATCACAAGTGGTCAGACCTCCTACAAGTAAGGGGCTTTTCGTTATGGAATTAACCCTCACTAAAGGGCGGC
KO02	GAGCCTTTCGGCTCCGTTATTCATTTACGCGGCTTCAACTTTCCGCACTTTAATACGACTCACTATAGGGCTCG
KO03	GCGTTTCCGCCGCTTCGTTCAGTTCG
KO04	CCTGGGTGATGAAAGGCGGTACTTATACTCC
OP primers	
OP01	GAGATATA<u>CATATG</u>GCGGCCCGTCTGCAGGAGCAAAAGG
OP02	ATA<u>GAATTC</u>TTAGAAGGCAAGGCTGTCCGTGGCGATGACCGAAG
OP03	AAACAATT<u>CATATG</u>CTTCGGCCCCCGTGCAAAAGAAGG
OP04	ATA<u>GAATTC</u>TTACAGCTTCTCGGCCGGGACGTATGTGTCATC
OP05	AAAGAATTCGGATCCGCGCCTGCAGGTCGACAAGCTTGC

OP06 GTGATGTGCCATATGTATATCTCCTTATTAAAGTTAAACAAAATTATTTCTACAGGG

OP07 AAAGAATTCATATGATTGAAATGTTCCGTCTTGGAATCCTCAC

OP08 GCGCACTGCGGTGCTACGGTGGTTGTTG

OP09 GCGTCAGCCGAAGCAACAGCCTTGG

OP10 GAGATATACATATGGCCGCTCGGAATGTGAGCGCCGCGCATGAGATG

OP11 GGTCGGAGATGAGACCGTTCTTCTTGG

OP12 GAGATATACATATGGCGCTCCGTGTCAAGACGAACAAGAAGC

OP13 ATAGAATTCTTAGAGCGCGTTGGTGGGCTCGTAGACAAAG

OP14 CATATGTATATCTCCTTCTTGTGAAATTGTTATCCGCTCACAATTCC

OP15 ACCATGATTACGAATTCGAGCTCGGTACC

OP16 TATAAGCTTCACGTGGACGCTCTCAGCCGCACTCGCACTGTTG

OP17 ATACTGCAGACGTCCTTGGCCTCGACGTTGAGCATGG

OP18 GGCCAGTGCCAAGCCGTACGAGCGTGAG

OP19 GGAGATGACATCCTTGAAGGCCGACGAGG

OP20 CAAGGATGTCATCTCCAAGGTCTCCTTCC

OP21 GGGATCCTCTAGAGTCGACCTGGTCGACGTCCTTGGCCTCG

OP22 CAGGTCGACTCTAGAGGATCCCCG

OP23 CGGCTTGGCACTGGCCGTCGTTTTAC

OP24 TGTGGATCCGAGGGAAGCCTTGGCGAACTTG

OP25 CAAGGACGTCGACGCTCTCAGCC

SP primers

SP01 ACGGAATTCATGAGCCATACCCCTTCACAG

SP02 ACGCTCGAGTCACTTAACACTTACCTC

SP03 GCACTCCAGTCGCCTTCCCGTT

SP04 CTGTGAAGGGGTATGGCTCATATGTATATCTCCTTCTTAAAGTTAAACAAAATTATTTC

SP05 GAGCCATACCCCTTCACAG

SP06 GGCAGGTCGATGGTTTCCTC

SP07 ACGCACGTGATGAGTTCTCAAATGCATACTCACCC

SP08 ACGCTCGAGCTATGCCTCTTCGATGCAGATG

SP09 GTCGGGTGAGTATGCATTTGAGAACTCATGGTATATCTCCTTATTAAAGTTAAAC

SP10 AGTTCTCAAATGCATACTCACCC

SP11 CCATTGTCGATACCCAACTGG

SP12 GCTTACATATGACGAATACCACACTCGATAATAACGC

SP13 TGTGAGGATCCTTAGCAGCGTTGCAGAGGTTTCC

SP14 GCGATACCATGGATGAAGATTGAGCTTTTTTTTATACC

SP15 TATATGGATCCTTAGTCAGCCAAACTAGCCGC

SP16 CTACATCATATGACACTCAACCCAATCGCACAT

SP17 TGTGCGGATCCTCAAAGGGGTTCTCCTTCTTGGAATACG

SP18 AATTGCGGCCGCGAGAGTAGGGAACTGCCAGGCATC

SP19 CGATTATGCGGCCGTGTACAATACGCAAAAAGGCCATCCGTCAG

SP20 CGTATTGTACACGGCCGCATAATCG

SP21 GCTAGTTATTGCTCAGCGG

SP22 GCCCTTGGATCCAACGCAGTGATGATACG

SP23 TTTAAGAATTCCGGATACGGCCGCAATTGGCGTGACAGCGCTGGCGACAACCTGAGGATTCG

SP24 GCTACACAATGCGCAGTAGCAGCAAGTGCAGCAGTTTCCAATGATGAGATTGAGCG

SP25 CCTATCGATGCCAACGCC

SP26 CTTTATGCTTCCGGCTCGTATGTTGTGTG

SP27 CCGATTCATTAATGCAGCTGGCACGACAG

SP28 CTTAGGGATCGATGCTATTAAGCGCGTAGAAATTCTAGGCACAGTG

SP29 AATAGCATCGATCCCTAAGTCCGCTTCCATATC

SP30 CCACACGTTTAATTGCGTCAATGCCAAGGTCGGCTTCC (FX07

SP31 GGCATTGACGCAATTAAACGTGTGGAAATTCTAGGCACAGTGCAGG (FX06)

SP32 GAATTGACGCCATTAAACGGGTGGAGATTTTAGG

SP33 CGTTTAATGGCGTCAATTCCAAGGTCGGCTTCC

SP34 GGTATCGATGCCATTAAGCGCGTGGAAATTCTAGG

SP35 CGCTTAATGGCATCGATACCAAGGTCGGCTTCC

SP36 TTAAGCAGCGCTCCAGTAACGTCAGCATCAAAC

SP37 CAACACGCTTAATAGCGTCGATACCCAAATCTGCTTCCATATCC

SP38 GGGTATCGACGCTATTAAGCGTGTTGAAATTCTTGGTACG

SP39 TTACGGCCGCTGACGCGACTGGAGCAGAAGCAAC

SP40 TTAAGAGCGCTACTACTGCTAACACTAACAACGGTCTTTC

SP41 CTCTTTTGATAGCATCAATACCCAAATCTGCTTCCATATCCATGTC

SP42 GATTTGGGTATTGATGCTATCAAAAGAGTAGAAATCTTTGGTGCTATGACC

SP43 TTGATCGGCCGTTTGTCGTACAGGAGCAGGTG

SP44 GTTATGCGCACCGTCTATCGATTTGAACCACATTC

SP45 CCACACGTTTGATAGCATCGATACCTAAATCAGCTTCCATGTC

SP46 GGTATCGATGCTATCAAACGTGTGGAAATATTAGGTGCAG

SP47 TTTAACGGCCGGAGAGCTTGTTGCTACAGAAGCCGTC

SP48 TTTAATGCGCAGCCGCCGCCCCTGCTGTC

SP49 GCTTGATCGCGTCAATGCCGAGCTCGGTCTC

SP50 CTCGGCATTGACGCGATCAAGCGTGTCGAGATTCTCTCCG

SP51 TTAATCGGCCGGCGCAGGGGCGGCAGCAG

SP52 TTGTCAGCTGCCTTCCCTCAATCAAAAAAGGAGTCGC

SP53 TTAATCGGCCGAGGGCATACTGAGGAGTTGATTAAAGG

SP54 TTAATCAGCTGAATCAGAGCATTTCACCCGGC

SP55 TTAAACGGCCGTGCCATTAGGGCCGATAATGGCG

AP primers

AP01 TATGAATTCTTTAAGAAGGAGATATACATATGAATTTAAACCACTCGCTTCGCAAAACTCCTG

AP02 CTGGCGAAAGGGGGATGTGCTGCAAGG

AP03 AAACTGCAGCATATGAAAATAGCAATCATAGGCTTATCTGGTTTGTTTC

AP04 ATAGGATCCTTAAGCTTCTTCTATACCTAGAGCCAAGTCCG

AP05 TATCTCGAGCTAGCTAATTGCTAGAGAAAAATTAGGGACTGGATTGG

AP06 AGAAGGAGCATATGATTACTTTTTCTGGAATAAAACAGCAGTTGTATTGG

AP07 AGACCATGGTTCATTTGCTTTATATCAACTCTGCTGTGGTTC

AP08 CGCGAATTCCTAGAATAAAGAATCTACATCTAGTAAATTAATAGAAAAATCTTTGAC

AP09 GAGTCAGCATATGATGCCTCAACCAGATTACCTAGACTTCACCCTC

AP10 GACGGATCCGCAAGCTTGTCGAGCTACCAAGTTAGTTCC

P primers

P01 GACAGTGAAATGCTGATTAAGAAATTCCAAG

P02 TTTGGATCCCTATGACAGAAGCTCCTTCTCTGGCTC

P03 TTTGGTCATATGGGTGTTAAGCGGAGACTCATGATG

P04 CTTGTGCCACTAGGAAGCTGCCAG

P05 TTTTCCCATATGCCATTGCGCATCGCTCTTTTAG

P06 TTTGGATCCTCACACTGGCTCTCCTTGTGTAGTGTTC

P07 TTCCTTCATATGCATTGCCCAGTTAATTACGCACC

P08 CCGACTTCAAGCTTTGCATCG

P09 CCTGCGAACGGTTCTGCGGC

P10 TTCGGATCCTCAGGCTTCTTCAATACAGATTGCAATGTC

P11 TTCACTCATATGACAACGCAAACTATGAATAATGAAAAGCTG

P12 TTCGGATCCTTAAATCATTTTCTCAACAGGCTTCCAACG

P13 GAGTCAGCATATGATGCCTCAACCAGATTACCTAGACTTCACCCTC

P14 GCAATGGCAAAATCTGTTTGTCCTACATTACCATAAAAACC

P15 GGACAAACAGATTTTGCCATTGCTAATGAAATTCTAAGCAAAG

P16 GCTAGTTATTGCTCAGCGGTGG

P17 CTTGAATAACGAAATGTTGTAAGAAAGGATTCTCAGAAGGTTCTAATG

P18 TTTCTTACAACATTTCGTTATTCAAGGGCAAGCCG

P19 AAACACTAGAGCCACAACAAGCCCTCATTC

P20 GTTATGCCATGGGCGAAAGTGCGGGCATGTG

P21 CGCACTTTCGCCCATGGCATAACCAAATGCCAAATCTGG

P22 ATAGGATCCTTAAGCTTCTTCTATACCTAGAGCCAAGTCCG

P23 GCACTCCAGTCGCCTTCCCGTT

P24 AGCGAATTCTACTAAATCTTCGTAATCCCAGATACAAG

P25 TTCCGAATTCGCAACAGGCAAAATTGCTAAAGTATTTG

P26 TGCGAATTCTTCCAAATCTTCCTGAGAAAAGATAATCGTC

P27 GAGATGTTACAGAAATGAACTCCATTTCTGATTTCTTTGC

P28 GCAAAGAAATCAGAAATGGAGTTCATTTCTGTAACATCTCC

P29 TTTGAATTCGCTGAAGGCGATATCGCCAATG

P30 TAGACCATGGAAATCGAAGAAGGTAAACTGGTAATCTGG

P31 ATAGGTACCTGGACATATGTGAAATCCTTCCCTCGATCC

P32 GGCGCATATGGTTGAAAACCTTGTAGAAGCGATTGCAGAA

P33 TTCCGCTCGAGTGACAGAAGCTCCTTCTCTGGCTCAGAC

P34 TGGCCGGCTAGCATTCGCAAACCTTGTATCTGGGATTACGAAG

P35 TTAGGCCATATGCCGAGCGCAACCGTTGCTATCTC

P36 TTCTCTCGAGTGACATATCGTTCAAAATGTCACTGACACTGAC

P37 GGCTAAGCTAGCGCTGCTACACAAGCTGGTTTTCAGATAAAAGGACC

P38 TTTAAGGATCCTTACGCTTCAACAATACTTAAAACGATGTTTTTAACTTC

P39 GGGGCCCATATGCAAGGAAAGACGATTATCTTTTCTCAGGAAG

P40 TTATGCCATATGGCAGTAGCAGCAAGTGCAGCAGTTTCC

P41 TTGCTCGAGGGCCGCAATTGGCGTGAC

P42 CGGCATATGAATTTTGAAGGAAAAATCGCACTG

P43 TTAAGGATCCTCAGACCATGTACATCCCGCC

PM primers

PM01 TTTAAACATATGGCTAAAAAGAACACCACATCGATTAAGCACG

PM02 TTTAAGCTTATCATGACATATCGTTCAAAATGTCACTGACACTGAC

PM03 TTCCCCATGGATGTACAGCGGCGTAAAAGATAAGCTCACCC

PM04 TTTCGGATCCCTATTTAGCGTCAGGTTTAAAATTAGTCTCAGG

PM05 GGTTGTCATATGACGGAATTAGCTGTTATTGGTATGGATG

PM06 CCTAAACCAACATAAGTAGCACCAATACCTGGGTACATGAAGG

PM07 ATTGGTGCTACTTATGTTGGTTTAGGGCGTGATCTATTTCATC

PM08 CATGTGGTATAGCTCAACCATGTGATCGTATTCGGCATAAGCTGGC

PM09 GATCACATGGTTGAGCTATACCACATGGATGTTACTCCACGTATTAATACCAAGATG

PM10 TTAAGGATCCCTATTTGTTCGTGTTTGCTATATGGCCTGC

PM11 TTTAAACCATGGAAAATATTGCAGTAGTAGGTATTGCTAATTTGTTC

PM12 TTTAAGGATCCTTACGCTTCAACAATACTTAAAACGATGTTTTTAACTTC

PM13 GTGGTTCATATGTCGAGTTTAGGTTTTAACAATAACAACGCAATTAACTGGG

PM14 CACCTTTAAGCATGTGCAAAGCAACATCTACAGCGCC

PM15 GGGGGATCCTTAATCACTCGTACGATAACTTGCCAATTCTG

PM16 GATGTTGCTTTGCACATGCTTAAAGGTGCTGCGTATTTACAACGTG

PM17 AGCGAATTCTACTAAATCTTCGTAATCCCAGATACAAG

PM18 GCACTCCAGTCGCCTTCCCGTT

PM19 TTTGAATTCGCTGAAGGCGATATCGCCAATG

PM20 TTCGGATCCTCAGGCTTCTTCAATACAGATTGCAATGTC

PM21 TTCCTTCATATGCATTGCCCAGTTAATTACGCACC

PM22 CTGAACTTGCAGCTGCTGCATCTAGGCTAAGCTGTACG

PM23 GATGCAGCAGCTGCAAGTTCAGTCTATTCTCTGAAATTAGCC

PM24 TTAGGATCCTTATGCAGAGTTAGCTGAATGAGCTTCAAGC

PM25 CAAGATGAAGCTGCAGCCGCATCCAGTGCAAAATGTGAAC

PM26 GATGCGGCTGCAGCTTCATCTTGTTATAGCGTTAAGTTAGCGTG

PM27 AAAGTGACAAGGGAAATACCAATGCTCAGGGTCTAAATCTTTCTG

PM28 TTTGGTCATATGGGTGTTAAGCGGAGACTCATGATG

PM29	TTCGGATCCTTACTTAATTGGCGTAGGTGTCGCGACTG
PM30	GCGTTCAAGCAACACATGTTGCAATCTGTTCGTTTCAGC
PM31	GCAACATGTGTTGCTTGAACGCTTTCTTAATGGC
PM32	TTCGGATCCTTAAGCAACGGGTTTAGCAATAGCTTGAATG
PM33	TTCGGATCCTTATGCTGGCGTAGTAGCGACTGTTGG
PM34	GGGGCCATATGGAAAATATTGCAGTAGTAGGTATTGCTAATTTGTTC
PM35	TTCGGATCCTTATGCTGATACAGGATTTGTTAGCACTGTATTG
PA primers	
PA01	GCACCAACGCCCATGCCGTCTTTGAGG
PA02	CAAGTGCGAGGCCAAAAGCAGCCTTGGGCGTGATGTTGAGAACG
PA03	GGCTGCTTTTGGCCTCGCACTTGGCGAGATTTCCATGATTTTTGC
PA04	GCTAGTTATTGCTCAGCGGTGG
PA05	TTTTCCCATATGCCATTGCGCATCGCTCTTTTAG
PA06	CGCTTTAGGTTACGCTAAAGGTGAAGCATCGATGTGG
PA07	GCTTCACCTTTAGCGTAACCTAAAGCGAAATCAGGCTTAACG

Underline showed restriction sites or mutation sites.

Plasmid construction of pET-*orfA*

The *orfA* gene (8,733 bp; accession number AF378327) of PUFA synthase from *Schizochytrium* sp. ATCC20888 was amplified by PCR with primers (OP01/OP02) and genomic DNA of *Schizochytrium* sp. according to the manufacturer's protocol. The amplified DNA fragment was digested with *Nde*I and *Eco*RI, and inserted into the corresponding sites of pET-21a (Merck).

Plasmid construction of pCDF-*orfB*

Previously, Metz *et al*. succeeded in expressing *orfB* with altered Ser codons suitable for *E. coli* though *orfB* encoded by the native codons was hardly expressed in *E. coli*[3]. Therefore, I constructed a plasmid carrying the *orfB* gene (6,180 bp; accession number AF378328) with the same altered Ser codons. The scheme is shown in Figure 6-1. First, DNA fragment 1 (4,568 bp to end of *orfB*) was amplified by PCR with primers (OP03/OP04) and genomic DNA of *Schizochytrium* sp. as a template. A pCDF-1b (Merck) derivative possessing *Nde*I and *Eco*RI sites was also constructed by PCR with two primers (OP05/OP06) and pCDF-1b as a template. The amplified fragment 1 was inserted into the *Nde*I and *Eco*RI sites of the pCDF derivative vector to obtain pCDF-*orfB1*.

Second, DNA fragment 2 (4,123 to 4,705 bp), which has the same altered Ser codons as those reported previously, was purchased from Thermo Fisher Scientific Inc. (Waltham, MA, USA). DNA fragment 3 (3,390 to 4,151 bp) was obtained by PCR with primers (OP07/OP08) and genomic DNA.

To obtain DNA fragment 4 (3,390 to 4,705 bp), DNA fragments 2 and 3 were assembled by overlap extension PCR with primers (OP07/OP09). Fragment 4 was digested with *Nde*I and *Sac*II, and then inserted into the corresponding sites of pCDF-*orfB1* to construct pCDF-*orfB4*.

Finally, DNA fragment 5 (1 to 3,478 bp) was amplified by PCR with primers (OP10/OP11), digested with *Nde*I and *Mfe*I, and inserted into the same sites of pCDF-*orfB4* to yield pCDF-*orfB*.

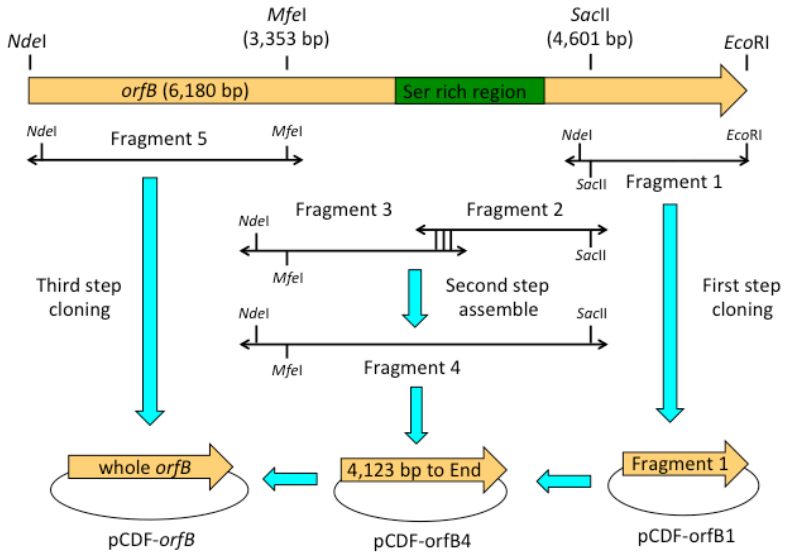

Figure 6-1. Strategy for pCDF-*orfB* construction.

Plasmid construction of pCOLA-*orfC*

The *orfC* gene (4,509 bp; accession number AF378329) was amplified by PCR with primers (OP12/OP13) and *Schizochytrium* sp. genomic DNA as a template. The fragment was digested with *Nde*I and *Eco*RI, and then inserted into the *Nde*I and *Mfe*I sites of pCOLADuet-1 vector (Merck).

Plasmid construction of pSTV-*hetI*

A 4′-phosphopantetheinyl transferase (PPTase) is required to activate acyl carrier proteins (ACPs). Though no genes encoding PPTase have been reported from *Schizochytrium* sp., Metz *et al*. successfully used a PPTase gene, *het*I, from *Nostoc* sp. as an alternative[3]. I therefore used the *hetI* gene (accession number L22883), the codons of which were optimized for *E. coli* expression (Thermo Fisher Scientific). The DNA fragment was digested with *Nde*I and *Eco*RI and then inserted into the same sites of pSTV28N, which is a derivative of the pSTV28 vector (Takara Bio Inc., Shiga, Japan) and was constructed by inverse PCR with pSTV28 as a template and primers (OP14/OP15), to create an *Nde*I site at the start codon for protein expression. The plasmid thus obtained was designated pSTV-*hetI*.

Plasmid construction of pET-*SopfaA*

The *SopfaA* gene (7,596 bp; accession number NC_004347) of PUFA synthase from *Shewanella oneidensis* MR-1 was amplified by PCR with primers (SP01/SP02) and *S. oneidensis* MR-1 genomic DNA as a template. The fragment was digested with *Eco*RI and *Xho*I, and inserted into the same sites of pET-21a (Merck) to obtain pET-*SopfaA′*. Then, the *N*-terminal His-tag sequences of the plasmid were deleted by overlap PCR extension with two sets of primers (SP03/SP04 and SP05/SP06) and pET-*SopfaA′* as a template. Thus, the DNA region between the *Apa*I and *Sal*I sites in pET-*SopfaA′* was replaced with the assembled DNA fragment to yield pET-*SopfaA*.

Plasmid construction of pCDF-*SopfaC*

The *SopfaC* gene (5,892 bp; accession number NC_004347) was amplified by PCR with primers (SP07/SP08) and genomic DNA as a template. The fragment was digested with *Pml*I and *Xho*I, and inserted into the same sites of pCDF-1b (Merck) to make pCDF-*SopfaC′*. The *N*-terminal His-tag sequences of the plasmid were deleted as described above with primers (SP03/SP09 and SP10/SP11).

Plasmid construction of pCOLA-*SopfaD*

The *SopfaD* gene (1,644 bp; accession number NC_004347) was amplified by PCR with primers (SP12/SP13) and genomic DNA as a template. The fragment was digested with *Nde*I and *Bam*HI, and inserted into the *Nde*I and *Bgl*II sites of pCOLADuet-1.

Plasmid construction of pACYC-*SopfaE-SopfaB*

For co-expression of *SopfaB* and *SopfaE* (accession number NC_004347), pACYCtrm, a derivative of pACYCDuet-1 (Merck), was constructed by inserting the *rrnB* terminator from pTrc99A between the first multi-cloning site and the second T7 promoter in pACYCDuet-1. Two DNA fragments possessing *rrnB* terminators and the second T7 promoter were prepared by PCR with primers (SP18/SP19 and SP20/SP21) and pACYCDuet-1 and pTrc99A as templates, and then assembled by overlap extension PCR. The DNA fragment thus obtained was digested with *Not*I and *Nde*I, and inserted into the same sites of pACYCDuet-1 to construct pACYCtrm.

The *SopfaE* gene was amplified by PCR with primers (SP14/SP15) and genomic DNA as a template, and then the *Nco*I and *Bam*HI fragment was inserted into the same sites of pACYCtrm to obtain pACYC-*SopfaE*. Then, the *SopfaB* gene was amplified by PCR with primers (SP16/SP17) and genomic DNA as a template, digested with *Nde*I and *Bam*HI, and inserted into the *Nde*I and *Bgl*II sites of pACYC-*SopfaE* to construct pACYC-*SopfaE-SopfaB*.

Plasmid construction of pET-*araA*

The *araA* gene (4,671 bp; accession number AB980240) of PUFA synthase from *Aureispira marina* was amplified by PCR with primers (AP01/AP02) and pSTV29-*Plac-pfaAB*[4] as a template. The fragment was digested with *Nde*I and *Bam*HI, and inserted into the same sites of pET-21a.

Plasmid construction of pCDF-*araC*

The *araC* gene (6,726 bp; accession number AB980240) was amplified with primers (AP03/AP04) and pMW219-*Plac-pfaCD*[4] as a template. The fragment digested with *Nde*I and *Bam*HI was replaced with that of pCDF-*orfB*.

Plasmid construction of pCOLA-*araD*

The *araD* gene (1,629 bp; accession number AB980240) was amplified with primers (AP05/AP06) and pMW219-*Plac-pfaCD*[4] as a template. The *Nde*I and *Bam*HI digested fragment was inserted into the *Nde*I and *Bgl*II sites of pACYCDuet-1.

Plasmid construction of pACYC-*araE-araB* and pACYC-*SopfaE-araB*

The *araE* gene (660 bp; accession number AB980240) and *araB* gene (2,406 bp; accession number AB980240) were each amplified with primers (AP07/AP08 and AP09/AP10, respectively) and template DNA (pUC19-*Plac-pfaE* and pSTV29-*Plac-pfaAB*[4], respectively). The former and latter fragments were digested with *Nco*I/*Bam*HI and *Nde*I/*Bam*HI, respectively, and inserted into the *Nco*I/*Bam*HI and *Nde*I/*Bgl*II sites of pACYCtrm to construct pACYC-*araE-araB*.

To construct pACYC-*SopfaE-araB*, pACYC-*araE-araB* was digested with *Nde*I and *Xho*I, and inserted into the same sites of pACYC-*SopfaE*.

Plasmids Construction of *orfA* genes with 4 to 11 acyl carrier protein domains

To investigate the relationship between PUFA productivity and the number of ACP domains in the *orfA* gene, I constructed *orfA* genes possessing 4×, 5×, 6×, 7×, 8×, 9×, 10×, and 11×ACP domains. Each of the ACP domains is highly conserved and separated by conserved and repeated regions with Ala and Pro rich sequences. I therefore considered the region between Ala/Pro rich sequences one ACP domain unit.

To construct the plasmids, I used the following technique. *Zra*I sites exist in every ACP domain except the first one (Figure 6-2). A *Pml*I site is also located downstream of the last ACP domain.

Deletion of the internal region between either *Zra*I or *Pml*I in the *orfA* gene results in no frame shift of codons. Moreover, the DNA fragment obtained by ligation at the *Zra*I and *Pml*I sites cannot be re-digested with either of the restriction enzymes.

First, each of the single ACP domains was randomly amplified by PCR with primers (OP16/OP17) using pET-*orfA* as a template. The fragment was digested *Hin*dIII/*Pst*I and inserted into the same sites of pUC18 (Takara Bio). By sequencing, I identified the original ACP domain and consequently obtained plasmids possessing each of the ACP domains (pUC18-ACP2nd, 3rd, 4th, 5th, 6th, 7th, 8th and 9th).

Next, an *orfA* gene fragment from 1,976 to 2,469 bp was amplified with pET-*orfA* as a template and primers (OP18/OP19); the primers were designed to remove the additional *Zra*I site located at 2,469 bp. An *orfA* gene fragment from 2,469 bp to 3,858 bp was amplified with primers (OP20/OP21) and pET-*orfA* as a template. A pHSG298 (Takara Bio) derivative plasmid possessing *Bsi*WI and *Zra*I sites was also constructed by inverse PCR with primers (OP22/OP23) and pHSG298 as a template. The three fragments thus obtained were assembled by in-fusion recombination (Takara Bio) to obtain pHSG298-ACP2′.

Next, I obtained the ACP fragment by digesting pUC18-ACP3 with *Pml*I and *Bam*HI. The fragment was inserted into the *Zra*I and *Bam*HI sites of pHSG298-ACP2′. This operation was repeated to construct plasmids possessing the desired number of ACP domains (pHSG298-4′ to 11′). Then, an *orfA* gene fragment from 6,162 to 6,503 bp was amplified with primers (OP24/OP25) and pET-*orfA* as a template. The fragment was digested with *Zra*I and *Bam*HI, and inserted into the same sites of pHSG298-ACP4′ to 11′ to construct pHSG298-ACP4 to 11. Finally, the *orfA* genes carrying the desired number of ACP domains were digested with *Bsi*WI and *Pml*I, and replaced with those of pET-*orfA* to make pET-*orfA4* to *11*, respectively.

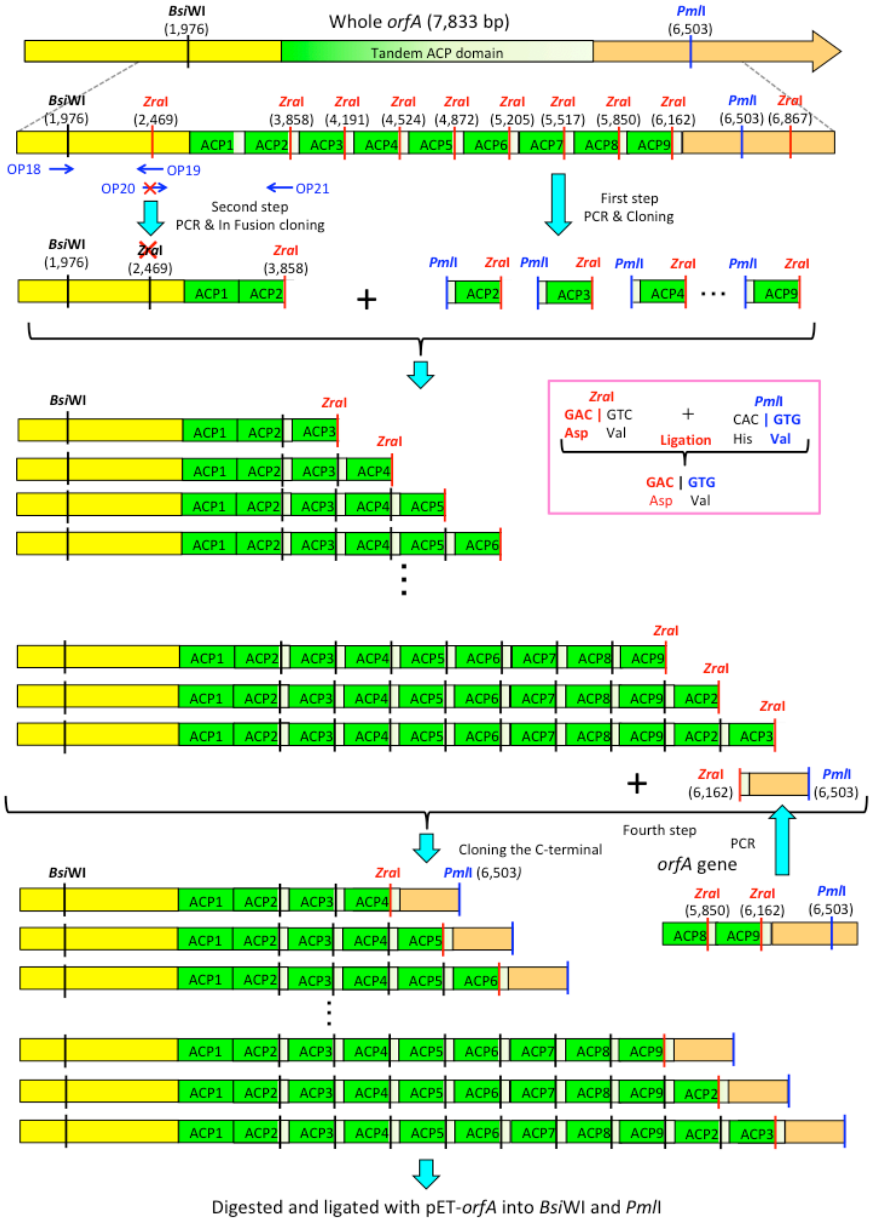

Figure 6-2. Strategy for construction of *orfAs* with 4× to 11× acyl carrier protein domains.

Plasmid construction of *SopfaA* genes with 5 to 9 acyl carrier protein domains

I also constructed *SopfaA* genes possessing 5×, 6×, 7×, 8×, and, 9×ACP domains. In this case, I employed the same technical strategy as that used to construct *orfA* genes with 4 to 11 ACP domains (Figure 6-3).

First, a fragment from the *Bam*HI to *Eag*I site was amplified by PCR with pET-*SopfaA* as a template and primers (SP22/SP23); the primers were designed to create an *Afe*I site in the Ser1431 and Ala1432 codons. The fragment was digested with *Bam*HI and *Eco*RI, and inserted into the same sites of pHSG298 to obtain pHSG298-ACP2. Then, a fragment carrying the second ACP domain was

amplified with primers (SP24/SP23) and pET-*SopfaA* as a template. In this case, the primer SP24 was designed to create a *Fsp*I site in the Ser1323 and Ala1324 codons. The fragment was digested with *Fsp*I and *Eco*RI, and inserted into the *Afe*I and *Eco*RI sites of pHSG298-ACP2 to obtain pHSG298-ACP3. This operation was repeated to construct plasmids with the desired number of ACP domains (pHSG298-ACP3 to 7). Finally, the *SopfaA* genes possessing the desired number of ACP domains were digested with *Bam*HI and *Eag*I, and replaced with the corresponding region of pET-*SopfaA* to construct pET-*SopfaA5* to *9*.

(A)

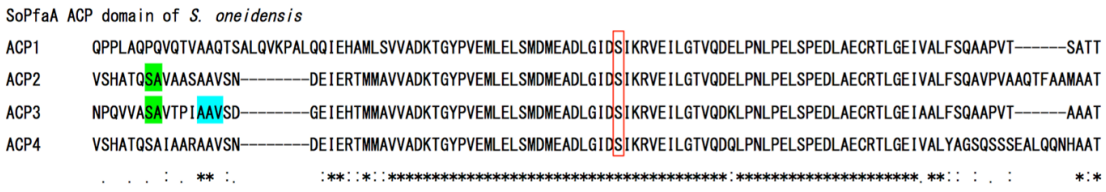

(B)

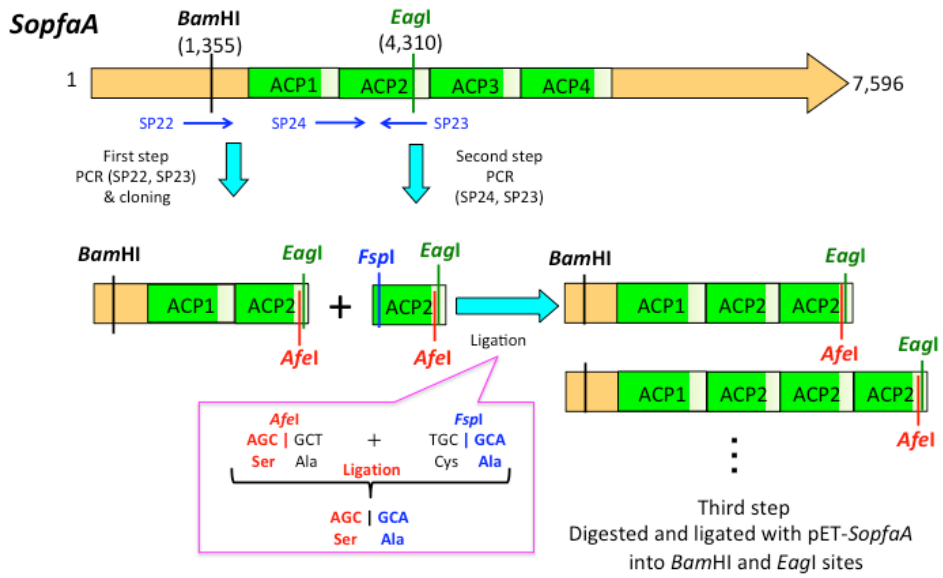

Figure 6-3. Strategy for construction of *SopfaA* genes with 5× to 9× acyl carrier protein domains. (A) Sequence alignment of the tandem acyl carrier protein domains of *SopfaA*. The red box, blue highlighting, and green highlighting show the active sites of the ACP domains, the *Eag*I site, and the boundary of one unit of ACP, respectively. (B) Plasmid construction is shown schematically.

Plasmid construction of pET-*SopfaA5-1M*

A DNA fragment, in which the first ACP was inactivated by replacing the active Ser with an Ala residue, was amplified by overlap PCR with primers (SP28/SP29/SP25/SP26) and pHSG298-ACP2 as a template. The fragment was digested with *Nde*I and *Eco*RI, and replaced with the corresponding region of pHSG298-ACP2 to obtain pHSG298-ACP2-1M. A DNA fragment with active ACP domains was amplified with primers (SP24/SP23) and pHSG298-ACP2 as a template, digested with *Fsp*I and *Eco*RI, and inserted into the *Afe*I and *Eco*RI sites of pHSG298-ACP2-1M. The *Eag*I and *Bam*HI fragment of the plasmid thus obtained was replaced with that of pET-*SopfaA.*

Plasmid construction of pET-*SopfaA5-2M*

A DNA fragment, in which the second ACP was inactivated, was obtained as described above with primers (SP30/SP31/SP25/SP26) and pHSG298-ACP2 as a template. The fragment was digested with *Nde*I and *Eco*RI, and replaced with the corresponding fragment of pHSG298-ACP2 to construct pHSG298-ACP2-2M. After this, the protocol for pET-*SopfaA5-1M* construction was employed; that is, the preparation of a DNA fragment with active ACP domains by PCR with primers (SP24/SP23), the cloning of the *Fsp*I and *Eco*RI fragment into pHSG298-ACP2-2M, and the replacement of the *Eag*I and *Bam*HI fragments.

Plasmid construction of pET-*SopfaA5-3M*

A DNA fragment, in which the third ACP was inactivated, was obtained as described above with primers (SP24/SP23/SP30/SP31) and pHSG298-ACP2 as a template. The fragment was digested with *Fsp*I and *Eco*RI, and replaced with the *Afe*I and *Eco*RI fragment of pHSG298-ACP2 to make pHSG298-ACP3-3M. After this, the protocol described above was employed.

Plasmid construction of pET-*SopfaA5-4M*

The *Eag*I and *Xho*I fragment possessing the *C*-terminal half region was inserted into the same sites of the pBluescript II SK(+) vector (Agilent Technologies Inc., Santa Clara, CA, USA) to make pBlue-ACP34. A DNA fragment, in which the fourth ACP was inactivated, was obtained as described above with primers (SP32/SP33/SP27/AP02) and pBlue-ACP34 as a template. The *Eag*I and *Sac*I fragment of the constructed plasmid was replaced with that of pBlue-ACP34 to obtain pBlue-ACP3M4. Finally, the *Eag*I and *SacI* fragment of pET-*SopfaA* was replaced with that of pBlue-ACP3M4.

Plasmid construction of pET-*SopfaA5-5M*

A DNA fragment, in which the fifth ACP was inactivated, was obtained as described above with primers (SP34/SP35/SP27/AP02) and pBlue-ACP34 as a template. The fragment was digested with *Eag*I and *Sac*I, and replaced with that of pBlue-ACP34 to make pBlue-ACP34M. Then, the *Eag*I

and *Sac*I fragment of pET-*SopfaA* was replaced with that of pBlue-ACP34M.

Plasmid construction of pET-*SopfaA-epaAM*

A DNA fragment carrying the second mutated ACP domain of *epaA* (accession number CR354531) from *Photobacterium profundum* SS9 was amplified by overlap PCR with primers (SP36/SP37/SP38/SP39) and the *P. profundum* SS9 genome as a template. The fragment was digested with *Afe*I and *Eag*I, and inserted into the same sites of pHSG298-ACP2. Then, the *Eag*I and *Bam*HI fragment of the constructed plasmid was replaced with that of pET-*SopfaA*.

Plasmid construction of pET-*SopfaA-araAM*

A DNA fragment carrying the second mutated ACP domain of *araA* from *A. marina* was amplified by overlap PCR with primers (SP40/SP41/SP42/SP43) and pET-*araA* as a template. After this, the method for pET-*SopfaA-epaAM* construction was employed.

Plasmid construction of pET-*SopfaA-dhaAM*

A DNA fragment carrying the second mutated ACP domain of *dhaA* (accession number AB025342) from *Moritella marina* was amplified by overlap PCR with primers (SP44/SP45/SP46/SP47) and the *M. marina* genome as a template. The fragment was digested with *Fsp*I and *Eag*I, and inserted into the *Afe*I and *Eag*I sites of pHSG298-ACP2. The replacement of the *Eag*I and *Bam*HI fragments was carried out using the method described above.

Plasmid construction of pET-*SopfaA-orfAM*

A DNA fragment carrying the third mutated ACP domain of *orfA* from *Schizochytrium* sp. was amplified by overlap PCR with primers (SP48/SP49/SP50/SP51) and pET-*orfA* as a template. The fragment was digested with *Fsp*I and *Eag*I, and inserted into the *Afe*I and *Eag*I sites of pHSG298-ACP2. The replacement of the *Eag*I and *Bam*HI fragments was done as described above.

Plasmid construction of pET-*SopfaA-S1*

A DNA fragment carrying *hlyB* sequence S1 (accession number NC_004347, 118th to 224th amino acids of HlyB), which is an ABC transporter from *S. oneidensis*, was amplified by PCR with primers (SP52/SP53) and the *S. oneidensis* genome as a template. The fragment was digested with *Pvu*II and *Eag*I, and inserted into the *Afe*I and *Eag*I sites of pHSG298-ACP2. The replacement of the *Eag*I and *Bam*HI fragments was done as described above.

Plasmid construction of pET-*SofaA-S2*

A DNA fragment carrying *hlyB* sequence S2 (accession number NC_004347, 383rd to 489th

amino acids of HlyB) was amplified by PCR with primers (SP54/SP55) and the *S. oneidensis* genome as a template. After this, the protocol for pET-*SopfaA-S1* was employed.

Plasmid construction of pET-*epa-A*

First, C-terminal DNA fragments carrying *epa-A* (from 633 bp to the end of *epa-A*) were amplified by PCR with primers (P01/P02) and genomic DNA of *Photobacterium profundum* SS9. The amplified fragments were inserted into the *Bam*HI and *Eag*I sites of pBluescript II SK(+) (Agilent Technologies Inc.) to obtain pBlue-*epa-A-C-terminus*. Second, DNA fragments of *epa-A* (from 1 to 633 bp) were amplified with primers (P03/P04), digested with *Nde*I and *Eag*I, and inserted into the same sites of pET-21a (Merck) to obtain pET-*epa-A-N-terminus*. Finally, *C*-terminal DNA fragments obtained by digestion of pBlue-*epa-A-C-terminus* with *Eag*I and *Xho*I were inserted into the corresponding sites of pET-*epa-A-N-terminus* to obtain pET-*epa-A*.

Plasmid construction of pACYC-*SopfaE-epa-B*

DNA fragments carrying the *epa-B* gene were amplified with primers (P05/P06) and genomic DNA of *P. profundum* SS9. The fragments obtained were digested with *Nde*I and *Bam*HI, and inserted into the *Nde*I and *Bgl*II sites of pACYC-*SopfaE* to obtain pACYC-*SopfaE-epa-B*.

Plasmid construction of pCDF-*epa-C*

DNA fragments carrying the *N*-terminus of the *epa-C* gene (from 1 to 993 bp of *epa-C*) were amplified with primers (P07/P08) and genomic DNA of *P. profundum* SS9. The fragments obtained were digested with *Nde*I and *Xba*I and inserted into the corresponding sites of pUC18 (Takara Bio Inc.). The plasmid thus constructed was digested with *Nde*I and *Bam*HI and inserted into the same sites of pCDF-*orfB* to obtain pCDF-*epa-C-N-terminus*. DNA fragments carrying the *C*-terminus of the *epa-C* gene (from 993 to 6,021 bp of *epa-C*) were amplified with primers (P09/P10), digested with *Nco*I and *Bam*HI, and inserted into the corresponding sites of pCDF-*epa-C-N-terminus* to yield pCDF-*epa-C*.

Plasmid construction of pCOLA-*epa-D*

DNA fragments carrying the *epa-D* gene were amplified with primers (P11/P12) and genomic DNA. The fragments obtained were digested with *Nde*I and *Bam*HI, and inserted into the *Nde*I and *Bgl*II sites of pCOLADuet-1 (Merck) to get pCOLA-*epa-D*.

Plasmid construction of pACYC-*SopfaE-ara-B-KR*^{0}

DNA fragments carrying a mutated *ara-B* gene, which encoded a mutated KR domain in which the catalytically essential Tyr432 was replaced with Phe, were amplified by overlap extension

PCR with primers (P13/P14/P15/P16) and pACYC-*SopfaE-ara-B* as a template. The amplified fragments were digested with *Nde*I and *Xho*I and used to replace the original fragment of pACYC-*SopfaE-ara-B* to construct pACYC-*SopfaE-ara-B-KR*^{0}.

Plasmid construction of pACYC-*SopfaE-ara-B-DH*^{0}

DNA fragments carrying a mutated *ara-B* gene, which encoded a mutated DH_{PKS} domain in which the catalytically essential His544 was replaced with Phe, were amplified by overlap extension PCR with primers (P13/P16/P17/P18) and pACYC-*SopfaE-ara-B* as a template. After this, the same protocol as for the construction of pACYC-*SopfaE-ara-B-KR*^{0} was employed.

Plasmid construction of pCDF-*ara-C-AT*^{0}

DNA fragments carrying a mutated *ara-C* gene, which encoded a mutated AT domain in which the catalytically essential Ser1094 was replaced with Ala, were amplified by overlap extension PCR with primers (P19/P20/P21/P22) and pCDF-*ara-C* as a template. The amplified fragments were digested with *Bgl*II and *Afe*I and used to replace the original fragment of pCDF-*ara-C*.

Plasmid construction of pCDF-*epa-C-ara-*DH_{FabA}*-chimera1*

DNA fragments carrying the KS-CLF genes of *epa-C* were amplified with primers (P23/P24) and pCDF-*epa-C* as a template. The amplified fragments were digested with *Nde*I and *Eco*RI and inserted into the same sites of pCDF-*orfB* to obtain pCDF-*epa-C-KS-CLF*. A DNA fragment carrying the *ara-C* DH_{FabA} gene was also amplified by PCR with primers (P25/P16) and pCDF-*ara-C* as a template. The primer P25 was designed to create an artificial *Eco*RI site. The amplified fragments were digested with *Eco*RI and *Bam*HI and inserted into the corresponding sites of pCDF-*epa-C-KS-CLF* to construct pCDF-*epa-C-ara-*DH_{FabA}*-chimera1*.

Plasmid construction of pCDF-*ara-C-epa-*DH_{FabA}*-chimera2*

DNA fragments carrying the KS, CLF, and AT genes of *ara-C* were amplified by overlap extension PCR with primers (P26/P27/P23/P28) to remove the native *Eco*RI site at 1,028 bp in *ara-C*. The amplified fragments were digested with *Nde*I and *Eco*RI and used to replace the corresponding fragment of pCDF-*epa-C-KS-CLF* to obtain pCDF-*ara-C-KS-CLF-AT.* We also amplified a DNA fragment carrying a DH_{FabA} gene of *epa-C* with primers (P29/P10). The amplified fragment was digested with *Eco*RI and *Bam*HI and inserted into the corresponding sites of pCDF-*ara-C-KS-CLF-AT* to obtain pCDF-*ara-C-epa-*DH_{FabA}*-chimera2*.

Plasmid construction of pET28-*epa-A-KR-*DH_{PKS}

To insert a gene encoding a maltose binding protein into pET-28a(+) (Merck), DNA fragments

were amplified with primers (P30/P31), digested with *Nco*I and *Nde*I, and inserted into the same sites of pET-28a to obtain pET28-maltose. DNA fragments carrying the KR and DH_{PKS} genes of *epa-A* were amplified with primers (P32/P33) and pET-*epa-A* as a template. The amplified fragments were digested with *Nde*I and *Xho*I and inserted into the same sites of pET28-maltose to construct pET28-*epa-A-KR-*DH_{PKS}.

Plasmid construction of pET28-*epa-C-*DH_{FabA}

DNA fragments carrying the consecutive DH_{FabA} genes of *epa-C* were amplified with primers (P34/P16) and pCDF-*epa-C* as a template. The fragments were digested with *Nhe*I and *Xho*I, and inserted into the corresponding sites of pET-28a to obtain pET28-*epa-C-*DH_{FabA}.

Plasmid construction of pET28-*dha-A-KR-*DH_{PKS}

The same method as for pET28-*epa-A-KR-*DH_{PKS} construction was employed with the primers P35/P36 using *M. marina* genome DNA.

Plasmid construction of pET28-*dha-C-*DH_{FabA}

DNA fragments carrying the consecutive DH_{FabA} genes of *dha-C* were amplified with primers (P37/P38) and *M. marina* genome DNA as a template. The amplified fragments were digested with *Nhe*I and *Bam*HI and inserted into the same sites of pET28-maltose to construct pET28-*dha-C-*DH_{FabA}.

Plasmid construction of pET28-*ara-B*

pACYC-*SopfaE-ara-B* was digested with *Nde*I and *Xho*I and the fragment carrying the *ara-B* gene was inserted into the corresponding sites of pET28-maltose to construct pET28-*ara-B*.

Plasmid construction of pET28-*ara-C-*DH_{FabA}

DNA fragments carrying the consecutive DH_{FabA} genes of *ara-C* were amplified with primers (P39/P16) and pCDF-*ara-C* as a template. The amplified fragments were digested with *Nde*I and *Xho*I and inserted into the same sites of pET28-maltose to obtain pET28-*ara-C-*DH_{FabA}.

Plasmid construction of pET28-*sfp*

pACYC-*sfp*[5] was digested with *Nde*I and *Xho*I, and the DNA fragment carrying the phosphopantetheinyl transferase *sfp* gene of the *Bacillus subtilis* was inserted into the corresponding sites of pET-28a.

Plasmid construction of pET28-*ACP*

DNA fragments carrying a single ACP gene from *SopfaA* of *S. oneidensis* MR-1 were

amplified with primers (P40/P41) and pHSG298-*ACP3* as a template. The amplified fragments were digested with *Nde*I and *Xho*I and inserted into the same sites of pET-28a.

Plasmid construction of pET28-*EcfabG*

DNA fragments carrying a *EcfabG* gene of *E. coli* were amplified with primers (P42/P43) and genomic DNA of *E. coli* BL21(DE3) as a template. The amplified fragments were digested with *Nde*I and *Bam*HI and inserted into the same sites of pET-28a.

Plasmid construction of pET-*dha-A*

DNA fragments carrying *dha-A* were amplified with primers (PM01/PM02) and genomic DNA of *M. marina*. The fragments obtained were digested with *Nde*I and *Hin*dIII, and inserted into the same sites of pET-21a to construct pET-*dha-A*.

Plasmid construction of pACYC-*dha-E-dha-B*

DNA fragments carrying a PPTase gene (*dha-E*) were amplified with primers (PM03/PM04), digested with *Nco*I and *Bam*HI, and inserted into the same sites of pACYCrrm to construct pACYC-*dha-E*. DNA fragments carrying *dha-B* were amplified by overlap extension PCR with primers (PM05/PM06/PM07/PM08/PM09/PM10). After digestion with *Nde*I and *Bam*HI, the fragments were inserted into the *Nde*I-*Bgl*II sites of pACYC-*dha-E* to obtain pACYC-*dha-E-dha-B*.

Plasmid construction of pCDF-*dha-C*

DNA fragments carrying *dha-C* were amplified with primers (PM11/PM12). The fragments obtained were digested with *Nco*I and *Bam*HI, and inserted into the same sites of pCDF-1b (Merck) to obtain pCDF-*dha-C*.

Plasmid construction of pCOLA-*dha-D*

DNA fragments carrying the *N*-terminus and *C*-terminus of *dha-D* were amplified with primers (PM13/PM14/PM15/PM16). The whole *dha-D* gene was obtained by overlap extension PCR with primers (PM13/PM15). The fragments obtained were digested with *Nde*I and *Bam*HI, and inserted into the *Nde*I and *Bgl*II sites of pCOLADuet-1 (Merck) to construct pCOLA-*dha-D*.

Plasmid construction of pACYC-*dha-E-SopfaB*

pACYC-*SopfaE-SopfaB* was digested with *Nde*I and *Xho*I and the DNA fragments carrying the *SopfaB* gene were inserted into the same sites of pACYC-*dha-E* to obtain pACYC-*dha-E-SopfaB*.

Plasmid construction of pACYC-*SopfaE-dha-B*

pACYC-*dha-E-dha-B* was digested with *Nde*I and *Xho*I and the DNA fragments carrying *dha-B* were inserted into the same sites of pACYC-*SopfaE* to construct pACYC-*SopfaE-dha-B*.

Plasmid construction of pACYC-*dha-E-epa-B*

pACYC-*SopfaE-epa-B* was digested with *Nde*I and *Xho*I and the DNA fragments carrying *epa-B* were inserted into the same sites of pACYC-*dha-E* to construct pACYC-*dha-E-epa-B*.

Plasmid construction of pCDF-*epa-C-dha-C-chimera1*

DNA fragments carrying the KS_C and CLF genes of *epa-C* were amplified with primers (PM17/PM18) and pCDF-*epa-C* as a template. The primer PM17 was designed to create an artificial *Eco*RI site without amino acid changes of Epa-C. The amplified fragments were digested with *Apa*I and *Eco*RI and inserted into the same sites of pCDF-*dha-C*.

Plasmid construction of pCDF-*dha-C-epa-C-chimera2*

DNA fragments carrying the consecutive DH_{FabA} genes of *epa-C* were amplified with primers (PM19/PM20) and pCDF-*epa-C* as a template. The primer PM19 was designed to introduce an artificial *Eco*RI site without amino acid changes of Epa-C. The amplified fragments were digested with *Eco*RI and *Bam*HI and inserted into the same sites of pCDF-*dha-C*.

Plasmid construction of pCDF-*epa-C-*KS^0

DNA fragments carrying a mutated *epa-C* gene, which encoded a mutated KS_C domain in which the catalytically essential Cys257 was replaced with Ala, were amplified by overlap extension PCR with primers (PM21/PM22/PM23/PM24). The amplified fragments were digested with *Nsi*I and *Nco*I and used to replace the original fragment of pCDF-*epa-C*.

Plasmid construction of pCDF-*dha-C-*KS^0

DNA fragments carrying a mutated *dha-C* gene, which encoded a mutated KS_C domain in which the catalytically essential Cys196 was replaced with Ala, were amplified by overlap extension PCR with primers (PM11/PM25/PM26/PM27). The amplified fragments were digested with *Nco*I and *Eco*RI and used to replace the original fragment of pCDF-*dha-C*.

Plasmid construction of pET28-*epa-A-*KS_A*-MAT*

DNA fragments carrying the KS_A and MAT genes of *epa-A* were amplified by overlap extension PCR with primers (PM28/PM29/PM30/PM31) and pET-*epa-A* as a template to remove the *Nde*I site at 2,588 bp in *epa-A*. The amplified fragments were digested with *Nde*I and *Bam*HI and

inserted into the corresponding sites of pET-28a to obtain pET28-*epa-A-KS$_A$-MAT*.

Plasmid construction of pET28-*epa-C-KS$_C$-CLF*

DNA fragments carrying the KS$_C$ and CLF genes of *epa-C* were amplified by PCR with primers (PM21/PM32) and pCDF-*epa-C* as a template. The amplified fragments were digested with *Nde*I and *Bam*HI and inserted into the corresponding sites of pET-28a to obtain pET28-*epa-C-KS$_C$-CLF.*

Plasmid construction of pET28-*dha-A-KS$_A$-MAT*

DNA fragments carrying the KS$_A$ and MAT genes of *dha-A* were amplified by PCR with primers (PM01/PM33) and pET-*dha-A* as a template. The same protocol used for the construction of pET28-*epa-A-KS$_A$-MAT* was employed to obtain pET28-*dha-A-KS$_A$-MAT*.

Plasmid construction of pET28-*dha-C-KS$_C$-CLF*

DNA fragments carrying the KS$_C$ and CLF genes of *dha-C* were amplified by PCR with primers (PM34/PM35) and pCDF-*dha-C* as a template. The amplified fragments were digested with *Nde*I and *Bam*HI and inserted into the same sites of pET28-maltose to construct pET28-*dha-C-KS$_C$-CLF.*

Plasmid construction of pCDF-*orfB-AT^0*

DNA fragments carrying a mutated *orfB* gene, which encoded a mutated AT domain in which catalytically essential residue Ser1140 was mutated to Ala, were amplified by overlap PCR extension with primers (PA01/PA02/PA03/PA04) and pCDF-*orfB* as a template. The Amplified fragments was digested with *Bam*HI and *Mfe*I and used to replace the original fragment of pCDF-*orfB*.

Plasmid construction of pACYC-*SopfaE-epa-B-AT^0*

DNA fragments of a mutated *epa-B* gene in which catalytically essential residue Ser403 was mutated to Ala were amplified by overlap PCR extension with primes (PA04/PA05/PA06/PA07) and pACYC-*SopfaE-epa-B* as a template. The DNA obtained was digested with *Nde*I and *Xho*I and replaced with the original fragment of pACYC-*SopfaE-epa-B*.

pET28-*maltose-orfB* and pET28-*maltose-orfB-AT^0*.

Whole DNA fragments of *orfB* or *orfB-AT^0* was obtained by digestion of pCDF-*orfB* or pCDF-*orfB-AT^0* with *Nde*I and *Eco*RI, respectively. The fragments obtained was inserted into a same restriction site of pET28-maltose to construct pET28-*maltose-orfB* or pET28-*maltose-orfB-AT^0*.

pET28-*maltose-epa-B* and pET28-*maltose-epa-B-AT*^{0}

I used the same strategy for construction of pET28-*maltose-orfB*. Whole DNA fragments of *epa-B* or *epa-B-AT*^{0} was obtained by digestion of pACYC-*SopfaE-epa-B* or pACYC-*SopfaE-epa-B-AT*^{0} with *Nde*I and *Xho*I. The fragments obtained was inserted into a same restriction site of pET28-maltose.

7. Synthetic methods

3-Oxobutyryl-SNAC.

3-Oxobutyryl-SNAC was synthesized according to a previous report[6]. Spectrum data: ^{1}H NMR (400MHz, $CDCl_3$): 3.63 (s, 2H, H-2), 3.32 (m, 2H, H-2′), 2.99 (t, 6.6 Hz, 2H, H-1′), 2.17 (s, 3H, H-4), 1.91 (s, 3H, H-4′), ^{13}C NMR (100MHz, $CDCl_3$): 199.8 (C-3), 191.7 (C-1), 170.2 (C-3′), 57.6 (C-2), 42.2 (C-2′), 38.6 (C-1′), 30.1 (C-4), 24.0 (C-4′).

3-Hydroxybutyryl-SNAC.

3-Hydroxybutyryl-SNAC was synthesized according to a previous report[7]. Spectrum data: ^{1}H NMR (400MHz, $CDCl_3$): δ 6.52 (br, 1H, NH), 4.19 (h, J = 5.8 Hz, 1H, H-3), 3.36 (q, J = 6.3 Hz, 2H, H-2′), 2.96 (m, 2H, H-1′), 2.65 (m, 1H, H-2), 1.90 (s, 3H, H-4′), 1.17 (dd, J = 6.2, 1.1 Hz, 3H, H-4), ^{13}C NMR (100MHz, $CDCl_3$) δ 199.1 (C-1), 171.1 (C-3′), 65.0 (C-3), 52.7 (C-2), 39.2 (C-2′), 28.8 (C-1′), 23.2 (C-4′), 22.9 (C-4).

3-Oxohexanoyl-SNAC. 3-Oxohexanoyl-SNAC was synthesized according to a previous report[8]. Spectrum data: ^{1}H NMR (400MHz, $CDCl_3$): δ 6.01 (br s, 1H, NH), 3.69 (s, 2H, H-2), 3.45 (q, J = 6.1 Hz, 2H, H-2′), 3.08 (t, J = 6.3 Hz, 2H, H-1′), 2.51 (t, J = 7.3 Hz, 2H, H-4), 1.97 (s, 3H, H-4′), 1.61 (q, J = 7.3 Hz, 2H, H-5), 0.92 (t, J = 7.4 Hz, 3H, H-6), ^{13}C NMR (100MHz, $CDCl_3$): δ 202.4 (C-3), 192.6 (C-1), 170.6 (C-3′), 57.3 (C-2), 45.4 (C-4), 39.3 (C-2′), 29.3 (C-1′), 23.3 (C-4′), 17.0 (C-5), 13.6 (C-6).

3-Oxooctanoyl-SNAC. 3-Oxooctanoyl-SNAC was synthesized according to the method used to synthesize 3-oxohexanoyl-SNAC from hexanoyl chloride. Spectrum data: ^{1}H NMR (400MHz, $CDCl_3$): δ 6.05 (br s, 1H, NH), 3.68 (s, 2H, H-2), 3.44 (q, J = 6.0 Hz, 2H, H-2′), 3.07 (t, J = 6.3 Hz, 2H, H-1′), 2.51 (t, J = 7.4 Hz, 2H, H-4), 1.96 (s, 3H, H-4′), 1.57 (m, 2H, H-5), 1.37–1.23 (4H, H-6 and H-7), 0.87 (t, J = 7.0 Hz, 3H, H-8), ^{13}C NMR (100MHz, $CDCl_3$) : δ 202.5 (C-3), 192.6 (C-1), 170.6 (C-3′), 57.3 (C-2), 43.5 (C-4), 39.3 (C-2′), 31.2 (C-6), 29.3 (C-1′), 23.3 (C-4′), 23.2 (C-5), 22.5 (C-7), 14.0 (C-8).

3-Oxooctanoyl-CoA and 3-hydroxyoctanoyl-CoA. 3-hydroxyoctanoyl-CoA was synthesized via 3-oxooctanoyl-CoA (Scheme 1).

3-Oxooctanoyl-CoA was synthesized according to a previous report[9]. 4-Dimethylaminopyridine (4-DMAP, 41.7 mmol, 2.0 eq) and Meldrum's acid (20.7 mmol, 1.0 eq) were dissolved in CH_2Cl_2 (30 ml) under a N_2 atmosphere. After the reaction mixture was cooled to 0 °C, hexanoyl chloride (20.7 mmol, 1.0 eq) was added dropwise over 30 min with stirring. After 16 h reaction at room temperature, the reaction was quenched by adding 1 M HCl (30 ml) and the product was extracted with CH_2Cl_2 three times, washed with brine, dried over anhydrous sodium sulphate, and concentrated. The crude mixture was dissolved in methanol (20 ml) and heated to 90 °C for 16 h under reflux. The reaction was evaporated and purified by column chromatography (ethyl acetate) to obtain 3-oxooctanoyl methyl ester. Spectrum data: ^{1}H NMR (400 MHz, $CDCl_3$) δ 3.66 (s, 3H), 3.38 (s, 2H), 2.46 (t, J = 7.4 Hz, 2H), 1.52 (d, J = 7.6 Hz, 2H), 1.25–1.18 (4H), 0.81 (t, J = 6.7 Hz, 3H), ^{13}C NMR (100 MHz, $CDCl_3$) δ 203.0, 167.8, 52.3, 49.0, 43.0, 31.1, 23.2, 22.4, 13.9.

To a solution of 3-oxooctanoyl methyl ester (4.38 mmol, 1.0 eq) and ethylene glycol (124.1 mmol, 28 eq) in CH_2Cl_2 (50 ml), chlorotrimethylsilane (26.3 mmol, 26 eq) was added dropwise and stirred at room temperature for 4 days. After the reaction was quenched with water, the organic layer was evaporated and the residue was used for the following reaction. The crude sample was dissolved in a solution (1 M aqueous sodium hydroxide:ethanol = 1:4, 20 ml) and heated under reflux for 16 h. After adjusting the pH to 5 with saturated NH_4Cl solution and formic acid, the reaction mixture was extracted with Et_2O and purified by column chromatography (ethyl acetate) to obtain 3-oxooctanoic acid ethylene acetal. Spectrum data: ^{1}H NMR (400 MHz, $CDCl_3$) δ 3.99 (m, 4H), 2.69 (s, 2H), 1.76 (d, J = 8.0 Hz, 2H), 1.37 (m, 2H), 1.34–1.23 (4H), 0.88 (t, J = 6.8 Hz, 3H), ^{13}C NMR (100 MHz, $CDCl_3$) δ 175.3, 109.4, 65.2, 42.5, 37.6, 31.9, 23.2, 22.7, 14.1.

CDI (0.28 mmol, 2.2 eq) and 3-oxooctanoic acid ethylene acetal (0.25 mmol, 2.0 eq) were dissolved in THF (10 ml) under a N_2 atmosphere and stirred for 1 h. After evaporation of the solvent, a CoA (0.13 mmol, 1.0 eq) solution (THF:H_2O =1:2, 1.0 ml) was added. After 2 h reaction, the solvent was evaporated, and the aqueous solution was acidified with formic acid. The CoA product was purified by HPLC using the following conditions: column, RP-18 GP Aqua (5 μm, 250 mm × 10 mm KANTO CHEMICAL Co. Inc.); flow rate, 3.0 ml/min; temperature, 35 °C; mobile phase, 5 mM CH_3COONH_4 (A) and methanol (B); gradient conditions, 10% B (0–10 min) and 10–80% B (10–40 min); detection, 260 nm.

3-Oxooctanoyl-CoA ethylene acetal (2.85 mg) was stirred at room temperature in a solution (H_2O 8.0 ml, acetone 10 ml, 1 M HCl 1.0 ml) for 2 days, and the product was purified by the same method as described above to obtain 3-oxooctanoyl-CoA. HR-MS: $[M+Na]^+$: observed 930.19098 $[M+Na]^+$: theo 930.18816 ($C_{29}H_{48}O_{18}N_7P_3SNa^+$). Spectrum data: ^{1}H NMR (400 MHz, D_2O) δ 8.50 (s, 1H, H-14′), 8.21 (s, 1H, H-15′), 6.12 (d, J = 6.8 Hz, 1H, H-13′), 4.52 (s, 1H, H-10′), 4.18 (br s, 2H, H-

9′), 3.96 (s, 1H, H-5′), 3.95 (s, 2H, H-2), 3.77 (m, 1H, H-8′), 3.49 (m, 1H, H-8′), 3.40 (m, 2H, H-4′), 3.30 (m, 2H, H-2′), 2.99 (m, 2H, H-1′), 2.54 (m, 2H, H-4), 2.40 (m, 2H, H-3′), 1.45 (m, 2H, H-5), 1.30–1.09 (4H, H-6 and H-7), 0.83–0.78 (6H, H-6′ and H-8), 0.69 (s, 3H, H-7′).

Finally, 3-hydroxyoctanoyl-CoA was enzymatically prepared by *in vitro* reaction with Epa-KR-DH$_{PKS}$, which was expressed as an *N*-terminus maltose binding protein-fused and *C*-terminus His-tagged enzyme and purified by amylose column. The mixture containing HEPES 100 mM, NADPH 1 mM, 3-oxooctanoyl-CoA 500 μM, Epa-KR-DH$_{PKS}$ 5 μM was incubated at 20 °C for 1 h. The formation of 3-hydroxyoctanoyl-CoA was confirmed by UPLC-ESI-MS and HR-MS. HR-MS: $[M+H]^+$: observed 910.22382 $[M+H]^+$: theo 910.22186 ($C_{29}H_{51}O_{18}N_7P_3S^+$).

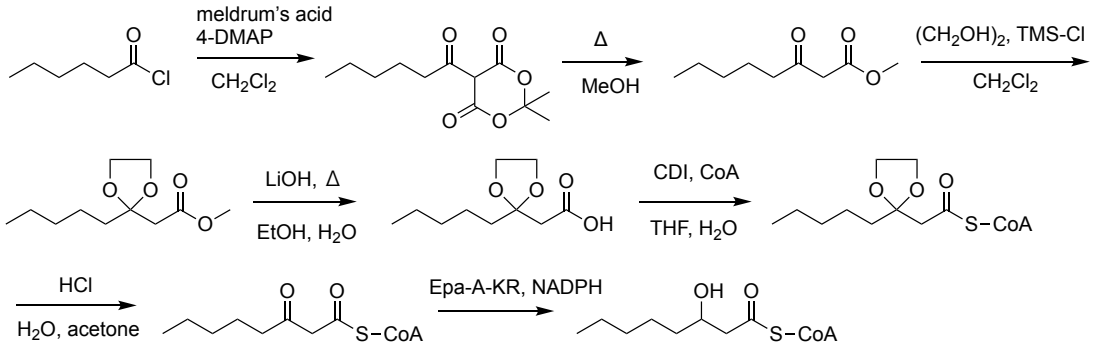

Scheme 1. Synthesis of 3-hydroxyoctanoyl-CoA.

3-Hydroxyhexanoyl-SNAC. 3-Oxohexanoyl-SNAC (0.1 mmol, 1.0 eq) was dissolved in methanol (5.0 ml) and $NaBH_4$ (0.1 mmol, 1.0 eq) was added to the mixture. After stirring at room temperature for 1 h, the reaction was quenched by adding saturated NH_4Cl solution (10 ml). The methanol was evaporated, and the compound was extracted with ethyl acetate three times, washed with brine, and purified by column chromatography (ethyl acetate). Spectrum data: ^{1}H NMR (400MHz, $CDCl_3$): δ 5.90 (br, 1H, NH), 4.07 (br s, 1H, H-3), 3.45 (m, 2H, H-2′), 3.04 (m, 2H, H-1′), 2.72 (m, 2H, H-2), 1.96 (s, 3H, H-4′), 1.56–1.32 (4H, H-4 and H-5), 0.93 (t, J = 6.9 Hz, 3H, H-6), ^{13}C NMR (100MHz, $CDCl_3$): δ 199.8 (C-1), 170.6 (C-3′), 68.7 (C-3), 51.2 (C-2), 39.4 (C-4), 38.9 (C-2′), 29.0 (C-1′), 23.4 (C-4′), 18.8 (C-5), 14.1 (C-6).

3-Hydroxyoctanoyl-SNAC. 3-Oxooctanoyl-SNAC (0.1 mmol, 1.0 eq) was dissolved in methanol (5.0 ml), and $NaBH_4$ (0.1 mmol, 1.0 eq) was added. After stirring at room temperature for 1 h, the reaction was quenched by adding saturated NH_4Cl solution (10 ml). After removing the methanol by evaporation, the product was extracted with ethyl acetate three times, washed with brine, and purified by column chromatography (ethyl acetate) and by HPLC using the following conditions: column, RP-

18 GP Aqua (5 μm, 250 mm × 10 mm KANTO CHEMICAL Co. Inc.); flow rate, 1.0 ml/min; temperature, 35 °C; mobile phase, water (A) and methanol (B); gradient conditions, 50% B (0–5 min) and 50–90% B (5–30 min); detection, 234 nm. Spectrum data: ^{1}H NMR (400MHz, $CDCl_3$): 5.85 (br s, 1H, NH), 4.06 (dt, J = 7.7 Hz, 4.1 Hz, 1H, H-3), 3.45 (dt, J = 10.2 Hz, 5.3 Hz, 2H, H-2′), 3.04 (m, 2H, H-1′), 2.74 (dd, J = 15.4, 3.4 Hz, 1H, H-2), 2.67 (dd, J = 15.4, 8.6 Hz, 1H, H-2), 1.97 (s, 3H, H-4′), 1.57–1.39 (8H, H-4, H-5, H-6, and H-7), 0.88 (t, J = 6.7 Hz, 3H, H-8), ^{13}C NMR (100MHz, $CDCl_3$): δ 199.8 (C-1), 170.6 (C-3′), 69.0 (C-3), 51.1 (C-2), 39.4 (C-2′), 36.8 (C-1′), 31.8 (C-4), 29.0 (C-6), 25.2 (C-5), 23.4 (C-4′), 22.7 (C-7), 14.2 (C-8).

2-*trans* Hexenoyl-SNAC. 2-*trans* Hexenoyl-SNAC was synthesized according to a previous report[10]. Spectrum data: ^{1}H NMR (400MHz, $CDCl_3$): δ 6.84 (m, 1H, H-3), 6.07 (d, J = 15.8 Hz, 1H, H-2), 3.36 (m, 2H, H-2′), 3.02 (m, 2H, H-1′), 2.12 (m, 2H, H-4), 1.90 (s, 3H, H-4′), 1.44 (m, 2H, H-5), 0.87 (t, J = 7.3 Hz, 3H, H-6), ^{13}C NMR (100MHz, $CDCl_3$): δ 190.5 (C-1), 170.5 (C-3′), 146.6 (C-3), 128.5 (C-2), 39.8 (C-2′), 34.3 (C-1′), 28.3 (C-4), 23.3 (C-4′), 21.3 (C-5) 13.8 (C-6).

2-*trans* Hexenoyl-CoA. 2-*trans* Hexenoyl-CoA was prepared according to a previous report[11]. Spectrum data: ^{1}H NMR (400 MHz, D_2O) δ 8.63 (s, 1H, H-14′), 8.38 (s, 1H, H-15′), 6.90 (m, 1H, H-3), 6.17–6.13 (m, 2H, H-2 and H-13′), 4.55 (s, 1H, H-10′), 4.20 (br s, 2H, H-9′), 3.97 (s, 1H, H-5′), 3.83 (m, 1H, H-8′), 3.56 (m, 1H, H-8′), 3.39 (t, J = 6.7 Hz, 2H, H-4′), 3.30 (t, J = 6.2 Hz, 2H, H-2′), 2.98 (t, J = 6.2 Hz, 2H, H-1′), 2.37 (t, J = 6.4 Hz, 2H, H-3′), 2.12 (m, 2H, H-4), 1.39 (m, 2H, H-5), 0.89 (s, 3H, H-6′), 0.81 (t, J = 7.4 Hz, 3H, H-6), 0.75 (s, 3H, H-7′).

3-*cis* Hexenoyl-SNAC. 3-*cis* Hexenoic acid was synthesized according to a previous report[12]. Spectrum data: ^{1}H NMR (400 MHz, $CDCl_3$) δ 11.59 (br s, 1H, COOH), 5.59 (m, 1H, H-3), 5.51(m, 1H, H-4), 3.11 (d, J = 7.2 Hz, 2H, H-2), 2.02 (m, 2H, H-5), 0.95 (t, J = 7.6 Hz, 3H, H-6), ^{13}C NMR (100 MHz, $CDCl_3$) δ 179.0 (C-1), 135.8 (C-4), 119.5 (C-3), 32.7 (C-2), 20.8 (C-5), 14.0 (C-6).

3-*cis* Hexenoic acid (0.88 mmol, 1.0 eq) and 1,1-carbodiimidazole (CDI, 171 mg, 1.2 eq) were dissolved in CH_2Cl_2 (5 ml) and stirred for 2 h. Then, *N*-acetylcysteamine (0.1 ml, 1.0 eq) was added and stirred at room temperature for 16 h. The reaction mixture was quenched by adding saturated NH_4Cl solution (30 ml) and the compound was extracted with ethyl acetate three times. After washing the organic layer with water and brine, the product was purified by column chromatography (ethyl acetate). Spectrum data: ^{1}H NMR (400 MHz, $CDCl_3$) δ 6.02 (br s, 1H, NH), 5.62 (m, 1H, H-3), 5.47 (m, 1H, H-4), 3.39 (q, J = 6.3 Hz, 2H, H-2′), 3.31 (d, 2H, H-2), 3.00 (t, J = 6.5 Hz, 2H, H-1′), 2.06 (p, J = 7.5 Hz, 2H, H-5), 1.94 (s, 3H, H-4′), 0.97 (t, J = 7.5 Hz, 3H, H-6), ^{13}C NMR (100 MHz, $CDCl_3$) δ 198.5 (C-1), 170.4 (C-3′), 136.9 (C-4), 119.4 (C-3), 42.5 (C-2), 39.7 (C-2′), 28.6 (C-1′), 23.3 (C-4′), 20.9 (C-5), 13.9 (C-6).

2-*trans* Octenoyl-SNAC. 2-*trans* Octenoyl-SNAC was prepared according to a previous report[13]. Spectrum data: ^{1}H NMR (400MHz, $CDCl_3$): δ 6.90 (dt, J = 15.2, 7.9 Hz, 1H, H-3), 6.13 (d, J = 15.2 Hz, 1H, H-2), 3.44 (q, J = 5.8 Hz, 2H, H-2′), 3.08 (t, J = 6.3 Hz, 2H, H-1′), 2.18 (q, J = 7.5 Hz, 2H, H-4), 1.95 (s, 3H, H-4′), 1.46 (p, J = 7.2 Hz, 2H, H-5), 1.39–1.24 (6H, H-6 and H-7), 0.88 (t, J = 6.7 Hz, 3H, H-8), ^{13}C NMR (100MHz, $CDCl_3$): δ 190.6 (C-1), 170.4 (C-3′), 147.0 (C-3), 128.3 (C-2), 40.0 (C-2′), 32.3 (C-1′), 31.4 (C-4), 28.3 (C-5), 27.7 (C-6), 23.4 (C-4′), 22.5 (C-7), 14.1 (C-8).

2-*trans* Octenoyl-CoA. 2-*trans* Octenoyl-CoA was synthesized according to a previous report using 2-*trans* octenoic acid[14]. HR-MS: $[M-2H]^{2-}$: observed 444.59510 theo 444.59473 ($C_{29}H_{46}O_{17}N_7P_3S^{2-}$). Spectrum data: ^{1}H NMR (400 MHz, D_2O) δ 8.48 (s, 1H, H-14′), 8.18 (s, 1H, H-15′), 6.86 (m, 1H, H-3), 6.10 (m, 2H, H-2 and H-13′), 4.52 (s, 1H, H-10′), 4.19 (br s, 2H, H-9′), 3.96 (s, 1H, H-5′), 3.77 (m, 1H, H-8′), 3.50 (m, 1H, H-8′), 3.37 (m, 2H, H-4′), 3.28 (m, 2H, H-2′), 2.96 (t, J = 6.2 Hz, 2H, H-1′), 2.35 (t, J = 6.3 Hz, 2H, H-3′), 2.10 (q, J = 7.0 Hz, 2H, H-4), 1.33 (p, J = 7.3 Hz, 2H, H-5), 1.24–1.11 (4H, H-6 and H-7), 0.83 (s, 3H, H-6′), 0.77 (t, J = 6.6 Hz, 3H, H-8), 0.70 (s, 3H, H-7′).

2-*cis* Octenoyl-SNAC. 2-*cis* Octenoic acid methyl ester was synthesized with the Horner-Wadsworth-Emmons reaction. To a suspension of NaH (1.0 eq, 10 mmol) in THF (30 ml), trimethyl phosphonoacetate (1.0 eq, 10 mmol) was added dropwise at 0 °C over 30 min with stirring. Hexanal (0.9 eq, 9 mmol) was then added dropwise at 0 °C and the mixture was stirred at room temperature for 16 h. The reaction was quenched by adding H_2O and extracted with ethyl acetate. After washing with brine, the organic layer was dried over Na_2SO_4 and concentrated. The crude product (2-*trans*:2-*cis* form = 9:1) was purified with column chromatography (hexane : ethyl acetate = 20 : 1) to yield 2-*cis* octenoic acid methyl ester. Spectrum data: ^{1}H NMR (400 MHz, $CDCl_3$) δ 6.20 (dt, J = 11.5, 7.5 Hz, 1H, H-3), 5.73 (dt, J = 11.5, 1.7 Hz, 1H, H-2), 3.68 (s, 3H, OCH_3), 2.61 (qd, J = 7.5, 1.8 Hz, 2H, H-4), 1.41 (m, 2H, H-5), 1.34–1.23 (4H, H-6 and H-7), 0.87 (t, J = 7.0 Hz 3H, H-8), ^{13}C NMR (100 MHz, $CDCl_3$) δ 167.0 (C-1), 151.2 (C-3), 119.2 (C-2), 51.0 (OCH_3), 31.5 (C-4), 29.0 (C-5), 28.8 (C-6), 22.5 (C-7), 14.1 (C-8).

To a solution of 2-*cis* octenoic acid methyl ester (1.28 mmol) in THF (10 ml), a mixture of 1.0 M LiOH solution (10 ml) and methanol (10 ml) was added. After 16 h reaction at room temperature, the solution was acidified by adding formic acid and the product was extracted with diethyl ether three times, washed with saturated NH_4Cl solution, water, and brine, dried over Na_2SO_4, and concentrated. 2-*cis* Octenoic acid was purified by column chromatography (ethyl acetate). Spectrum data: ^{1}H NMR (400 MHz, $CDCl_3$): δ 6.36 (dt, J = 11.5, 7.6 Hz, 1H, H-3), 5.78 (dt, J = 11.5, 1.8 Hz, 1H, H-2), 2.66 (qd, J = 7.5, 1.8 Hz, 2H, H-4), 1.46 (m, 2H, H-5), 1.37–1.20 (4H, H-6 and H-7), 0.89 (t, J = 6.8 Hz, 3H, H-8), ^{13}C NMR (100 MHz, $CDCl_3$) δ 172.7 (C-1), 153.8 (C-3), 119.2 (C-2), 31.6 (C-4), 29.3 (C-5), 28.8 (C-6), 22.6 (C-7), 14.1 (C-8).

2-*cis* Octenoic acid (0.42 mmol, 1.0 eq) and triethylamine (0.5 mmol, 1.2 eq) in CH_2Cl_2 (5 ml) kept for 30 min at room temperature under a N_2 atmosphere was cooled to 4 °C, and ethyl chloroformate (0.5 mmol, 1.2 eq) was added dropwise. After 2 h, *N*-acetylcysteamine (0.42 mmol, 1.0 eq) was added and stirred at room temperature for 30 min. The reaction was quenched by adding saturated $NaHCO_3$ solution (20 ml). The compound was extracted with CH_2Cl_2 three times. The organic layer was washed with water and brine, and then dried with anhydrous sodium sulphate. The product was purified by column chromatography (ethyl acetate). Spectrum data: ^{1}H NMR (400 MHz, $CDCl_3$): δ 6.08–6.04 (2H, H-2 and H-3), 5.90 (br s, 1H, NH), 3.47 (q, J = 5.9 Hz, 1H, H-2′), 3.08 (t, J = 6.4 Hz, 1H, H-1′), 2.63 (m, 2H, H-4), 1.96 (s, 3H, H-4′), 1.45 (m, 2H, H-5), 1.36–1.28 (4H, H-6 and H-7), 0.88 (t, J = 6.9 Hz, 3H, H-8), ^{13}C NMR (100 MHz, $CDCl_3$) δ 190.1 (C-1), 170.1 (C-3′), 148.6 (C-3), 125.9 (C-2), 39.9 (C-2′), 31.6 (C-1′), 30.1 (C-4), 28.8, 28.7 (C-5 and C-6), 23.4 (C-4′), 22.6 (C-7), 14.1 (C-8).

3-*cis* Hexenoyl-CoA. 3-*cis* Hexenoic acid (0.44 mmol, 1.0 eq) and CDI (0.53 mmol, 1.2 eq) were dissolved in THF (5.0 ml) and the mixture was stirred for 2 h. After evaporation of the solvent, a CoA (0.088 mmol, 0.2 eq) solution (H_2O:THF = 1:2, 1.0 ml) was added, and the reaction was stirred for 1 h. THF was evaporated and the solution was acidified by adding 0.1% aqueous acetic acid. The mixture was stirred at room temperature for 16 h. The CoA product was purified by HPLC using the following conditions: column, RP-18 GP Aqua (5 μm, 250 mm × 10 mm KANTO CHEMICAL Co. Inc.); flow rate, 3.0 ml/min; temperature, 35 °C; mobile phase, 5 mM CH_3COONH_4 (A) and methanol (B); gradient conditions, 10% B (0–10 min) and 10–80% B (10–40 min); detection, 260 nm. HR-MS: $[M+H]^+$: observed 864.17985 theo 864.18000 ($C_{27}H_{45}O_{17}N_7P_3S^+$). Spectrum data: ^{1}H NMR (400 MHz, D_2O) δ 8.50 (s, 1H, H-14′), 8.16 (s, 1H, H-15′), 6.10 (d, J = 6.7 Hz, 1H, H-13′), 5.65 (m, 1H, H-3), 5.40 (m, 1H, H-4), 4.52 (s, 1H, H-10′), 4.18 (br s, 2H, H-9′), 3.96 (s, 1H, H-5′), 3.77 (m, 1H, H-8′), 3.59 (m, 1H, H-8′), 3.39 (m, 2H, H-4′), 3.25 (m, 2H, H-2′), 3.01 (d, J = 7.5 Hz, 2H, H-2), 2.69 (t, J = 6.3 Hz, 2H, H-1′), 2.37 (m, 2H, H-3′), 2.00 (d, J = 9.6 Hz, 2H, H-5), 0.90 (t, J = 7.5 Hz, 3H, H-6), 0.82 (s, 3H, H-6′), 0.68 (s, 3H, H-7′).

4,7-*cis* Decadienoyl-CoA. 4,7-*cis* Decadienoyl-CoA was synthesized by the same method as for 3-*cis* hexenoyl-CoA with 4,7-*cis* decadienoic acids. HR-MS: $[M+H]^+$: observed 918.22857 theo 918.22695 ($C_{31}H_{51}O_{17}N_7P_3S^+$). Spectrum data: ^{1}H NMR (400 MHz, D_2O) δ 8.50 (s, 1H, H-14′), 8.20 (s, 1H, H-15′), 6.11 (d, J = 6.4 Hz, 1H, H-13′), 5.44–5.20 (4H, H-4, H-5, H-7, and H-8), 4.54 (s, 1H, H-10′), 4.18 (br s, 2H, H-9′), 3.97 (s, 1H, H-5′), 3.79 (dd, J = 9.4, 4.6 Hz, 1H, H-8′), 3.50 (dd, J = 9.7, 4.5 Hz, 1H, H-8′), 3.39 (t, J = 6.7 Hz, 2H, H-4′), 3.26 (t, J = 6.3 Hz, 2H, H-2′), 2.91 (t, J = 6.3 Hz, 2H, H-1′), 2.71–2.55 (4H, H-2 and H-6), 2.36 (m, 4.7 Hz, 2H, H-3′), 2.31 (m, 2H, H-3), 1.97 (p, J = 7.2 Hz, 2H, H-9), 0.86 (m, 3H, H-10), 0.84 (s, 3H, H-6′), 0.70 (s, 3H, H-7′).

3,6,9,12,15-*cis* Octadecapentaenoyl-CoA. 3,6,9,12,15-*cis* Octadecapentaenoic acid was synthesized according to previous reports (scheme 2)[15,16]. Spectrum data: ^{1}H NMR (400 MHz, $CDCl_3$) δ 5.68–5.54 (2H, H-3 and H-4), 5.46–5.28 (8H, H-6, H-7, H-9, H-10, H-12, H-13, H-15, and H-16), 3.18 (m, 2H, H2), 2.88–2.79 (8H, H-5, H-8, H-11, and H-14), 2.07 (q, J = 7.2 Hz, 2H, H-17), 0.97 (t, J = 7.5 Hz, 3H, H-18), ^{13}C NMR (100 MHz, $CDCl_3$) δ 178.0 (C-1), 132.2, 132.0, 128.9, 128.7, 128.5, 128.0, 127.9, 127.3, 127.1, 120.7 (C-3, C-4, C-6, C-7, C-9, C-10, C-12, C-13, C-15, and C-16), 32.7 (C-2), 25.9, 25.8, 25. 7 (C-5, C-8, C-11, and C-14), 20.7 (C-17), 14.4 (C-18).

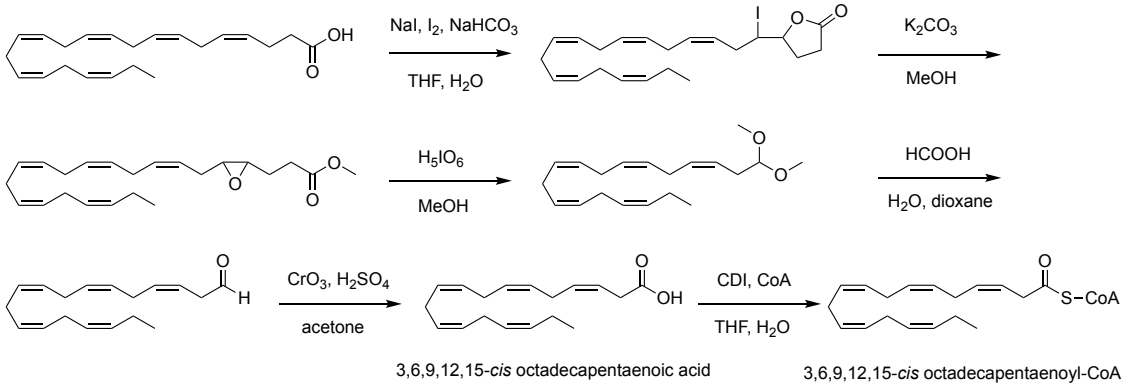

Scheme 2. Synthesis scheme of 3,6,9,12,15-*cis* octadecapentaenoyl-CoA.

3,6,9,12,15-*cis* Octadecapentaenoyl-CoA was synthesized by the same method as that for 3-*cis* hexenoyl-CoA with 3,6,9,12,15-*cis* octadecapentaenoic acid. 3,6,9,12,15-*cis* Octadecapentaenoyl-CoA was purified by HPLC. Analytical conditions were as follows: column, RP-18 GP Aqua (5 μm, 250 mm × 10 mm KANTO CHEMICAL Co. Inc.); flow rate, 3.0 ml/min; temperature, 35 °C; mobile phase, 5 mM CH_3COONH_4 (A) and methanol (B); gradient conditions, 50% B (0–10 min) and 50–80% B (10–40 min); detection, 260 nm. HR-MS: $[M+H]^+$: observed 1024.30621 theo 1024.30520 ($C_{39}H_{61}O_{17}N_7P_3S^+$). Spectrum data: ^{1}H NMR (400 MHz, D_2O) δ 8.50 (s, 1H, H-14′), 8.20 (s, 1H, H-15′), 6.11 (d, J = 5.1 Hz, 1H, H-13′), 5.69–5.53 (2H, H-3 and H-4), 5.51–5.22 (8H, H-6, H-7, H-9, H-10, H-12, H-13, H-15, and H-16), 4.53 (s, 1H, H-10′), 4.18 (br s, 2H, H-9′), 3.97 (s, 1H, H-5′), 3.79 (m, 1H, H-8′), 3.50 (m, 1H, H-8′), 3.38 (m, 2H, H-4′), 3.33–3.21 4H, H-2 and H-2′), 2.91 (m, 2H, H-1′), 2.76–2.71 (8H, H-5, H-8, H-11, H-14), 2.35 (m, 2H, H-3′), 1.98 (m, 2H, H-17), 0.88–0.84 (6H, H-18, and H-6′), 0.69 (s, 3H, H-7′).

Docosahexaenoyl-CoA. 1,1-Carbodiimidazole (CDI, 0.18 mmol) and docosahexaenoic acids (0.15 mmol) were stirred in dry THF (1 ml) for 40 min at room temperature. A CoA (0.075 mmol) in water (1 ml) was added into the mixture, and the reaction mixture was stirred for 30 min. Excess fatty acids was removed by extraction with EtOAc three times. The water layer was evaporated, and the residues

were dissolved in MeOH. Docosahexaenoyl-CoA was purified by HPLC (SHIMADZU) on RP-18 GP Aqua (5 μm, 250 mm x 10 mm KANTO CHEMICAL Co., Inc). Flow rate, 3.0 ml/min; temperature, 35℃; mobile phase A, 5 mM CH_3COONH_4:MeOH = 9:1; mobile phase B, 5 mM CH_3COONH_4:MeOH = 2:8; gradient conditions, 50% B (0-10 min); 50-90% (10-40 min); 90% B (40-45 min); detection, 260 nm. HR-ESI-MS: $[M+H]^+$: 1078.35437 ($C_{43}H_{67}N_7O_{17}P_3S$: 1078.35215).

Eicosapentaenoyl-CoA. Eicosapentaenoyl-CoA was synthesized and purified by the same methods for docosahexaenoyl-CoA using eicosapentaenoic acids. HR-ESI-MS: $[M+H]^+$: 1052.33850 ($C_{41}H_{65}N_7O_{17}P_3S$: 1052.33650).

8. *In vitro* analysis of the KR domain

A mixture containing 1 mM 3-oxobutyryl-SNAC, 3-oxohexanoyl-SNAC, or, 3-oxooctanoyl-SNAC, 2 mM NADPH, 100 mM HEPES, and 5 μM purified Epa-KR-DH_{PKS} or ketoacyl reductase EcFabG of *E. coli* was incubated for 1 h at 20 °C. Then, the reaction mixture was boiled and analyzed by LC-ESI-MS to examine the ketoacyl reductase activity. Analytical conditions were as follows: Waters ACQUITY UPLC system equipped with a SQ Detector2 (Waters, MA, USA); column, InertSustain C18 (2.1 × 150 mm, 3.0 μm, GL Science Inc., Tokyo, Japan); flow rate, 0.2 ml/min; temperature, 35 °C; mobile phase, water (A) and methanol (B); gradient conditions, 5% B (0–5 min) and 5–80% B (5–50 min); detection, 234 nm and positive ion mode; injection volume, 2 μl. For chiral analysis, the reaction mixture was extracted with ethyl acetate three times and the extracts were dissolved in isopropanol. Stereochemical analysis of the reaction products was carried out with a Waters ACQUITY UPLC system equipped with a SQ Detector2. Analytical conditions were as follows: column, CHIRALPAK IA-3 (2.1 × 150 mm, 3.0 μm, DAICEL CORPORATION, Tokyo, Japan); flow rate, 0.2 ml/min; temperature, 25 °C; mobile phase, isopropanol (A) and hexane (B); isocratic conditions, A:B = 10:90, detection, 234 nm; injection volume, 2 μl.

9. *In vitro* hydration reaction with DH domains and acyl-ACP substrates

A mixture containing 100 μM *apo*-ACP, 20 μM phosphopantetheinyl transferase (Sfp), 80 mM Tris-HCl, 80 mM NaCl, 25 mM $MgCl_2$ and 300 μM crotonyl-CoA, 2-*trans* hexenoyl-CoA, or 2-*trans* octenoyl-CoA was incubated for 10 min at 20 °C. Then, a purified dehydratase, Ara-KR-DH_{PKS}, Ara-DH_{FabA}, Epa-KR-DH_{PKS}, Epa-DH_{FabA}, Dha-KR-DH_{PKS}, or Dha-DH_{FabA}, was added into the mixture at a concentration of 0.91 μM. After incubation for 1, 10, or 60 min at 20 °C, the reaction was quenched by adding the same volume of 1% trifluoroacetic acid (TFA) solution. The reaction mixtures were analyzed on an HPLC instrument (Shimadzu, Kyoto, Japan) equipped with an amaZon SL DB-1 (Bruker, MA, USA). Analytical conditions were as follows: column, ZORBAX 300SB-C8 (2.1 × 150 mm, 3.5 μm, Agilent Technologies Inc., CA, USA); flow ratio, 0.2 ml/min; temperature, 40 °C;

mobile phase, 0.1% TFA in water (A) and 0.1% TFA in acetonitrile (B); gradient conditions, 20–70% B (40 min); detection, 210 nm and positive ion mode; injection volume, 10 µl. The reaction products were also analyzed with an HPLC instrument (Agilent Technologies Inc.) equipped with a Maxis Plus (Bruker) for HR-MS. Analytical conditions were as follows: column, Sunshell C8-30HT (2.1 × 150 mm, 3.4 µm, ChromaNik Technologies Inc., Osaka, Japan); flow ratio, 0.3 ml/min; temperature, 70 °C; mobile phase, 0.1% TFA in water (A) and 0.1% TFA in acetonitrile (B); gradient conditions, 30–60% B (30 min); detection, 280 nm and positive ion mode; injection volume, 5 µl. The mass spectra of multiply charged ions were deconvoluted using the DataAnalysis ver. 4.0 software (Bruker) to provide molecular weight information of proteins.

10. *In vitro* dehydration reaction with DH domains and 3-hydroxyoctanoyl-ACP

A mixture containing 50 µM *apo*-ACP, 20 µM Sfp, 80 mM Tris-HCl, 80 mM NaCl, 25 mM $MgCl_2$ and 100 µM 3-hydroxyoctanoyl-CoA was incubated for 10 min at 20 °C. Then, purified Ara-KR-DH_{PKS} or Ara-DH_{FabA} was added into the mixture at a concentration of 0.91 µM. After incubation for 60 min at 20 °C, the product was analyzed by the same method of *in vitro* hydration reaction assay.

11. *In vitro* isomerization reaction with Epa-DH_{FabA} and 3-*cis* hexenoyl-SNAC

A reaction mixture containing 1 mM 3-*cis* hexenoyl-SNAC, 100 mM HEPES, and 5 µM Epa-DH_{FabA} was incubated for 1 h at 20 °C. Then, the reaction mixture was extracted with ethyl acetate and analysed with an ACQUITY UPLC system equipped with a SQ Detector2 (Waters). Analytical conditions were as follows: column, InertSustain C18 (2.1 × 150 mm, 3.0 µm, GL Science Inc.); flow rate, 0.2 ml/min; temperature, 35 °C; mobile phase, water (A) and methanol (B); gradient conditions, 5% B, (0–5 min) and 5–80% B (5–50 min); detection, 260 nm and positive ion mode; injection volume, 2 µl.

12. *In vitro* analysis of Ara-DH_{FabA} with 3-hydroxyoctanoyl-SNAC or 2-*cis* octenoyl-SNAC

A reaction mixture containing 1 mM 3-hydroxyoctanoyl-SNAC or 2-*cis* octenoyl-SNAC, 100 mM HEPES, and 50 µM Ara-DH_{FabA} was incubated for 16 h at 20 °C. Then, the reaction mixture was analyzed by the same method as that for the ketoacyl reductase assay.

13. *In vitro* reactions with the KS domains and acyl-ACPs

A mixture containing 100 µM *apo*-ACP of EPA synthase of *Shewanella oneidensis* MR-1, 20 µM phosphopantetheinyl transferase Sfp, 80 mM Tris-HCl, 80 mM NaCl, 25 mM $MgCl_2$ and 300 µM acyl-CoA was incubated for 10 min at 20 °C to prepare acyl-ACP substrates. Malonyl-ACP was also prepared by the same method. Into the mixture containing acyl-ACP substrates (50 µl) and malonyl-ACP (50 µl), dithiothreitol (DTT) and the recombinant KS domains were added at concentrations of 250 µM and 4.5 µM (Epa-KS_A, Epa-KS_C, Dha-KS_A, or Dha-KS_C), respectively. After incubation for

1 h at 20 °C, the reactions were quenched by adding the same volume of 1% TFA solution. The reaction mixtures were analyzed on an HPLC instrument (Shimadzu, Kyoto, Japan) equipped with an amaZon SL DB-1 (Bruker, MA, USA). Analytical conditions were as follows: column, ZORBAX 300SB-C8 (2.1 × 150 mm, 3.5 μm, Agilent Technologies Inc., CA, USA); flow ratio, 0.2 ml/min; temperature, 40 °C; mobile phase, 0.1% TFA in water (A) and 0.1% TFA in acetonitrile (B); gradient conditions, 20–70% B (40 min); detection, 210 nm and positive ion mode; injection volume, 10 μl. The reaction products were also analyzed with an HPLC instrument (Agilent Technologies Inc.) equipped with a Maxis Plus (Bruker) for HR-MS. Analytical conditions were as follows: column, Sunshell C8-30HT (2.1 × 150 mm, 3.4 μm, ChromaNik Technologies Inc., Osaka, Japan); flow ratio, 0.3 ml/min; temperature, 70 °C; mobile phase, 0.1% TFA in water (A) and 0.1% TFA in acetonitrile (B); gradient conditions, 30–60% B (30 min); detection, 280 nm and positive ion mode; injection volume, 5 μl. The mass spectra of multiply charged ions were deconvoluted using the DataAnalysis ver. 4.0 software (Bruker) to provide molecular weight information of proteins.

14. *In vitro* reaction of the KS domains with malonyl-ACP.

A mixture containing 100 μM *apo*-ACP, 20 μM Sfp, 80 mM Tris-HCl, 80 mM NaCl, 25 mM $MgCl_2$, and 300 μM malonyl-CoA was incubated for 10 min at 20 °C, and then 4.5 μM Epa-KS_A, Epa-KS_C, Dha-KS_A, or Dha-KS_C was added and incubated in the presence of DTT (250 μM) for 1 h at 20 °C. The reaction mixture was quenched by adding the same volume of 1% TFA solution and analyzed by the same methods as those for the *in vitro* reaction with KS domains.

15. *In vitro* combination reaction with Dha-KS_C and 3,6,9,12,15-*cis* octadecapentaenoyl-ACP.

Epa-KR-DH_{PKS} (3.8 μM) and NADPH (1 mM) were added to a reaction mixture containing Dha-KS_A and 3,6,9,12,15-*cis* octadecapentaenoyl-ACP and incubated for 1 h at 20 °C. Then, Epa-DH_{FabA} (5.3 μM), Dha-KS_C (4.7 μM) and malonyl-ACP (100 μM) were added and incubated for 1 h at 20 °C. The reaction mixture was quenched by adding the same volume of 1% TFA solution. The reaction products were analyzed by the same methods as the abovementioned *in vitro* reactions of KS domains.

16. *In vitro* reactions of AT domains with acyl-ACPs.

A mixture containing 50 μM *apo*-ACP, 10 μM Sfp, 5 mM $MgCl_2$, 80 mM Tris-HCl, 80 mM NaCl, and 1 mM butyryl-CoA, 600 μM hexanoyl-CoA, 1 mM 4,7-*cis* decadienoyl-CoA, 1 mM myristoyl-CoA, 1 mM palmitoyl-CoA, 1 mM stealoyl-CoA, 1 mM 3,6,9,12,15-*cis* octadecapentaenoyl-CoA, 600 μM eicosapentaenoyl-CoA, or 600 μM docosahexaenoyl-CoA were incubated for 10 min at 20℃ to prepare acyl-ACPs. Then, recombinant enzymes, Epa-B, Epa-B-AT^0, OrfB, or OrfB-AT^0 was added into the mixture at concentration or 1μM (OrfB enzymes) or 5 μM

(Epa-B enzymes). The reaction mixture was incubated for 1 h at 20℃ (Epa-B enzymes) or 30℃ (OrfB enzymes). The reaction was quenched by addition of three times the volume of solution (acetonitrile:water = 2:1) to mixture. The reaction mixtures were analyzed by the same methods as the abovementioned *in vitro* reactions of KS domains.

For analysis of free fatty acids, excess free fatty acids in the mixture was removed using Amicon Ultra 3K after preparation of DHA- and EPA-ACPs. Recombinant enzymes, EpaB, EpaB-AT^0, OrfB, or OrfB-AT^0 was added into the mixture at concentration of 1μM (OrfB enzymes) or 5 μM (EpaB enzymes). The reaction mixture was incubated for 1 h at 20℃ (Epa-B enzymes) or 30℃ (OrfB enzymes). The reaction was quenched by addition of twice volume of solution (acetonitrile:water = 2:1) to mixture. The reaction mixtures were analyzed on an HPLC instrument equipped with an amaZon SL DB-1 (Bruker). Analytical conditions were as follows: column, InertSustain C18 (2.1 × 150 mm, 3.0 μm, GL Science Inc.); flow ratio, 0.2 ml/min; temperature, 40 °C; mobile phase, 0.1% formic acid in water (A) and 0.1% formic acid in acetonitrile (B); gradient conditions, 50–90% B (0–40 min); detection, 210 nm and positive ion mode; injection volume, 5 μl.

References

1. E. G. Bligh, W. J, Dyer, A rapid method of total lipid extraction and purification. *Can. J. Biochem. Physiol.,* **37**, 911–917 (1959).
2. B. Andersson, R. Holman, Pyrrolidides for mass spectrometric determination of the position of the double bond in monounsaturated fatty acids. *Lipids* **9**, 185–190 (1974).
3. A. Hauvermale, J. Kuner, B. D. Guerra, S. Diltz, J. G. Metz, Fatty acid production in Schizochytrium sp.: Involvement of a polyunsaturated fatty acid synthase and a type I fatty acid synthase. *Lipids* **41**, 739–747 (2006).
4. T. Ujihara, M. Nagano, H. Wada, S. Mitsuhashi, Identification of a novel type of polyunsaturated fatty acid synthase involved in arachidonic acid biosynthesis. *FEBS Lett.* **588**, 4032–4036 (2014).
5. K. Takeda, K. Kemmoku, Y. Satoh, Y. Ogasawara, K. Shin-Ya, T. Dairi, *N*-Phenylacetylation and nonribosomal peptide synthetases with substrate promiscuity for biosynthesis of heptapeptide variants, JBIR-78 and JBIR-95. *ACS Chem. Biol.* **12**, 1813–1819 (2017).
6. S. K. Piasecki, C. A. Taylor, J. F. Detelich, J. Liu, J. Zheng, A. Komsoukaniants, D. R. Siegel, A. T. Keatinge-Clay, Employing modular polyketide synthase ketoreductases as biocatalysts in the preparative chemoenzymatic syntheses of diketide chiral building blocks. *Chem. Biol.* **18**, 1331–1340 (2011).
7. S. Gruschow, T. J. Buchholz, W. Seufert, J. S. Dordick, D. H. Sherman, Substrate profile analysis and ACP-mediated acyl transfer in *Streptomyces coelicolor* type III polyketide synthases. *ChemBioChem* **8**, 863–868 (2007).
8. R. A. Cacho, J. Thuss, W. Xu, R. Sanichar, Z. Gao, A. Nguyen, J. C. Vederas, Y. Tang, Understanding programming of fungal iterative polyketide synthases: The biochemical basis for regioselectivity by the methyltransferase domain in the lovastatin megasynthase. *J. Am. Chem. Soc*., **137**, 15688–15691 (2015).
9. C. Kanchanabanca, W. Tao, H. Hong, Y. Liu, F. Hahn, M. Samborskyy, Z. Deng, Y. Sun, P. F. Leadlay, Unusual acetylation-elimination in the formation of tetronate antibiotics. *Angew. Chem. Int. Ed.,* **52**, 5785–5788 (2013).
10. C. R. Huitt-Roehl, E. A. Hill, M. M. Adams, A. L. Vagstad, J. W. Li, C. A. Townsend, Starter unit flexibility for engineered product synthesis by the nonreducing polyketide synthase PksA. *ACS Chem. Biol.*, **10**, 1443–1449 (2015).
11. B. B. Bond-Watts, A. M. Weeks, M. C. Y. Chang, Biochemical and structural characterization of the trans-enoyl-CoA reductase from *Treponema denticola. Biochemistry* **51**, 6827–6837 (2012).
12. J. A. Gurak Jr., K. S. Yang, Z. Liu, K. M. Engle, Directed, regiocontrolled hydroamination of unactivated alkenes via protodepalladation. *J. Am. Chem. Soc*., **138**, 5805–5808 (2016).
13. M. L. Tse, R. E. Watts, C. Khosla, Substrate tolerance of module 6 of the epothiline synthetase. *Biochemistry* **46**, 3385–3393 (2007).

14. M. Yang, K. E. Guja, S. T. Thomas, M. Garcia-Diaz, N. S. Sampson, A distinct MaoC-like enotl-CoA hydratase architecture mediates cholesterol catabolism in *Mycobacterium tuberculosis. ACS Chem. Biol*. **2014**, *9*, 2632–2645.
15. S. Flock, M. Lundquist, L. Skattebol, Syntheses of Some Polyunsaturated Sulfur- and Oxygen-containing Fatty Acids Related to Eicosapentaenoic and Docosahexaenoic Acids. *Acta. Chemica. Scandinavica.*, **53**, 436–445 (1999).
16. D. V. Kuklev, N. A. Latyshev, V. V. Bezuglov, A simple synthesis of *all-cis*-3,6,9,12,15-octadecapentaenoic acid. *Russian Journal of Bioorganic Chemistry* **17**, 1433–1436 (1991).

Acknowledgements

This study “Studies on the Biosynthetic machinery in Polyunsaturated Fatty-Acid Synthases” was supervised by Prof. Tohru Dairi (Division of Applied Chemistry, Faculty of Engineering, Hokkaido University). This work was done from April 2014 to March 2020 in laboratory of Applied BioChemistry in Hokkaido University.

First, I would like to express the deepest appreciation to Prof. Tohru Dairi. His invaluable advises and great guidance led this project forward, and his warm encouragements always supported and motivated me. Thank you for giving me a chance to work on this project. I learned important and essential things as a researcher from him.

I also would like to express my gratitude to Assistant Professors, Dr. Yasuharu Satoh and Dr. Yasushi Ogasawara. Dr. Yasuharu Satoh gave me a lot of helpful advises and taught me biological techniques and knowledge. Dr Yasushi Ogasawara taught me chemical techniques and knowledge, and his helpful discussion about chemistry of natural products led this study forward.

I carried out this study with cooperation of some researchers. I want to thank Prof. Yoshimitsu Hamano and Associate Prof. Chitose Maruyama (Graduate School of Bioscience and Biotechnology, Fukui Prefectural University) for helpful discussion and technical helps about high-resolution MS analysis. I also thank Dr. Ujihara Tetsuro (Kyowa Hakko Bio. Co., Ltd.) for cooperation on this study.

I also thank previous and current lab members, Ms. Mai Naka, Mr. Kota Kobayashi, Mr. Kenshin Ikeuchi, and Mr. Makoto Ohtsuka, for contributions to this project, and the other members for discussion, encouragement, and enjoyable time.

I have received a support from Japan Society for the Promotion of Science (JSPS) Research Fellowship DC2 since April 2018. This work was supported by a Grant-in-Aids for Scientific Research from JSPS.

Finally, I am deeply grateful to my parents, Dr. Tsuguo Hayashi, Mrs. Yukie Hayashi, and my older brother and sisters, Dr. Kenichi Hayashi, Mrs Hiroko Saitoh, Ms. Nami Hayashi, for all encouragements and supports.

March 2020
Sapporo

Shohei Hayashi